ABSTRACT

Title of Dissertation: INVESTIGATION OF INTERCELLULAR ADHESION MOLECULE-1 TARGETED DRUG TRANSPORT ACROSS THE GASTROINTESTINAL EPITHELIUM

Rasa Ghaffarian, Doctor of Philosophy, 2015

Dissertation directed by: Associate Professor, Silvia Muro
Fischell Department of Bioengineering & Institute for Bioscience and Biotechnology Research

Contrary to systemic injection of therapeutics, oral formulations represent clear advantages to patients, healthcare systems, and pharmaceutical companies including safety, low cost and patient compliance. However, oral delivery remains a major obstacle due to (1) drug instability in the harsh environment of the gastrointestinal (GI) tract owing to low gastric pH and enzymatic hydrolysis; (2) low permeability through the mucus layer and subsequent adhesion to the GI epithelium; and (3) suboptimal transport into or across the GI epithelium- the cell barrier responsible for selective absorption of substances into the circulation, for local or systemic delivery. While encapsulation methods have been developed to overcome barriers to stability and adhesion to the GI epithelium, safe and effective transport into and across this lining has not yet been achieved for several drugs, especially biotherapeutics. Hence, our goal is to overcome these challenges for delivery of therapeutics (including biotherapeutics) via the oral route. For this purpose, we targeted drugs to intercellular adhesion molecule-1 (ICAM-1), a protein expressed on the GI epithelium and other

cell types. We previously demonstrated, that polymer nanocarriers (NCs) coated with antibodies to bind multiple copies of ICAM-1 (multimeric targeting) triggered uptake and transport across cultured GI epithelial cells, enabling intracellular and transcellular drug delivery. To implement this strategy *in vivo*, we successfully encapsulated antibody-coated NCs in chitosan-alginate microspheres for gastric protection of labile targeting antibodies, site-specific release in the intestinal environment (the site of drug absorption) and retention of targeting ability following release *in vitro*, in cell culture, and *in vivo*. Furthermore, to expand the utility of the ICAM-1 targeting approach, we explored a novel drug delivery system that binds only one to two molecules of ICAM-1 (monomeric targeting), which provides distinct advantages for oral drug delivery compared with multimeric strategies. In order to elucidate the advantages offered by this monomeric targeting approach, we compared the uptake and intracellular trafficking of ICAM-1 targeted monomeric antibodies vs. multimeric antibody-coated NCs in cultured endothelial cells, a commonly used cellular model to study ICAM-1 transport. We then revealed that the distinct itinerary of transport offered by monomeric ICAM-1 targeted antibodies led to enhanced uptake and transport across cultured GI epithelial cells, showing promise for oral delivery. Finally, in order to exploit this transport pathway for oral drug delivery, we conjugated a model drug cargo to monomeric ICAM-1 targeted antibodies, which was shown to endow drug targeting and delivery into and across cultured GI epithelial cells, while preserving the functional activity of the drug cargo. These findings demonstrate that monomeric vehicles serve as a viable alternative to multimeric strategies, expanding the range of oral delivery applications afforded by ICAM-1 targeting. Taken together, the work performed in this dissertation advocates the potential of ICAM-1 targeting strategies for improving oral absorption of therapeutics, and provides a foundation for studying these strategies *in vivo*.

INVESTIGATION OF INTERCELLULAR ADHESION MOLECULE-1 TARGETED DRUG TRANSPORT ACROSS THE GASTROINTESTINAL EPITHELIUM

By

Rasa Ghaffarian

Dissertation submitted to the Faculty of the Graduate School of the
University of Maryland, College Park, in partial fulfillment
of the requirements for the degree of
Doctor of Philosophy
2015

Advisory Committee:

Associate Professor Silvia Muro, Chair

Professor Srinivasa R. Raghavan, Dean's Representative

Professor Peter Kofinas

Professor Peter Swaan

Professor Xiaoping Zhu

Acknowledgements

First and foremost, I'd like to thank my advisor, Dr. Silvia Muro, for her guidance, encouragement, and trust over the years I've been here. I appreciate all of your relentless hard work that you put into mentoring me and my other lab mates. Thanks to you, I couldn't be happier with my progress as a professional and understanding who I am in the face of challenges. You pushed me to do outstanding work and succeed the many challenges that I never before believed I could do. As a result, you set me up for the opportunities that I've always dreamed of.

I would also like to thank all the members of the Muro lab, both past and present, including our post-docs, Carmen, Tridib, Viraj, Melani, and Edgar; graduate students, Daniel "Sir Rhino", Jason, Janet (aka Flanet), Rachel (aka Ray Ray), Zois (aka Poseidon), Jon; the undergraduate students, Maria, Jeff (aka Geoffrey), Deep, Josh, Austin, Peter, Ashwin, Hyunjo, Anna; and high school students, Michael and Meilin. You all have been so incredibly kind to me and supportive of who I am as a person, and I truly appreciate you making our lab such a warm and friendly environment. I couldn't have asked for better lab mates and friends.

I especially want to thank Daniel and Janet, my first true friends in grad school. I love Daniel for your quirkiness, drawings, genius, sense of humor, and the countless times you've helped me. I love you Flanet for your cuteness, sharing your baked goods, foodie adventures, being the glue that held all of the lab mates together, your advice, generosity, and hugs. Last but certainly not least, I'd like to thank my Ray Ray. I can't even begin to describe how much I respect, admire, and value you as a friend. You have been there to help me through some of the hardest times. I am constantly dumbfounded by your boundless generosity, hard work, resilience, grit, and your ability to stick to your values. Honestly, you are one of my greatest role models. Also, you are freaking

hilarious. I love you all, I don't know what I would've done without you. I hope to continue our friendships until old age. And I can't wait to see all the incredible things you will accomplish.

Bentley lab! You guys are awesome! Special thanks to DQ, Jess, Tanya, Amin, Naren, Hanna, Chelsea, Karen, Chen Yu, Hsuan Chien, for your amazing friendship and Plant Science partners in crime. I admire each and every one of your quirks, your creativity, your countless support, and passion for knowledge. You brought out the "good kind" of nerd in me, and made me feel welcome here. With that being said, I'd like to thank Dr. Bentley for fostering the creative, unique, kind, warm, collaborative, and spirited nature of his lab members. You are truly a great leader. Your lab and the department is so lucky to have you empowering them and allowing them to do great things. Lastly, I'd like to thank my girls, Jess and Tanya, for being my right-hand women, and DQ, one of the kindest, most selfless people I've ever met.

I also extend my appreciation to my thesis committee members, Dr. Raghavan, Dr. Kofinas, Dr. Swaan, and Dr. Zhu, who have taken the time and effort to guide my research in a positive direction. I especially thank Dr. Raghavan, who has served as a valuable mentor to me. Your class on the physical principles of nanotechnology was one of the best I've ever taken. It gave me so much insight and knowledge on how physics and biology are intertwined, how everything in nature is connected, which validated why I sought the transition from life sciences to engineering. You helped me bridge the gap between those two fields. In addition, without your intellectual contribution on polymers, my research on encapsulation strategies (Chapter 4 of this dissertation) would not have been possible. I'd also like to thank several of Dr. Raghavan's graduate students, including Hyuntaek (or "MacGyver" of graduate students), Chanda, Kevin, Jasmine, Anand, and Annie, for their intellectual contribution and warmly welcoming me into their lab.

I also want to thank my collaborators at the National Institute of Standards and Technology, Abraham Abouzeid and Wyatt Vreeland, for their intellectual contribution and lending me their time, effort, lab space, and fancy equipment to characterize my anti-ICAM-enzyme conjugates.

Without their help, my work on monomeric ICAM-1 ligands (Chapters 2 and 3 and their associated publications) would not have been completed.

To the professors and administrative staff in the Fischell Department of Bioengineering, especially Dr. Herold, Dr. Shah, Dr. Payne, Helim, Kim Stroka, Tracy, Dr. White, Dr. Hsieh, Theresa, and Debbie, thank you for your inspiring, warm, encouraging, and supportive attitude in creating such an amazing environment for grad school, treating me like an equal, and making me feel at home. You all are so cool, and I will miss our candid bonding over drinks! Special thanks to Dr. Herold, who like Dr. Raghavan, helped me to bridge the gap between biology and engineering and rekindled my love for math. You are also a great person with great intentions, and I appreciate all your help, support, and dry humor. I also want to especially thank Dr. Payne. I will miss your enthusiasm and warm greetings in the Plant Sciences hallway. Thank you so much for all of your advice and help about life and fellowships. Kim Stroka, you are an awesome woman and will continue to be my role model. I also want to thank Wendy, my lab Mom, for her warmth, support, and delicious baked goods.

To all of my friends I've made at College Park, Ting, Emily, Eric, Kevin, Sarah, Chinchu, Omar, Chris, Amin Alm, Patrick, Mohammad, Nariman, and Amir. Thank you for all the good memories and supporting me in times of need. Special thanks to my all my soccer buddies on and off campus, including those mentioned above as well as Sonia, Matteo, Adel, Luis, Michael Wiederoder, John Schardt, Shadi, Daniel, Johnny, Greg, and Nathan. Soccer is my biggest passion outside of work and has been a consistent source of stress relief throughout my life. Thank you so much for giving me the opportunity to play with you all, those experiences and connections, both on and off the field, meant so much to me.

Of course, my accomplishments would not have been possible without the unconditional love and support of my immediate family, Momzo, Dadzo, Benj, and Tara, and extended family, Mamoo, Uncle Fink, Nooshin, Maman Maimanat, Auntie Zahry, Auntie Pinthong, Dai Mamad,

Ashraf, Ted, Houri, Augusto, Navin, Kristen, Mona, Mina, Yoshi, and Ceyda. I especially want to extend my heartfelt appreciation to Momzo and Dadzo, who have established my sense of self-worth and integrity, made me who I am, and picked me up over and over again without any hesitation. Their selflessness in sacrificing all that they had to give me better life, to ensure my freedom, education and exploration of my interests, has not gone unnoticed. My achievements, including this dissertation, and more importantly, my happiness, is largely due to them.

Last but oh my goodness definitely not least, my dear love, Jonathan Kim aka Mouse. Where do I even start? You have been THE most incredible person I've ever met: selfless, mature, kind, understanding, open-minded, generous, warm, "geneeus," perceptive, freaking hilarious, weird (in the best way possible), fun, quince, sqwaad, beautiful in and out. I love your integrity and that you stick to your values, that you call people out when they are wrong, that you bring out the best in me, and that you make this world worth living in. You are the first person who has loved me for literally ALL that I am, much more than I could possibly love myself, and I can't thank you enough for all that you've done and how much you've allowed me to grow. I cannot wait to share more memories with you, whether it's outdoors (adventuring, camping, climbing, rafting, backpacking, snowboarding, jogging, and even mountain biking…perhaps….however), in the city, at home, enjoying each other one on one or with friends and family, I love it all. I can't wait to see what amazing things you'll accomplish in your life.

Table of Contents

List of Figures and Tables

Chapter 6

List of Abbreviations

α Gal .....α Galactosidase

Anti-ICAM.....Antibody targeted to intercellular adhesion molecule-1

AF4 .....Asymmetric flow field-flow fractionation

Amil. .....Amiloride

BSA.....Bovine serum albumin

Caco-2.....Human colorectal adenocarcinoma cells

CAM .....Cell adhesion molecule

EIPA .....5-(N-ethyl-N-isopropyl) amiloride

Fil......Filipin

FITC .....Fluorescein isothiocyanate

ICAM-1 .....Intercellular adhesion molecule-1

HRP .....Horseradish peroxidase

HUVEC .....Human umbilical vein endothelial cells

IgG.....Immunoglobulin G

^{125}I.....125-Iodine

LAMP-1 .....Lysosomal-associated membrane protein 1

LSD.....Lysosomal storage disorder

MALS .....Multi-angle light scattering

MDC .....Monodansylcadaverine

NC.....Nanocarrier

PBS .....Phosphate buffered saline

QELS.....Quasi-elastic light scattering

RI .....Refractive index

TEER.....Transepithelial electrical resistance

TxR.....Texas red

TNFα .....Tumor necrosis factor alpha

Wtm......Wortmannin

Chapter 1: Introduction and Overview

1.1 Problem Description and Motivation

Among the various routes of drug administration, oral delivery through the gastrointestinal (GI) tract, whereby tablets, capsules, or drops are taken orally, remains the most favorable [1]. Relative to parenteral, or injectable therapies, oral formulations present clear advantages to patients, healthcare workers, and pharmaceutical industries. Patients prefer oral forms for the convenience of self-administration, which allows a flexible dosing schedule and fewer healthcare appointments, and comfort of swallowing a drug relative to receiving an injection. Oral formulations also minimize costs to patients, healthcare workers, and manufacturers, since they can be formulated in bulk, and do not necessitate specialized personnel and sterilization procedures [1]. In addition, given that oral therapies do not necessitate sterility, they pose lower safety concerns associated with potential contamination and systemic infections [1]. As a result of these advantages, there is a substantial demand for making pharmaceuticals available in oral form. Indeed, oral formulations presently comprise 90% of all medicines and a USD $49 billion market (as of 2010), which represents over half of the total pharmaceutical market [1]. The market value of oral dosages is expected to grow by 10% each year [1]. Physiologically, the GI tract is relatively suitable for systemic absorption of drugs owing to its high surface area (500 sq. meters), dense vasculature, and significant blood perfusion supporting sink conditions [1].

Access to the systemic circulation via the oral route, or oral bioavailability, requires transport across the GI epithelial lining, a layer of cells responsible for selective absorption of nutrients and drugs from the GI tract into the systemic circulation [2, 3]. Yet, oral bioavailability is curtailed by a number of physiological barriers, including (A) premature degradation or deactivation by the low pH and proteolytic activity in the stomach, (B) suboptimal mucus permeation and subsequent adhesion to the GI epithelium, and (C) poor penetration into and/or across these cells for the treatment of disorders that affect the GI lining or those that require delivery into the circulation, respectively [2, 3].

While encapsulation, in hydrogels or drug vehicles for instance, has circumvented issues of gastric stability as well as have facilitated release and adhesion at the site of drug absorption [4, 5], transport of therapeutics into/across the GI tract that is both efficient and safe (i.e., maintains the integrity of the GI permeability barrier) has not yet been achieved for numerous drugs and drug vehicles. This is particularly the case for biotherapeutics, a rapidly emerging class of drugs composed of biological components, including monoclonal antibodies, peptide and protein hormones, enzymes, vaccines, etc. [3], designed to treat a number of autoimmune, cardiovascular, gut, metabolic, and neurological disorders and cancers [3]. Oral delivery of such therapeutics can be enhanced by active targeting strategies, which involves coupling drugs or their vehicles to targeting moieties, such as antibodies, peptides, sugars, and vitamins (see Fig. 1.1 below) [2, 6]. These targeting moieties recognize and bind to specific markers, such as transporters and receptors, on the GI epithelial cell lining, which not only improves adhesion to the GI epithelium, but may additionally enhance transport into and/or across cells by natural processes [2, 6]. Hence,

the **goal of this work** is to utilize active targeting strategies to improve absorption of therapeutics, particularly biotherapeutics, via the oral route.

1.2 Our Approach

Targeting of therapeutics can be achieved by: (A) direct conjugation of targeting ligands to the drug itself (drug conjugates), or by (B) coupling targeting ligands to the surface of drug-loaded nanocarriers (NCs) (Fig. 1.1) [7]. NCs are macromolecular vehicles composed of a variety of natural or synthetic biomaterials, which may be functionalized to optimize drug solubility, protection, biodistribution, release kinetics, metabolism, elimination, etc. for GI or systemic delivery [8]. Prominent examples of NCs include dendrimers, liposomes, metallic nanoparticles, micelles and polymer particles [8]. Both of these targeting strategies are valuable in that they may provide distinct advantages from a manufacturing and drug delivery standpoint. For example, ligand-drug conjugates constitute a less complex formulation and in most cases, better mimic ligands found in nature [7], while targeted NCs allow for high drug loading and control over the parameters noted above. Importantly, these strategies differ in targeting valency, or the number of binding interactions with cell-surface markers (Fig. 1.1). Drug conjugates often contain a single ligand that binds 1-2 markers (monomeric targeting), whereas NCs present multiple copies of ligands that bind 2 or more markers (multimeric targeting). The differences in such binding interactions typically trigger alternative itineraries of drug transport though the cell, the knowledge of which is essential to selecting an appropriate therapeutic application.

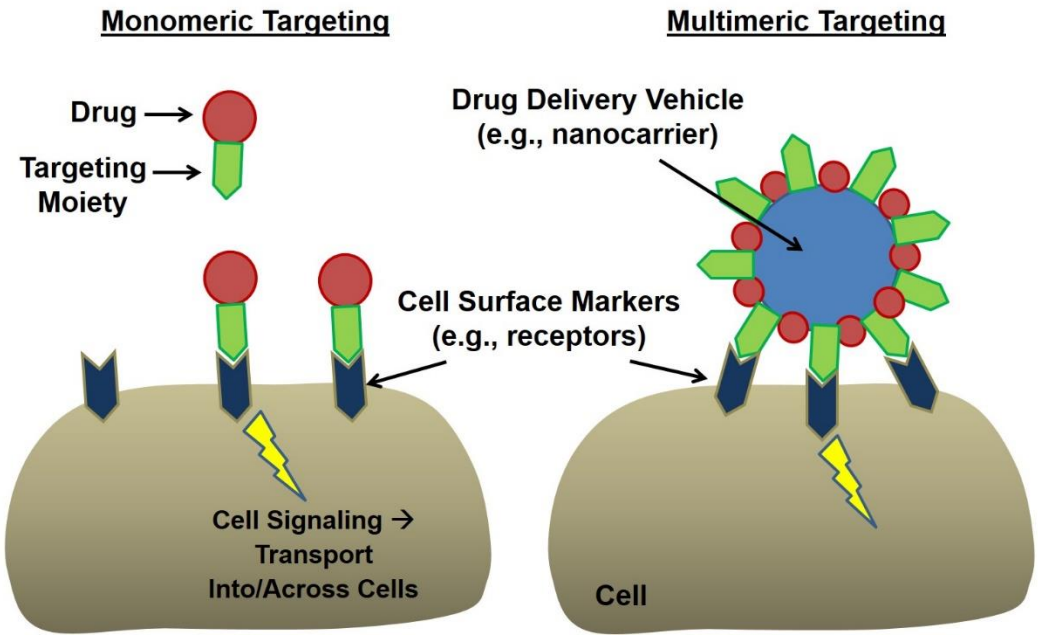

Figure 1.1. Monomeric vs. multimeric targeting strategies.

In this dissertation, we have focused on one such cell-surface marker, intercellular adhesion molecule-1 (ICAM-1) that triggers differential transport outcomes upon monomeric vs. multimeric targeting [9]. ICAM-1 is a transmembrane glycoprotein that is typically involved in the attachment and transmigration of leukocytes across cellular barriers [10]. ICAM-1 represents an attractive target for drug delivery in both the GI tract and other tissues accessed from the systemic circulation, as it is expressed on the GI epithelium and other epithelial cell types, vascular endothelial and immune cells, astrocytes and neurons, among others [10]. Another valuable feature is upregulation of ICAM-1 in pathological conditions, which promotes specific targeting to sites of disease [10, 11].

In a previous publication, we established the potential of ICAM-1 targeting for oral delivery into and across the GI epithelial cell barrier. This work employed a multimeric targeting approach consisting of coating multiple copies of an ICAM-1 targeted antibody

onto polymeric drug nanoparticles (anti-ICAM NCs; Fig. 1.2), which bind multiple ICAM-1 molecules [12]. Multimeric targeting to ICAM-1 on cultured GI epithelial and vascular endothelial cells induces a novel pathway of transport into and across these cells, referred to as cell adhesion molecule (CAM)-mediated transcytosis [13, 14]. CAM-mediated transcytosis is a non-classical avenue of transport that is independent of clathrin or caveolin [13]. Importantly, this pathway does not compromise cell barrier integrity, suggesting a safer means of oral delivery [13]. Hence, utilizing this multimeric targeting strategy provided significant delivery of a model therapeutic enzyme (α-Galactosidase, used for the treatment of Fabry disease) into and across GI epithelial cells [13].

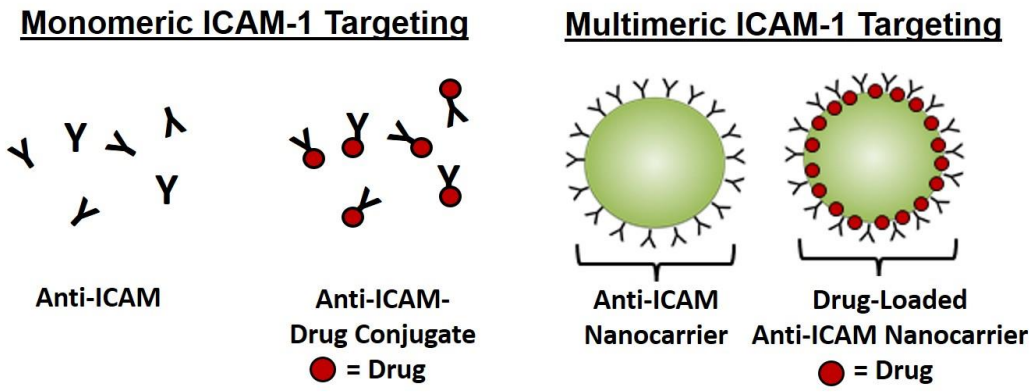

Figure 1.2. Monomeric and multimeric ICAM-1 targeting models.

A very important point to consider in designing an oral drug delivery system is the instability of many drug delivery vehicles in the acidic milieu of the stomach. In fact, although oral administration of anti-ICAM NCs in mice demonstrated the ability of these strategies to adhere to GI tissue [15], premature degradation of the targeted antibodies during transit through the stomach precluded the efficacy of this strategy by limiting intestinal biodistribution [15]. Hence it is necessary to effectively encapsulate ICAM-1 targeted systems in order to properly evaluate their oral delivery potential *in vivo*. Ideally,

encapsulation should provide: (A) protection of targeting moieties from gastric degradation; (B) site-specific release in the intestine, the main site of drug absorption; and (C) retention of targeting ability to allow ICAM-1 binding and subsequent transport into cells. For this purpose, we employed hydrogels, which are three-dimensional networks of natural or synthetic polymers [4, 5]. More specifically, we have chosen natural and biocompatible chitosan and alginate hydrogels, since they are well-established for their ability to preserve biological cargoes, including targeted antibodies, in the GI environment and provide pH-triggered release in the intestine [16, 17]. To meet the size requirements for oral gavage in mice, in this dissertation, we formulated chitosan-alginate microspheres loaded with antibody-coated NCs, which reflect our multimeric ICAM-1 targeting strategy that has previously demonstrated efficacy for oral delivery (Fig. 1.3) [13].

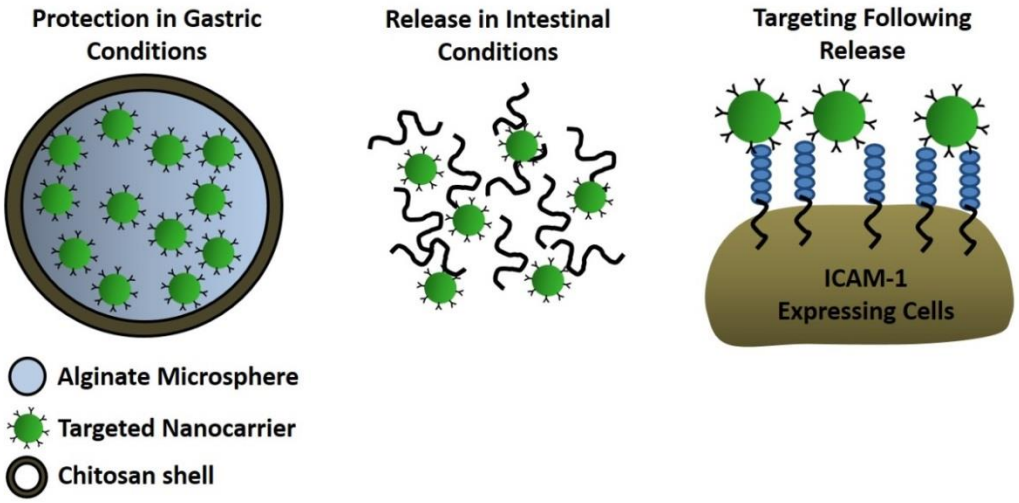

Figure 1.3. Requirements for encapsulation of ICAM-1 targeted nanocarriers.

In the case of monomeric ICAM-1 ligands, however, previous work demonstrating low cellular uptake precluded further characterization of transport by this strategy [9]. Herein, we evaluated, for the first time, the potential of monomeric ICAM-1 ligands as

alternative vehicles for drug delivery into and across GI epithelial cells, which would expand the range of oral delivery applications afforded by ICAM-1 targeting. As a model, we utilized single copies of antibodies against ICAM-1 (anti-ICAM; Fig. 1.2 shown above), which bind one to two ICAM-1 molecules, directly conjugated to an enzyme (drug cargo).

In light of previous literature supporting our research approach, we **hypothesized** that encapsulation of targeted NCs (i.e., antibody-coated NCs) in chitosan-alginate microspheres will provide protection of targeting antibodies in gastric conditions, release in intestinal conditions, and retention of targeting ability following release from microspheres. In order to determine the oral delivery potential of monomeric ICAM-1 targeting moieties as an alternative to multimeric targeting vehicles, we also **hypothesized** that, similar to anti-ICAM NCs, anti-ICAM and anti-ICAM-drug conjugates will provide binding, uptake, and transport across GI epithelial cells, and that this pathway provides an avenue for the delivery of active therapeutics. This hypothesis was evaluated with the following specific aims:

Specific Aim 1: Encapsulate ICAM-1 targeted NCs in chitosan-alginate microspheres for oral delivery.

- Sub-aim 1: Formulate and characterize chitosan-alginate microspheres loaded with targeted NCs (i.e., antibody-coated NCs).
- Sub-aim 2: Study protection of encapsulated targeted NCs from degradation in gastric conditions and pH-triggered release in intestinal conditions.

- Sub-aim 3: Evaluate degradation status and cellular binding of targeted NCs after release from microspheres.

Specific Aim 2: Assess targeting and cellular transport of monomeric ICAM-1 ligands.

- Sub-aim 1: Compare binding, uptake, and intracellular trafficking of anti-ICAM antibody vs. anti-ICAM NCs in vascular endothelial cells.
- Sub-aim 2: Quantify binding, uptake, and transepithelial transport of anti-ICAM antibody in GI epithelial cells.

Specific Aim 3: Evaluate monomeric ICAM-1 targeting for delivery of an active drug cargo into and across GI epithelial cells.

- Sub-aim 1: Formulate and characterize anti-ICAM antibody directly conjugated to a therapeutic cargo, using the enzyme horseradish peroxidase as a model.
- Sub-aim 2: Determine whether anti-ICAM-enzyme conjugates delivers and preserves the activity of enzymes into and across GI epithelial monolayers.

In achieving the above aims, this dissertation provided insight on ICAM-1-mediated transport across the GI tract and set the stage for future exploration of ICAM-1-targeted oral platforms in animal models, hence contributing to the future clinical translation of this approach.

1.2 Significance

As described in Section 1.1, oral delivery of drugs, particularly biotherapeutics, is restricted by (A) instability in the harsh environment of the GI tract due to low gastric pH and digestive enzymes in the stomach and small intestine, (B) poor transport through the mucus layer and/or adhesion to the GI epithelial barrier, and (C) suboptimal transport into and/or across this barrier for local GI interventions or delivery into the circulation [2, 3]. Whereas present strategies have effectively overcome the luminal barriers encompassing (A) and (B), safe and effective transport into/across the intestinal barrier remains unachieved for certain therapies, such as macromolecular biotherapeutics and drug vehicles [3]. Active targeting strategies, such as the example explored herein, are significant in that it may overcome these challenges to improve absorption of such agents via the oral route.

First, targeting therapeutics to specific markers on the GI epithelium has been shown to improve affinity to the cell surface (i.e. mucoadhesion), minimizing clearance from the body and improving biodistribution to the site of drug absorption [2, 3, 6]. This would ultimately reduce dosages needed for therapeutic efficacy. An example that shows particular promise in this regard is targeting drugs to ICAM-1. ICAM-1 is expressed on the apical surface of GI epithelial cells, allowing targeting to this tissue for oral delivery. Upon entering the systemic circulation, targeting ICAM-1 may also provide enhanced biodistribution to other cells that express this marker, including vascular endothelial cells on blood vessels, immune cells, various epithelial cells, neurons, etc. [10]. In addition, ICAM-1 is upregulated during inflammation [18], allowing specific targeting to diseased sites. This is the case for many gut pathologies, including infections, Crohn's disease, peptic ulcer, and GI cancers [19-22]. Moreover, utilizing anti-ICAM antibodies as a model

targeting moiety, either free in solution or bound to drug NCs, may improve permeation through hydrophobic mucus in light of their high charge density, yet neutral net charge [23].

Targeting drugs to certain markers also triggers transport into and/or across the GI epithelium, which is significant for treating intracellular GI pathologies or providing entry into the systemic circulation [2, 3]. We have previously shown that targeting to ICAM-1 triggers a non-classical pathway of transport into and across GI epithelial cells [13]. ICAM-1 mediated transport is valuable because unlike classical modes of cellular transport that are selective to carrier geometry, the CAM pathway accommodates drugs and drug carriers of various sizes (e.g., 100 nm to several μm), shape, chemistry, targeting valency, dose, etc. [9, 12, 24-34]. In addition, ICAM-mediated transport does not appear to breach the GI permeability barrier [13], whose function is to prevent non-specific transport of pathogens and other undesired substances into the body. Therefore, ICAM-1-targeting could provide a novel opportunity for safe transport across the GI epithelium. The proposed work is also expected to provide mechanistic insight about transport, particularly non-classical pathways, in the GI and other cell barriers (e.g., the blood-brain-barrier), an important yet unanswered question in cell biology. This information would also allow for the design of more effective therapeutics with the ability to access target sites restricted by such barriers.

By exploiting such transport, ICAM-1-targeted systems have been used for effective delivery of various imaging and therapeutic agents in cell culture and animal models [9, 25-28, 31-35], particularly biotherapeutics [25, 27, 30, 31, 36-38]. While these applications were intended for intravenous administration, the research proposed herein will, for the first time, advance the translation of such applications for oral delivery. Among

the biotherapeutics explored by our group for ICAM-1-mediated delivery, replacement enzymes for lysosomal storage disorders (LSDs) including α-Galactosidase (α-Gal) for the treatment of Fabry disease has been a large focus [25, 27, 30, 31, 36-38]. Current therapy involves frequent injections from an early age and costs ~150K per year [39]. Manufacturers, healthcare systems, and patients would greatly benefit from oral forms of these enzymes, yet no strategies exist for delivery into and across the GI tract for local and systemic treatment. ICAM-1-targeted NCs have shown promise in resolving this issue, as demonstrated using α-Gal as a model enzyme [13]. The significance of using enzymes as a model biotherapeutic for our targeting strategies is an attractive and novel application to treat LSDs via the oral route.

While ICAM-1 mediated drug delivery into and across cells has been demonstrated using multimeric targeting strategies, such as anti-ICAM NCs, this dissertation examines drug delivery by monomeric ICAM-1 targeting moieties (i.e., single anti-ICAM molecules). The significance of utilizing monomeric drug carriers with a different targeting valency is to provide alternative drug delivery outcomes, such as loading, biodistribution, intracellular trafficking, transport across cells, etc. A wider range of therapeutic applications can thus arise from studying both monomeric and multimeric anti-ICAM as oral drug carriers.

Mice studies by our group revealed that multimeric anti-ICAM NCs administered orally without protective coatings were degraded by gastric enzymes and retained in the stomach tissue due to premature targeting [15]. Encapsulation, in hydrogels and NCs for instance, has circumvented issues of stability, solubility, mucus permeation, and release in the GI tract [4, 5, 40, 41]. Encapsulation of ICAM-1-targeted platforms in chitosan-alginate

capsules would serve as the first attempt to preserve their activity in the stomach and provide release in the intestine, a suitable target due to high absorptive capacity. Characterization of an encapsulation strategy is significant for future translation of these targeting strategies for oral delivery *in vivo*.

1.4 Innovation

Ligands that have been used to target biotherapeutics to receptors in the GI tract include lectins, toxins, viral haemmaglutinins, invasins, transferrin, and vitamins [3, 6, 42-44]. A recent publication by our group revealed for the first time the potential of targeting ICAM-1 on the GI epithelium for oral drug delivery [13]. While this study employed multiple copies of ICAM-1-targeted antibodies coated onto drug NCs, the opportunity to target therapeutics directly conjugated to single antibody molecules has not been explored for oral delivery. Characterization of this strategy, using monomeric anti-ICAM as a model, is important because, compared to multivalent counterparts, it provides a simpler formulation method and can endow drugs with different delivery features, such as loading, targeting and biodistribution, intracellular trafficking, metabolism, clearance, etc., which may be better suited for certain therapeutic applications.

Intravenously injected antibodies and antisense nucleotides were previously used to target ICAM-1 on vascular endothelial cells in the gut to neutralize its involvement in gut pathologies such as inflammatory bowel disease [45]. However, ICAM-1 has not been exploited for the purpose of delivering therapeutics into and across the GI epithelium for the treatment of GI disorders and/or diseased tissues accessible from the systemic

circulation. While, classical clathrin- and caveolin-dependent endocytosis and transcytosis have been described fundamentally and in the context of oral delivery [6, 46], our previous study utilizing anti-ICAM NCs was the first observation of a non-classical, CAM-mediated pathway providing such transport in cultured GI epithelial cells [13]. It was also the first documented instance of CAM-mediated transcytosis in any cell type. Thus, our work involving characterization of anti-ICAM uptake and trafficking in vascular endothelial and GI epithelial cells (Aim 2) will for the first time, evaluate the potential of this strategy as an oral drug vehicle as well as elucidate the role of valency and size of targeting agents on CAM-mediated transport and GI transport in general. Moreover, the ability of ICAM-1-targeted strategies to preserve the activity of drug cargoes during transit through GI epithelial cells (Aim 3) has not yet been performed, and will provide insight for both fundamental knowledge of CAM-mediated transcytosis and future translation of these approaches for oral delivery.

Encapsulation of ICAM-1 targeted platforms for protection in transit through stomach and release in the intestine also has yet to be characterized. While chitosan-alginate capsules have been previously used for oral delivery applications involving large biological entities, such as proteins, antibodies, cells, etc., [47-49], applications involving targeted NCs have not been explored. In Aim 1, characterization of loading, protection, and release of targeted NCs, and the effect of encapsulation on the integrity of targeted NCs, are novel outcomes.

Therefore, the research performed herein is innovative because targeting ICAM-1 on the GI epithelium, using single or multiple copies of antibodies, has not been explored to improve the bioavailability of oral therapeutics. The outcomes of our specific aims are

novel in terms of advancing these strategies for future pre-clinical studies. Overall, the findings of this dissertation can elicit positive impact and advancement in the field of epithelial transport and its drug delivery applications for GI and systemic disorders.

Chapter 2: Background

2.1 Targeting Therapeutics to the Gastrointestinal Epithelium

As described in Section 1.1, oral delivery through the GI tract is the preferred form of drug administration by patients, healthcare workers, and pharmaceutical industries [1]. However, owing to the physiochemical nature of numerous drugs, there are no present solutions for safe and effective transport into and/or across the GI epithelial lining, the cell barrier responsible for selective absorption of substances into the circulation, for local or systemic delivery [2, 3]. As previously noted, active targeting is a promising strategy for overcoming these obstacles. Hence, the physiological and design principles underlying targeting strategies will be the focus of the following section.

2.1.1 Binding to the Gastrointestinal Epithelium

As noted above, one of the major challenges to oral drug delivery is poor attachment to the small intestinal mucosa, the innermost lining of the intestine exposed to the GI lumen which is responsible for absorbing ~90% of all ingested contents. The mucosa is divided into three sections: (1) the epithelium, which has protective and absorptive or secretory functions; (2) the lamina propria, a network of loose connective tissue, capillaries, and lymphatic vessels that carry substances transported across the epithelium to the systemic circulation; and the (3) muscularis mucosae, a double layer of inner circular and outer longitudinal smooth muscle. Within the mucosa, the GI epithelium serves as the interface between the luminal contents and the underlying circulatory vessels in the lamina propria (Fig. 2.1). Hence, it is essentially the barrier responsible for selective absorption of

nutrients (e.g., protein, carbohydrates, lipids, water, vitamins, and minerals) and drugs, while simultaneously excluding harmful substances, such as toxins and pathogens, from entering the circulation. [50]

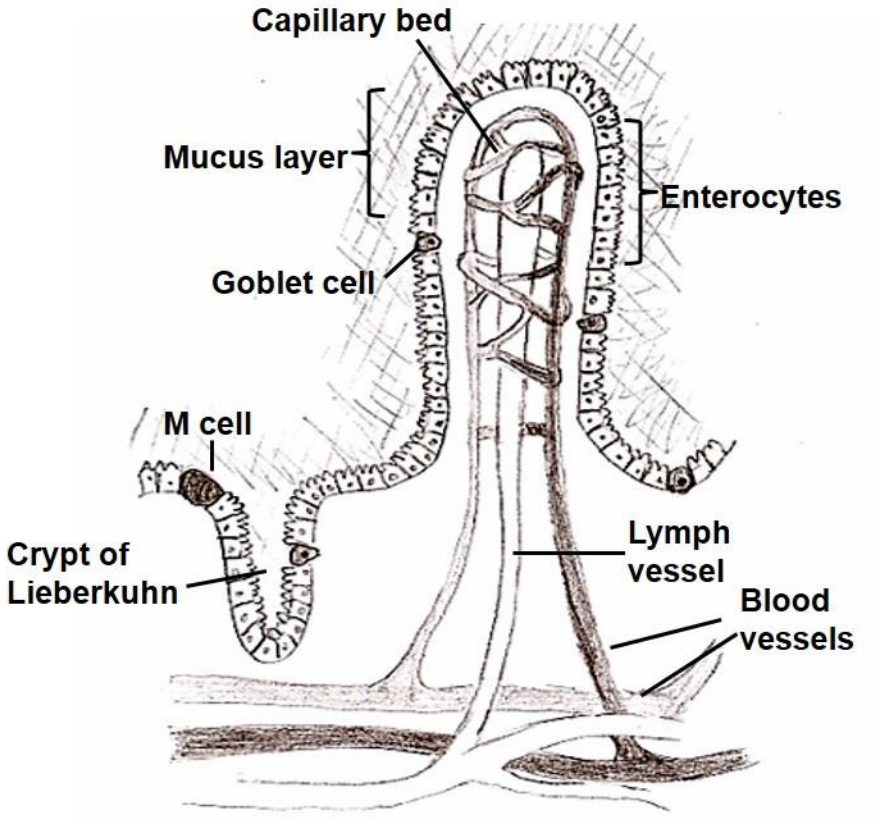

Figure 2.1. The gastrointestinal epithelium.

The epithelial lining is folded into large villi projections and invaginations (crypts of Lieberkühn), maximizing the absorptive surface area of the intestine. Within the lining are mainly columnar epithelial cells referred to as absorptive enterocytes, and less populated secretory cells, such as goblet cells, which secrete mucus into the lumen, and bicarbonate-secreting cells, which serve to neutralize stomach acid. A minor portion of the GI epithelium also consists of M cells or microvilli-lacking immune cells that deliver antigens from the lumen to underlying lymphatic system [50]. Absorptive enterocytes

present several distinctive features upon differentiation that are geared for nutrient and drug absorption: the apical membrane or brush border contains numerous folds, or microvilli, as a means of increasing surface area in contact with the intestinal lumen, as well as hydrolytic enzymes and transporters/receptors embedded in the membrane to breakdown essential nutrients and transport them into cells [50]. The basolateral membrane facing the abluminal space, containing underlying capillary and lymphatic networks, lacks microvilli and contains different types and amounts of transporters to maintain ionic concentration gradients used to drive transport. Due to the distinction between the apical and basolateral cell surfaces, enterocytes are referred to as polarized cells. In addition, the lateral membrane connecting adjacent epithelial cells is also responsible for regulating the permeability barrier. Within this lateral space, restricted passage of luminal substances is regulated by the (A) the tight junctions, a branching network of sealing strands mainly composed of the proteins occludins and claudins, and (B) anchoring junctions known as adherens junctions, which maintain cell-cell adherence by linking transmembrane proteins on adjacent cells to the cytoskeleton. [50, 51]

Binding to the intestinal epithelium, which increases residence time for absorption, is precluded by poor penetration of drugs through the mucus layer overlying epithelial cells as well as suboptimal affinity to the epithelial surface. Regular shedding of the mucus layer results in clearance and elimination of entrapped drugs, lowering biodistribution to the intestine [2, 3]. Another factor limiting binding is clearance by phagocytic immune cells present in the small intestine [2, 3]. Endowing therapeutics with specific affinity to the GI epithelium (i.e., active targeting) has shown much success for overcoming these obstacles [2, 6]. Active targeting is achieved by conjugation of therapeutics to natural ligands (e.g.,

vitamins, sugars, amino acids, lectins, etc.), other affinity molecules (e.g., antibodies, antibody fragments, peptides, aptamers, etc.), or molecules derived from pathogens (e.g., toxins and viral hemagglutinins) that bind specifically to membrane transporters and receptors on the apical surface of GI cells [2, 7, 52, 53]. Common markers that have been exploited for this purpose include transporters for amino acids, glucose, and vitamins, as well as receptors that bind transferrin, vitamin B12, lectins, toxins, and viral hemagglutinins [2, 3, 6, 42, 44, 54-56]. Transmembrane receptors of the immunoglobulin superfamily, such as integrins, cell adhesion molecules, and cytokine receptors have also been explored for targeted therapies aimed at treating GI disorders, as they are overexpressed in inflammatory conditions [45, 57, 58]. Molecular recognition and binding to these markers enhances biodistribution to the intestinal lining. This increases the residence time at the site of absorption and reduces the likelihood of clearance and excretion from the GI tract, which ultimately minimizes the effective dosage required for therapy and potential drug toxicity [3, 6, 42, 44].

2.1.2 Transport Into and Across Gastrointestinal Epithelial Cells

In addition, targeting to markers on the GI epithelium not only enhances intestinal biodistribution, but may also trigger transport into these cells, a significant requirement for treating intracellular pathologies, such as those affecting the GI epithelium itself, and/or across cells for delivery into the systemic circulation [2, 3]. As shown in Fig. 2.2, there are four main mechanisms of transport of nutrients/drugs from the apical space to the basolateral space: the (A) transcellular routes, whereby substances cross the cell body, include (1) passive diffusion, (2) carrier-mediated transport (facilitated and active), and (3)

transcytosis, whereas (B) paracellular transport takes place between adjacent cells [2, 3, 51].

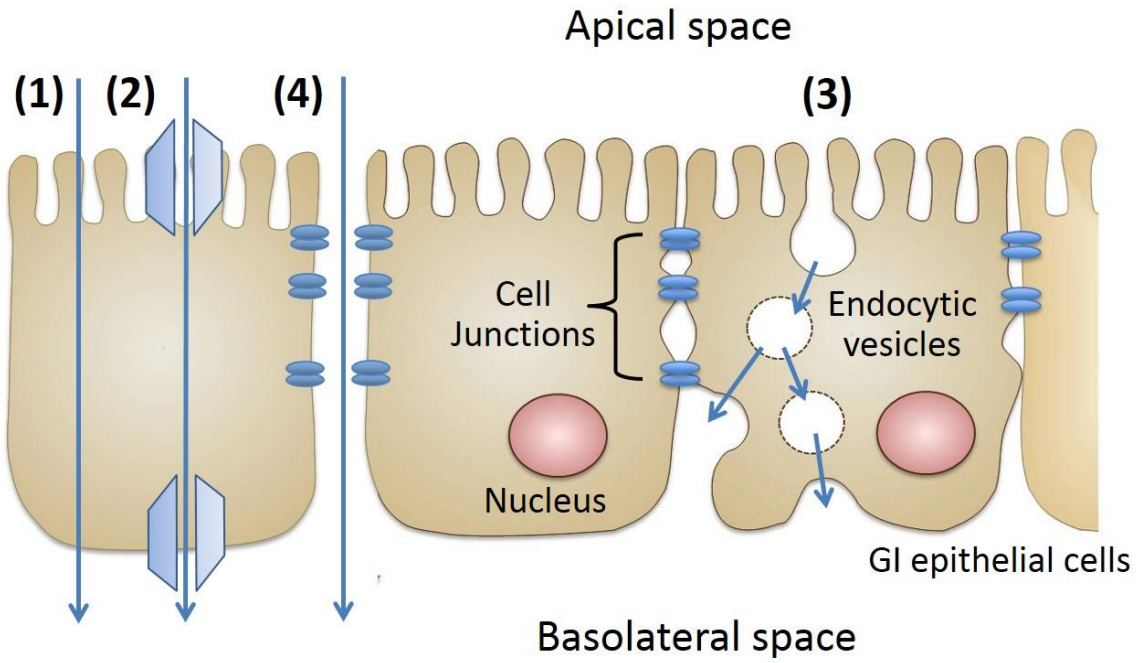

Figure 2.2. Mechanisms of transport across gastrointestinal epithelial cells. (A) Transcellular routes of transport, which involve passage across the cell body, include: (1) passive diffusion, (2) carrier-mediated transport (facilitated or active), and (3) transcytosis. Alternatively, (B) the paracellular route involves transport through the junctions between adjacent cells.

2.1.2.1 Passive Transcellular Diffusion

In passive diffusion, small solutes, such as water, gases, ethanol, and lipids, diffuse across the apical and basolateral membranes as a result of a concentration gradient. Drugs employing this pathway must exhibit a similar small size and certain degree of hydrophobicity, allowing permeation through the phospholipid bilayer of cell membranes [59]. A predictive measure of hydrophobicity may be represented by a drug's partition coefficient, or log *P*, which is a ratio of a concentrations in a mixture of two immiscible

solvents (hydrophobic and aqueous) [59]. The optimal range of log *P* for passive diffusion of these drugs lies between -1 and 3.5 [59]. Therefore, large, hydrophilic drugs, such as biotherapeutics, cannot innately undergo this pathway. Enhanced transcellular permeability of these compounds has been achieved using agents that enhance membrane fluidity, such as surfactants, bile salts, and fatty acids and their derivatives [3, 60-63]. However, a major drawback of these absorption-enhancement agents is that they are non-specific, and in turn risk importing toxins, allergens, or pathogens that may reside in the GI tract, along with the drug of interest, into the bloodstream [3, 63]. Furthermore, modulating membrane fluidity of the GI epithelial barrier often cause cytotoxicity, inflammation, and mucosal damage [3, 63]. Moreover, although passive diffusion is an efficient mode of transport, the rate of diffusion cannot be well regulated. Targeting of therapeutics to markers involved in the transport pathways described below, on the other hand, may offer greater regulation of transport into and/or across the GI epithelium.

2.1.2.2 Carrier-Mediated Transcellular Transport

Facilitated, carrier-mediated transport is another passive mechanism, as it is driven by a concentration gradient, which relies on membrane transporters on the apical and basolateral membranes to carry small polar compounds that are membrane-impermeable, including amino acids, oligopeptides, mono- and disaccharides, micronutrients (e.g., water-soluble vitamins), nucleic acids, bile acids, monocarboxylic acids, and phosphates [51]. Active, carrier-mediated transport of these compounds also uses membrane transporters, yet is driven by ATP or coupled to H^+ or Na^+ transporters, to mediate transport against a concentration gradient [51]. As noted above, drugs may be targeted to these carriers on the

apical surface of epithelial cells, by coupling them to the said substrates that undergo facilitated and active transport. For example, a strategy that has shown much success involves targeting to the PepT1 transporter, which is specific to a wide range of substrates, but mainly di- and tripeptides [6, 64]. Derivatization of the parent drugs aclovir and enalaprilat, an ACE inhibitor, with substrates for PepT1 significantly increased their oral bioavailability [6, 64]. However, as a result of the size constraint required to access membrane transporters, this targeting strategy is limited to relatively small drugs. In addition, carrier-mediated transport is not limited to influx of drugs to the cell interior but is also responsible for efflux to the intestinal lumen, namely by the P-glycoprotein (P-gp) efflux transporter [6]. As a result, drugs that enter the cell by carrier-mediated transport may also undergo efflux by P-gp transporters, resulting in reduced oral absorption [2, 3, 6].

2.1.2.3 Transcellular Transcytosis

As opposed to transcellular diffusion and carrier-mediated pathways, transcellular transcytosis provides transport of bulky compounds, such as transferrin, vitamin B12-intrinsic factor complexes, immunoglobulins, globular proteins, lectins, and viral hemagglutinins [6, 46]. Binding to cell-surface receptors involved in this pathway triggers internalization of materials on the apical surface via membrane invagination (endocytosis), traffic of endocytic vesicles across the enterocyte, and exocytosis at the basolateral membrane [46]. The classical endocytic pathways include: (A) macropinocytosis, a mechanism allowing uptake of extracellular fluid into large micrometer size vesicles and mainly associated with cells of the immune system; (B) phagocytosis, a process also

utilized by specialized immune cells, which involves uptake of large particulate ligands via formation of large endocytic vesicles called phagosomes; (C) clathrin-mediated endocytosis, the major route of endocytosis in most cell types, which is triggered by binding of specific ligands to their receptors in the plasma membrane, leading to internalization of extracellular macromolecules along with extracellular fluid into vesicles coated by the cytosolic protein, clathrin (clathrin-coated pits); and (D) caveolae-mediated endocytosis, a mechanism used by many cell types, characterized by uptake of materials into flask-shape vesicles enriched with the protein caveolin-1, which occurs in areas of the plasma membrane concentrated with cholesterol and glycolipids [6, 51, 52, 65].

In many cases, these uptake pathways determine the subsequent intracellular trafficking of the internalized materials. Macropinocytosis, phagocytosis, and clathrin-mediated pathways generally deliver materials via endosomes to lysosomes for degradation, whereas caveolae-mediated endocytosis delivers materials to various compartments including the cytosol, the Golgi complex, and the endoplasmic reticulum, in addition to lysosomes [51, 52, 65, 66]. Importantly, both clathrin- and caveolae-mediated endocytosis can transport materials across cells via transcellular transcytosis [6, 46]. However, classical endocytic pathways exploited by current targeting strategies may be sub-optimal in that they undergo non-specific uptake, as in the case of phagocytosis and macropinocytosis, or are restricted to ligands typically <100 nm, as in the case of clathrin- and caveolae-mediated endocytosis. Non-classical endocytic pathways that are independent of clathrin pits and caveoli may also trigger transcytosis [13, 46], yet these pathways are less understood from a mechanistic and drug delivery standpoint.

Targeting to receptors involved in transcytosis has shown significant promise for enhanced oral delivery of high molecular weight drugs and drug carriers that do not meet the size restrictions for carrier-mediated transport, such as numerous peptide and protein therapeutics and their delivery vehicles [2, 6]. Notable examples include targeting drugs to vitamin B12 and transferrin receptors, which results in clathrin-mediated endocytosis and transcytosis of the ligand-drug complex [6, 46, 67], and targeting to the folate receptor, which triggers caveolae-dependent vesicular transport [46, 68]. Another well characterized strategy is coupling of drugs or their vehicles to plant- or pathogen-derived lectins, such as wheat germ agglutinin, concavalin A, and tomato lectin, that bind to carbohydrate receptors on the apical cell membrane [3, 69]. Such binding has been shown to induce transport into and across GI epithelial cells by classical and non-classical vesicular pathways, depending on the type of carbohydrate receptor that is engaged [69].

2.1.2.4 Paracellular Transport

On the other hand, the paracellular pathway involves transepithelial transport of molecules across the aforementioned junctions that interlock adjacent epithelial cells. For instance, small and hydrophilic compounds <200 Da may diffuse through small pores (~4.5 Å) of tight junctions. Passive diffusion via the paracellular route also depends on other physicochemical properties, such as molecular dimension and overall ionic charge [70, 71]. For example, anionic peptides with α-helix conformation are transported to a significant extent, while β-sheet conformers of the same peptide do not [72]. Therefore, the ability of drugs to adopt a flexible conformation may bypass size constraints for paracellular diffusion. Moreover, similar to passive transcellular diffusion, paracellular diffusion of

substances is difficult to regulate. Alternatively, paracellular transport can be induced by disturbance of intercellular junctions, leading to the passage of macromolecules from the lumen [73]. The latter phenomenon can be induced by targeting to certain cell-surface receptors, such as those that bind cytokines, toxins, and pathogenic factors [73, 74], which in turn, cause cytoskeletal changes that regulate opening of epithelial junctions [73]. Another strategy for this purpose is co-administration of reagents to enhance paracellular transport of drugs, including calcium chelators and cationic and anionic polymers used for drug delivery [3]. However, similar to the strategies described above for enhancing passive transcellular diffusion, prolonged modulation of epithelial junctions may compromise barrier integrity in that it leads to non-specific passage of undesired materials across the mucosa. Hence, the specificity of carrier- or receptor-mediated transcellular mechanisms may offer a safer and more controlled route of oral absorption.

In summary, targeting therapeutics to membrane transporters and endocytic receptors that mediate transcellular and paracellular transport may provide: (A) improved biodistribution to the GI epithelium, the site of drug absorption; and (B) delivery into and/or across this barrier, valuable for interventions aimed at treating the lining itself or entering the systemic circulation for treating tissues beyond the GI tract. While paracellular transport is indiscriminate in its passage of substances, risking entry of pathogens, the specificity of transcellular pathways to the drug of interest may better maintain the permeability barrier and allow greater regulation of transport. Moreover, relative to carrier-mediated transport, receptor-mediated transcytosis is less restrictive in terms of the size and chemistry of drugs that may employ these pathways. In addition, the cellular fate of receptor-mediated transcytosis, including the kinetics and destination of transport, largely

depends on the design of the targeted systems. For example, transport parameters are influenced by the type of receptor targeted as well as the number of receptor-ligand engagements during binding, which we will describe in more detail in the following section. In light of the flexibility of receptor-mediated pathways, and the ability to better regulate delivery outcomes, the work herein explores this avenue for improving oral drug delivery.

2.2 Targeting of Drug Conjugates vs. Drug-Loaded Nanocarriers

Targeting of therapeutics can be achieved by (A) direct conjugation of targeting ligands to the drug itself (drug conjugates), or by (B) coupling targeting ligands to the surface of drug-loaded NCs. NCs are macromolecular nano-assemblies fabricated from a variety of biocompatible materials, designed to carry therapeutic agents by encapsulation or surface-loading [8, 41]. Functions of nanocarriers include solubilization of hydrophobic drugs, protection of drugs against premature inactivation and en route to the target, optimization of a drug's pharmacokinetics (including circulation and tissue distribution), control of drug release kinetics, and control of drug metabolism and elimination [8, 41]. A great diversity of NCs has been designed with this purpose, including (but not restricted to) nanotubes and other carbon nanostructures, branched dendrimers, phospholipid liposomes, and amphiphilic polymers formulated as self-assembled micelles or polymer particles (Fig. 2.3) [8, 41].

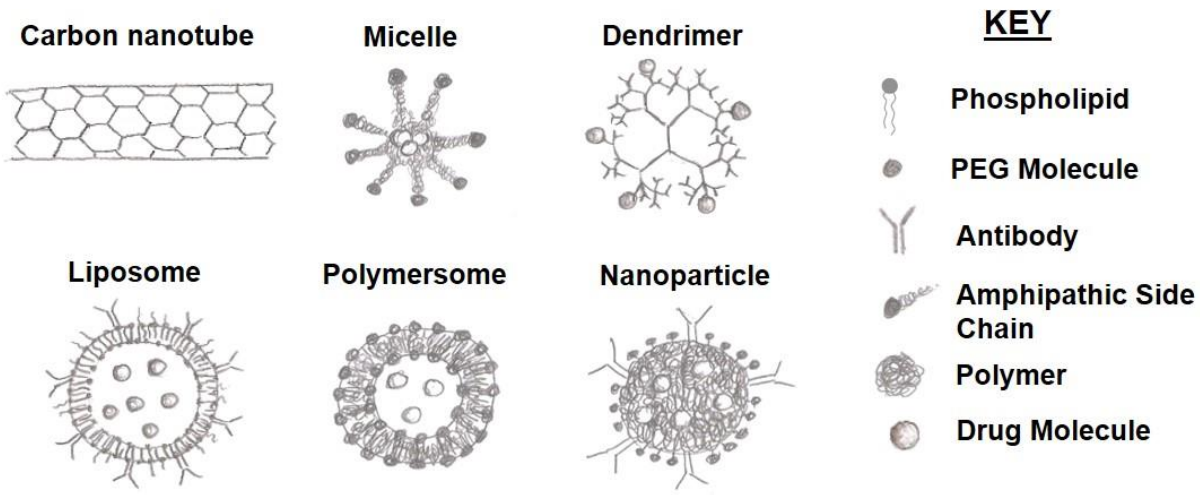

Figure 2.3. Nanocarriers for drug delivery.

Dendrimers are the smallest of NCs, with a diameter of only a few nanometers, yet their extensive branching allows for high drug loading [75-78]. However, their small size makes it difficult to control their passive diffusion through tissues within the body, which may be an advantage or disadvantage depending on the application [76, 78]. Phospholipid-based vehicles, called liposomes, arguably represent the most extensively studied drug vehicles [8, 79]. Liposomes are highly unstable in the GI tract, as a result of degradation by low gastric pH, pancreatic lipases, and bile salts, as well as the circulation, due to uptake by macrophages in the reticuloendothelial system [8]. To prolong circulation time and lower side effects of immune activation, "stealth" liposomes have been formulated by surface-grafting of poly(ethylene glycol) (PEG) [80]. However, the stability of "stealth" liposomes is limited, given that they are unable to bear more than 15% PEG on their surface without destruction of the phospholipid membrane. Polymersomes, the polymer analog of liposomes, have overcome these limitations, as they are capable of handling up to 100% loading of PEG onto their surface, allowing for a more stable vesicle membrane and

prolonged circulation half-life of days as compared to hours for "stealth" liposomes [81, 82]. In addition, polymer nanoparticles can be designed to present varied shapes, sizes, and drug loading capacities, almost entirely modulated by the processing conditions used [83-85]. Once formed, they are the most stable of the NCs [83, 85]. Hydrophobic drugs can be incorporated into the polymer matrix during formulation, and hydrophilic drugs can be loaded into interior compartments during formulation or subsequently attached to the particle surface [83, 85].

Solid polymer nanoparticles served as model NCs in this dissertation, provided that they are capable of adsorbing hydrophilic targeting agents and therapeutics onto their surface, while retaining the stability of these components in physiological conditions [12-15, 27, 30, 31, 37]. As a result, this model provides ample targeting and subsequent endocytosis and intracellular trafficking in cell culture and *in vivo*, according to numerous studies by our lab [27, 30, 31, 37].

Both receptor-targeting conjugates and carriers are valuable drug vehicles, yet it is expected that they would significantly differ in their ligand-receptor interactions and, therefore, subsequent drug delivery outcomes, such as biodistribution, cellular uptake, intracellular trafficking, transcytosis, metabolism, and elimination [7]. In particular, different targeting outcomes are influenced by the valency of such ligand-receptor engagement: a small, monomeric drug conjugate typically involves interaction of one ligand with one receptor (or two if a divalent antibody is used), while larger, multimeric drug conjugates and NCs employ multiple copies of a ligand to engage multiple copies of a cell surface receptor [7]. Therefore, understanding the cellular fate of monomeric (one targeting ligand per drug) vs. multimeric (two or more targeting ligands per drug) targeting

systems is important in order to determine the efficacy of these strategies and the selection of suitable therapeutic applications, while also providing insight on the biological regulation of their cell surface receptors.

In addition to providing distinct physiological outcomes, monomeric and multimeric carriers may endow different formulation advantages and drawbacks. For example, monomeric ligand-drug conjugates constitute a simpler formulation that lack exogenous materials and processing steps in synthesizing NCs. Due to the reduced complexity of these systems, they better reflect natural ligands, and in turn, may minimize immunogenicity and toxicity. However, direct conjugation to drugs by physical or chemical means may compromise the structure and activity of drug compounds. Encapsulation into nanocarriers may help to preserve drug activity, as well as provide higher drug payload. In light of these varying benefits from the perspectives of manufacturing and therapeutic efficacy, it is worthy to evaluate the potential of direct conjugation and carrier methods in parallel, as we aimed to do in this work.

2.3 ICAM-1 Targeting for Oral Delivery

2.3.1 Targeting to the ICAM-1 Receptor

Among the various endocytic receptors targeted for drug delivery, extensive work by our lab has demonstrated that ICAM-1 is particularly favorable for circumventing various challenges encountered in oral and systemic drug delivery. Constitutive expression of ICAM-1 on the GI epithelium and various other cell types, including endothelial cells in large and small blood vessels, neurons, astrocytes, etc. allows enhanced bioadhesion to

these sites, as demonstrated by efficient binding of ICAM-1-targeted platforms in GI epithelial and endothelial cell cultures [12, 13, 31, 86] and biodistribution to various organs (e.g., heart, lung, and brain) in mice [9, 24, 25, 27, 31]. ICAM-1 is a transmembrane glycoprotein that contains 5 extracellular domains that extend out into the luminal space [10, 11]. For endothelial cells, this has been shown to provide access to drug delivery systems from the circulation even in conditions with high shear stress (i.e. rapid blood flow) [31, 87]. This may also be the case for the GI tract, which exhibits high shear from peristalsis and mucus turnover. Indeed, anti-ICAM and anti-ICAM NCs were able to target GI tissue *in vivo* to a greater extent than non-targeted counterparts [15]. In addition, ICAM-1 is overexpressed in many pathologies in light of its role in leukocyte binding and transmigration during inflammation [10], favorable for targeting sites of disease in the GI and other tissues. Indeed, moieties with affinity to ICAM-1, including peptides and antibodies and their fragments, are currently being explored as therapeutics and targeting agents for intervention against inflammation, immune disorders, cardiovascular disease, genetic and metabolic syndromes, and cancers, among other conditions, as evaluated in cell cultures, animal models, and clinical trials, and do not seem to induce adverse side effects [9, 25-27, 33, 36, 88-92].

2.3.2 CAM-Mediated Endocytosis and Transcytosis

As depicted in Fig. 2.4, binding of polymer carriers bearing multiple copies of ICAM-1-targeting moieties (multimeric binding) induces ICAM-1 clustering followed by uptake into cells by a pathway known as CAM-mediated endocytosis, which is distinct from the classical endocytic mechanisms described in Section 2.1.2.3 [12]. This phenomenon was

not previously observed for anti-ICAM antibodies in solution, which were shown to remain on the cell surface [9]. Carrier binding causes ICAM-1 to cluster in membrane domains that are enriched in sphingomyelin and Na^+/H^+ exchanger 1 (NHE1) [12, 93]. These domains promote recruitment of acid sphingomyelinase (ASM) from intracellular compartments to sites of NC binding. ASM hydrolyzes sphingomyelin into ceramide, a lipid involved in plasmalemma deformability and cytoskeletal reorganization [93]. Multimeric binding to ICAM-1 also initiates a signal transduction pathway that activates protein kinase C, Src kinase, and Rho-dependent kinase (ROCK). Along with ceramide production, these signals regulate the interaction of ICAM-1 with the cytoskeleton (e.g., through alpha-actinin and ezrin-radixin-moesin -ERM- proteins) and also help regulate the recruitment of other effectors to the plasma membrane, such as dynamin-2, which associates with the actin cytoskeleton to induce vesiculization and subsequent vesicle traffic [12]. Following internalization, ICAM-1-targeted NCs traffic to early and late endosomes, a process that takes 1-2 hours, during which the NCs dissociate from ICAM-1 and ICAM-1 recycles to the plasma membrane [92]. The NCs then arrive at lysosomes about 3 hours after internalization [92]. CAM-mediated endocytosis has been shown to pervade various cell types that express ICAM-1, including cultured vascular endothelial cells, GI epithelial cells, neurons, astrocytes, and fibroblasts, as well as vascular endothelial cells *in vivo* [12-14, 25, 36, 94].

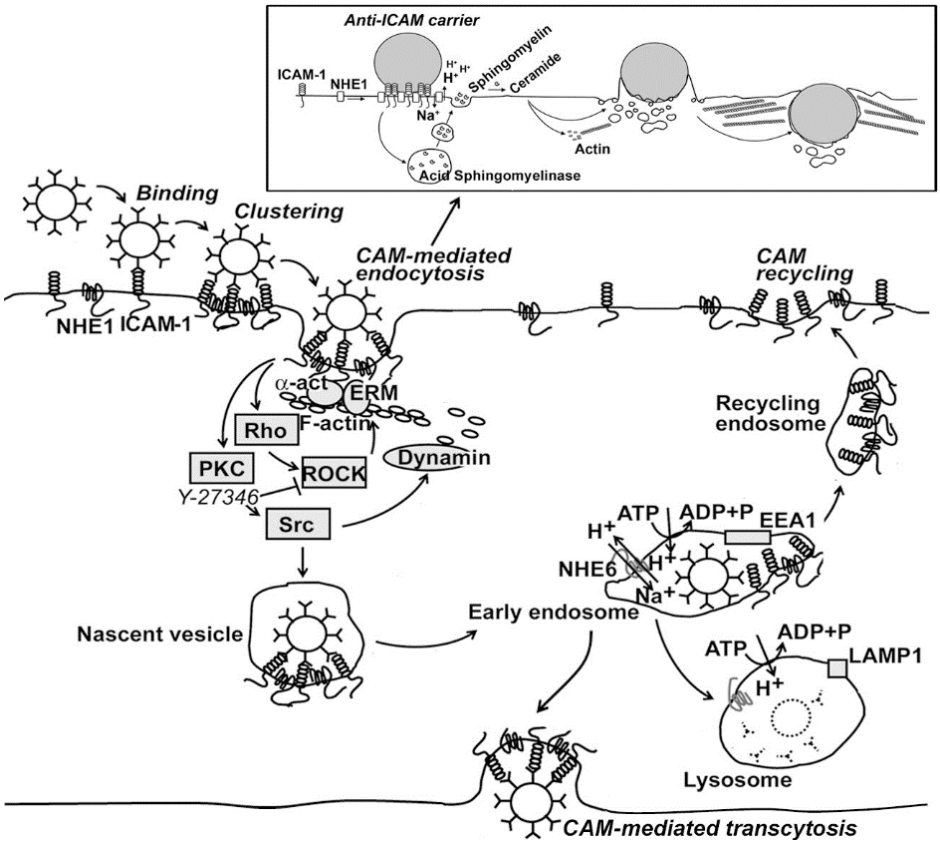

Figure 2.4. CAM-mediated endocytosis and transcytosis. Reprinted with permission [95].

Relative to classical endocytic routes, this pathway provides much flexibility in terms of internalizing carriers of different size (100 nm – 10 μm), shape, chemistry, targeting valency, and bulk concentration [24, 25, 27]. The kinetics of trafficking and subcellular destination can further be controlled by certain pharmacological agents and the size, shape, and targeting valency of carriers [24, 25, 91]. Fundamental characterization of CAM-mediated endocytosis and strategies for optimizing uptake and intracellular trafficking has allowed us to exploit this pathway for effective and precise intracellular delivery of various therapeutic and imaging agents, while preserving their functional activity [9, 25, 28, 30-32, 36]. Efforts by our lab have specifically focused on ICAM-1

mediated delivery of biotherapeutics for improving systemic delivery upon intravenous injections. Among the biotherapeutics studied for this purpose, delivery of replacement enzymes for the treatment of lysosomal storage disorders (LSDs) has shown much success over non-targeted counterparts, in terms of biodistribution to target organs in mice, as well as binding, trafficking to the target intracellular destination (lysosomes), and attenuation of disease symptoms in cell culture [30, 31, 36]. As a result of these promising results, our subsequent studies, including the work shown herein, evaluated the potential of this strategy for oral delivery of enzymes as a model therapeutic.

In addition to providing intracellular uptake, ICAM-1 has been shown to mediate transcellular transport of anti-ICAM NCs across an in vitro models of the GI epithelial and brain vascular endothelial barriers [13, 14]. Our results suggest this occurs by CAM-mediated transcytosis (Fig. 2.4) that does not lead to passive leakage of substances associated with the paracellular route. We also observed efficient transport of a model biotherapeutic enzyme, alpha-galactosidase (α-Gal), into and across GI epithelial cells [13]. These results show the promise of using ICAM-1-targeted platforms for oral delivery. In addition, the plasticity demonstrated in terms of the targeting valency in addition to the chemistry and size of carriers and cargo molecules that can efficiently use the CAM pathway over more restrictive vesicular mechanisms (e.g., clathrin, caveolar) [9, 12, 24-34], as described above, make this strategy particularly attractive to explore GI delivery using a variety of carrier formulations.

2.3.3 Potential for Oral Delivery using Monomeric Ligands against ICAM-1

Whereas previous literature alluded to minimal uptake of monomeric anti-ICAM by radioisotope tracing, precluding further characterization [9], recent findings utilizing fluorescence microscopy revealed that uptake of monomeric anti-ICAM is indeed significant (Chapter 5). Unlike multimeric ICAM-1-targeting strategies used in the past, this revealed a novel opportunity for oral delivery of agents directly coupled to single copies of ICAM-1-targeting moieties. Monomeric ligand-drug conjugates offer greater simplicity relative to anti-ICAM NCs, which could ultimately reduce manufacturing costs. As mentioned above, moieties that do not bear drugs bind to and neutralize ICAM-1, which demonstrated therapeutic efficacy and safety in clinical trials [45, 89]. Therefore, targeting by monomeric anti-ICAM may serve a double function by anchoring drugs to the GI mucosa to improve oral bioavailability and diminishing ICAM-1-involvement in pathology. In addition, as seen in previous literature and unpublished findings by our group, ICAM-1-targeting valency affects the mode of intracellular and transcellular trafficking [37]. Hence, anti-ICAM may provide alternative avenues of delivery that are more amenable to certain therapeutic applications than those provided by multimeric carriers. However, these avenues have yet to be fully characterized to understand the oral delivery potential of this strategy.

2.3.4 Need for Encapsulation of ICAM-1 Targeted Systems

To evaluate the potential of ICAM-1 targeting strategies for oral delivery *in vivo*, non-encapsulated anti-ICAM NCs were orally gavaged in mice [15]. Whereas this study

revealed targeting of these systems to GI tissue, the efficacy of these strategies was limited by gastric degradation, which in turn, curtailed intestinal biodistribution [15]. This prompted the need to encapsulate ICAM-1 targeted platforms to more accurately evaluate oral delivery *in vivo*. Encapsulation of anti-ICAM NCs was performed in this dissertation, since the efficacy of this system for delivery into and across GI epithelial cells has been previously demonstrated in cell culture [13]. As shown in Fig. 1.3 (Section 1.2), the main requirements of encapsulation would therefore be to provide protection of the targeting antibody from harsh gastric conditions, site-specific release of targeted NCs in intestinal conditions, and preservation of targeting ability following release.

2.4 Encapsulation for Oral Delivery

Whereas targeting of therapeutics may address various cellular barriers to oral delivery, such as mucosal adhesion and transport, the efficacy of these strategies *in vivo* is nevertheless limited by premature degradation or deactivation of labile drugs and targeting components, as in the case of ICAM-1 targeted systems. For instance, the low gastric pH and proteolytic enzymes of the stomach may prematurely deactivate, denature, or degrade drugs, particularly those that are protein-based or acid-sensitive [3]. In addition, therapeutics may experience changes in hydrophobicity, ionization, and aqueous solubility upon transitioning from low gastric pH to neutral intestinal pH, leading to potential destabilizing effects and/or suboptimal absorption [1]. The lumen of the small intestine, mainly the duodenum, as well as the brush border of enterocytes, also contains a variety of digestive enzymes responsible for drug degradation [3].

2.4.1 Hydrogels as Controlled Release Vehicles for Drug Delivery

The obstacles described above can be overcome by encapsulation in controlled release vehicles. Ideally, controlled release vehicles meet the following requirements: (A) protection of encapsulated contents from premature degradation/deactivation in the stomach, and (B) release at the site of drug absorption, with the most common site being the small intestine owing to its large absorptive capacity [4]. Encapsulation strategies may also provide controlled release, which entails maintaining the drug concentration within a therapeutic window over an extended period of time. This, in turn, minimizes the amount and frequency of dosages, and reduces potential toxicity and ineffectiveness associated with a rapid burst and fall of drug concentration, respectively [4].

Among the encapsulation materials used for this purpose, hydrogels offer significant potential for oral delivery in that they fulfill the essential requirements of controlled release vehicles [4]. Hydrogels are composed of hydrophilic polymers that are crosslinked by physical or chemical means to form three-dimensional networks entrapping a drug of interest [4]. They may employ one or more natural polymers which are biodegradable and biocompatible, such as alginate, chitosan, agarose, gellan, carrageenan, pectin, gelatin, etc., and/or synthetic polymers that can be tailored with desired biodegradability and functionality, including polyacrylic and polymethacrylic acids, PEG, and poly(vinyl alcohol) [4, 5, 16, 96]. These materials are also approved for commercial use [5]. A variety of processing methods allows flexibility in creating hydrogels of different size, shape, morphology, and other physical characteristics suiting the desired application. Many natural and synthetic hydrogel polymers, such as those listed above, are also

mucoadhesive, whereby they adhere to the mucus layer on the GI epithelium, thereby reducing the rate of clearance from the absorption site [4, 5, 16, 97].

2.4.2 Characteristics of Hydrogels for Oral Drug Delivery

2.4.2.1. Stability in Storage Conditions

When hydrogel networks are intact, they retain aqueous media from its surrounding environment. Hence, hydrophilic drugs, such as biotherapeutics, are likely to remain stable when loaded into hydrogels. The degree of drug loading and diffusion in or out of the hydrogel network is dependent on the chemical structure of polymers and mesh size, as determined by the density of a crosslinking agent [98, 99]. For instance, a higher crosslinking density limits the expansion of the polymer strands that contribute to swelling and drug leaching [98]. Mesh size also affects the physical properties of the gel, including mechanical strength and degradation, both of which affect stability in storage conditions [98].

2.4.2.2. Stimuli-Responsive Release

Hydrogels are also highly favorable for oral drug delivery because of their ability to respond to environmental changes in the GI tract that alter their structure, swelling, permeability, or mechanical strength, all of which contribute to controlling drug release [100]. In the context of oral delivery, responsiveness to stimuli allows hydrogels to protect therapeutics in storage and gastric conditions, and to provide release in the desired location

of the GI tract, e.g. the small intestine. Hydrogels have been designed to respond to various physical and chemical stimuli, yet those relevant for oral delivery mainly exploit the pH transition between the acidic environment of the stomach and neutral environment of the intestine [4, 101].

The pH-dependent properties of hydrogels often relies on the presence of ionizable pendant groups on the polymer chain [4, 16, 101]. Charged pendant groups impart electrostatic repulsion between the polymer chains, influx of water, and swelling and/or dissolution the network, leading to drug release [4]. Anionic pendant groups, such as those containing carboxylic acids (pKa ~3), remain neutral when the pH is below its pKa, and negatively charged when the pH is above its pKa [17, 102, 103]. The opposite is true for cationic pendant groups (e.g., amines), which are positively charged when the pH is below their pKa and neutral when the pH is above their pKa, amenable for release in the stomach rather than the intestine [101]. Since cationic polymers remain intact in neutral conditions, they are often incorporated with anionic polymers to prevent drug leakage in storage or provide a more controlled release pattern at intestinal pH [16, 47-49, 104-107]. The release kinetics of pH-responsive polymers can be further optimized by modulating the type and number of ionizable pendant groups as well as cross-linking density [101]. Moreover, since the strategies utilized to provide stability in storage also affect release patterns in the GI tract, optimization of these formulation parameters must be undertaken to satisfy both requirements.

2.4.3 Types of Hydrogels

2.4.3.1 Synthetic vs. Natural Hydrogels

Both synthetic and natural polymers offer pH-responsive properties, among other important functionalities for drug delivery. Engineering of synthetic polymers and their derivatives permits greater control and fine-tuning of these functionalities, yet their harsh processing conditions may compromise the integrity of loaded drugs, particularly biotherapeutics [4, 16]. Many synthetic hydrogels also lack biocompatibility and trigger adverse immune reactions in the body [16]. Although formulations consisting of natural polymers display lower mechanical stability and control of drug delivery parameters, advantages are that they are well characterized, biocompatible, and involve gentle and simple encapsulation methods for loading biological materials of diverse size, shape, and function [4, 17, 47-49, 105-109]. Their physiochemical properties are also more suitable for biological agents, as these polymers are derived from nature [4, 96]. For these reasons, natural polymers, namely alginate and chitosan, were utilized for the encapsulation of the therapeutic delivery platforms employed in this work. Nevertheless, no hydrogel system is ideal, and the benefits and drawbacks of each polymer type must be accounted for when selecting a drug delivery application.

2.4.3.2 Alginate Hydrogels

Alginate is a natural polysaccharide derived from brown algae. It is a linear, anionic copolymer comprised of 1→4 linked β-D-mannuronic acid and α-L-guluronic acid residues arranged in alternating or homopolymeric regions (Fig. 2.5A-B) [17]. It is

inexpensive, biocompatible, and biodegradable, justifying its widespread use in the food and pharmaceutical industries [17]. Dropwise addition of alginate containing a drug of interest into a crosslinking solution of divalent cations, such as Ca^{2+}, is a simple method that forms solid beads with a mesh size between 3 and 200 nm, amenable for entrapment of macromolecules [17]. Unlike covalent crosslinking methods, such as free radical polymerization, physical crosslinking by ionic interactions minimizes side reactions that may alter or deactivate the drug and avoids the need for loading after gel formation. Also, alginate microspheres can be formed at room temperature [17, 48, 49]. The gentle processing conditions associated with this encapsulation strategy has been widely used for efficient loading of labile biological entities, such as microbial and eukaryotic cells, globular proteins, antibodies, vaccines, etc., without compromising their structure or functional activity [16, 17, 47-49, 105-111]. This also demonstrates the flexibility of loading a wide range of size and structures. The presence of negatively charged carboxyl end groups confers other favorable qualities that improve biodistribution to the intestine and ultimately enhanced bioavailability of drugs. These include high mucoadhesion and pH sensitivity, whereby alginate beads shrink at low pH and dissolve at neutral or basic pH [16, 17, 48, 49, 105, 106, 109]. One caveat of unmodified alginate beads includes poor loading if the network mesh size is larger than the encapsulated content. Increasing the cation concentration may circumvent this issue and confer greater stability in terms of mechanical strength, yet only to certain extent [49]. Another problem is rapid dissolution of the alginate matrix at higher pH, leading to burst release in the intestine [16, 48, 49]. Hence, techniques for sustained release patterns are being studied for the purpose of optimizing drug absorption rates.

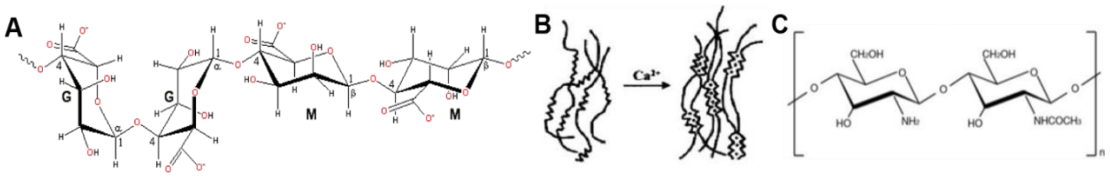

Figure 2.5. Alginate and chitosan hydrogels. (A) Chemical structure of alginate, a linear anionic polymer (pKa ~ 3.5) composed of guluronic (G) and mannuronic acid (M) residues arranged in consecutive or alternating order. (B) Consecutive G-blocks of alginate are crosslinked with Ca^{2+} in the form of egg box structures. (C) Chemical structure of chitosan, a linear cationic polymer (pKa ~ 6.5) containing D-glucosamine and N-acetyl-D-glucosamine residues.

2.4.3.3 Chitosan Hydrogels

To improve drug entrapment and control over release, alginate beads can be reinforced with a chitosan shell by addition of chitosan during or after bead formation [16, 47-49]. Chitosan is a natural polysaccharide produced by N-deacetylation of chitin, found in crustacean shells (Fig. 2.5C). Like alginate, chitosan is also widely used in the food and pharmaceutical industries owing to its affordability and biocompatibility among other features. The presence of positively charged amine groups within this copolymer, comprised of β-(1,4)-linked D-glucosamine and N-acetyl-D-glucosamine, form spontaneous electrostatic complexes with alginate and other anionic polymers [16]. In addition to providing greater mechanical stability and drug loading in alginate beads, chitosan swells and forms a hydrogel in acidic conditions. This helps to slow release of drugs from alginate matrices in intestinal conditions [49]. Chitosan is also a mucoadhesive agent, which prolongs residence time at the site of absorption [16]. This strategy also provides versatility for optimizing loading, stability, and release, for example by varying the capsule size, crosslinking density of the polymer core, thickness and crosslinking density of chitosan, type of polymer in the capsule core (e.g., alginate, gellan gum, xanthan

gum, carrageenan, etc.) [16, 48, 49, 96, 105, 106, 109]. As a result, chitosan alone or in combination with other polymers has been utilized for many applications, including oral delivery of various biological agents with high instability [16, 96].

Encapsulation in alginate and chitosan hydrogels has not previously been utilized for oral delivery of targeting systems, including ICAM-1 targeted systems. These systems may particularly benefit from this strategy due to the aforementioned advantages of these polymers, including gentle and simple encapsulation, protection in gastric conditions, release in intestinal conditions, and functional preservation of various labile materials, such as the targeting antibodies used herein [4, 17, 47-49, 105-109]. With these benefits in mind, the goal of this work was to encapsulate anti-ICAM NCs, which previously shown to target and traverse GI epithelial cells [13], in chitosan-alginate hydrogels for oral delivery *in vivo*.

Chapter 3: Materials and Methods

3.1 Reagents

Mouse monoclonal immunoglobulin G (IgG) against human ICAM-1 (clone R6.5) and rat monoclonal IgG against mouse ICAM-1 (clone YN1), herein collectively called anti-ICAM, were isolated from the respective hybridomas from ATCC (Manassas, VA, USA). Non-labeled mouse IgG, rat IgG, goat anti-mouse IgG, rabbit anti-human lysosomal-associated membrane protein 1 (LAMP-1), rabbit anti-HRP, as well as FITC- and Texas Red (TxR)-labeled secondary antibodies were from Jackson Immunoresearch (West Grove, PA, USA). HRP-conjugated secondary antibodies were from General Electric Healthcare Bio-Sciences (Pittsburg, PA, USA). Goat anti-human Rab11a was from Abcam (Cambridge, MA, USA). Green Alexa Fluor 488-labeled streptavidin, TxR dextran, blue Alexa Fluor 350-labeled secondary antibodies, and FluoReporter FITC Protein Labeling Kit® were from Invitrogen (Grand Island, NY, USA). Horseradish peroxidase (HRP) conjugation kit was from Innova Biosciences (Cambridge, UK). Green Fluoresbrite® 100 nm diameter polystyrene particles were from Polysciences (Warrington, PA, USA). Medium molecular weight chitosan (200-800 cps; 75-85% deacetylated), alginic acid sodium salt from brown algae (low viscosity), pepsin, and pancreatin were purchased from Sigma Aldrich (St. Louis, MO, USA). Protease inhibitor cocktail was from Thermo Scientific (Rockford, IL, USA). Simulated gastric fluid without enzymes (SGF) and simulated intestinal fluid without enzymes (SIF) were from Cole-Parmer (Vernon-Hills, IL). Reagents for gel electrophoresis were from Bio-Rad (Hercules, CA, USA). Chemiluminescent detection reagents for Western blot assays were from General Electric Healthcare Bio-Sciences, and autoradiography film was from Denville Scientific (South

Plainfield, NJ, USA). $Na^{125}I$ was from Perkin Elmer-Analytical Sciences (Wellesley, MA). Iodination tubes and tetramethylbenzidine (TMB) substrate for HRP was from Thermo Fisher Scientific (Rockford, IL, USA). Unless otherwise stated, all other reagents were from Sigma Aldrich (St. Louis, MO, USA).

3.2 Cell Culture

As a model of GI epithelial cells, we used human colorectal adenocarcinoma (Caco-2) cells, which were kindly provided by Dr. Jerrold Turner (Department of Biological Sciences, University of Chicago, IL). Cells were cultured in Dulbecco's Modified Eagle Medium (DMEM) (GibcoBRL, Grand Island, NY, USA) supplemented with 10% fetal bovine serum, 100 U/ml penicillin and 100 mg/ml streptomycin, and maintained at 37 °C, 5% CO_2 and 95% relative humidity. Cells between passages 4-5 were either seeded onto 12-mm^2 gelatin-coated coverslips in 24-well plates, or as shown in Fig. 3.1, onto transwell filter inserts (polyethylene terephthalate, 0.4-µm-pore size; BD Falcon, Franklin Lakes, NJ) at ~100,000 cells/cm^2. When indicated, cells were treated with 10 ng/ml tumor necrosis factor-alpha (TNFα; BD Biosciences, Franklin Lakes, NJ, USA) 16 h prior to assays to mimic an inflammation-like status, as it pertains to many diseases [13].

In the transwell system, the status of the cell monolayer was assessed by measuring the transepithelial electrical resistance (TEER) using an EVOM™ volt-ohm meter and STX100 electrodes (World Precision Instruments, Sarasota, FL). Confluent monolayers with TEER $\geq 230\ \Omega\times cm^2$ over background (16-21 days post-seeding), whose differentiated

status was previously verified by the presence of tight junctions and microvilli [13], were selected for experiments.

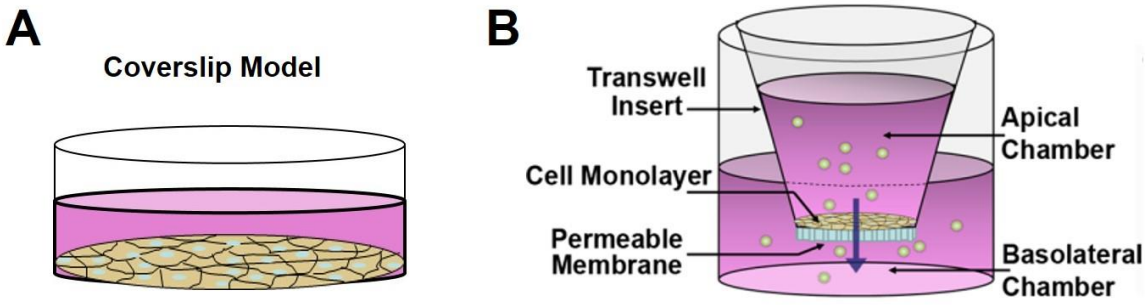

Figure 3.1. Cell culture models. (A) Cells cultured onto coverslips in 24-well plates. (B) Cells cultured onto transwell inserts for evaluating transepithelial transport from the apical chamber to the basolateral chamber.

Some mechanistic studies were also assessed in a model of vascular endothelial cells, i.e. human umbilical vein endothelial cells (HUVECs) from Clonetics (San Diego, CA, USA). This model was used due to its known ICAM-1 expression, which is relatively high, and previous experience in our laboratory testing targeting of anti-ICAM NCs on these cells [12, 31, 93, 112]. HUVECs were grown in M199 medium (GibcoBRL, Grand Island, NY, USA) supplemented with 15% fetal bovine serum, 2 mM glutamine, 15 mg/mL endothelial cell growth supplement, 100 mg/mL heparin, 100 U/mL penicillin, and 100 mg/mL streptomycin. Cell cultures were maintained at 37 °C, 5% CO_2, and 95% relative humidity. Cells between passages 4 and 5 were seeded onto 12 mm diameter gelatin-coated coverslips in 24-well plates and treated with 10 ng/mL TNF-α for 16 h to induce ICAM-1 expression, which is otherwise low in these cells [25, 113].

3.3 Iodination of Antibodies

Radioisotope labeling of antibodies with ^{125}Iodine (^{125}I) was done by incubating ~20 µCi of Na^{125}I and iodination tubes with 100 µL of 1 µg/µL protein for 5 minutes over ice. Free ^{125}I not bound to the protein was removed from the iodinated protein mixture through centrifugation (1000 × g for 4 min) in a 6 kDa cutoff gel size exclusion column (Biorad, Hercules, CA), which eluted only the iodinated protein. Prior to filtering the iodinated protein, the column was inverted several times to thoroughly homogenize the gel, then washed with 2 mL of phosphate-buffered saline (PBS), and packed by centrifugation (1000g for 1 minute). The concentration of the eluted iodinated protein was determined with a Bradford assay compared to known bovine serum albumin (BSA) concentrations. The amount of free ^{125}I remaining in the eluted iodinated sample was estimated by performing a trichloroacetic acid (TCA) precipitation assay by mixing 2 µL of iodinated protein with 1 mL of 3% BSA-PBS and 0.2 mL of 100% TCA to precipitate the iodinated protein. After a 15 minute incubation period at room temperature, TCA samples were centrifuged (2755 × g for 5 min) and the supernatant was measured for ^{125}I content using a gamma counter (2470 Wizard2; PerkinElmer; Waltham, MA). From this, the percent of free ^{125}I was determined and subtracted to estimate the specific activity, denoted as ^{125}I counts-per-minute (CPM) per µg protein.

3.4 Preparation of Model Antibody-Coated Nanocarriers

For the following monomeric and multimeric ICAM-1 targeting models, a well characterized monoclonal antibody to human ICAM-1 (R6.5) was used. As a NC model,

non-specific IgG or anti-ICAM were coated onto 100 nm diameter, green fluorescent (Fluoresbrite®) polystyrene particles to render IgG NCs or anti-ICAM NCs. Where indicated, antibodies were labeled with ^{125}I for quantification using a gamma-radiation counter. As previously described [30, 114], 5 μM antibody was incubated with ~10^{13} particles/mL for 1 h at room temperature to allow adsorption of the antibody on the particle surface. Non-coated antibody was removed by centrifugation at 13,800 × g for 3 min, and coated particles were resuspended at ~7 × 10^{11} NCs/mL in 1% BSA-PBS, and sonicated to remove aggregates [30, 114]. The hydrodynamic diameter of the resulting antibody-coated NCs was determined by nanoparticle tracking analysis (NanoSight LM10, Malvern Instruments, Westborough, MA), and the polydispersity index and ζ-potential were measured by dynamic light scattering (DLS; Zetasizer NanoZS90, Malvern Instruments, Westborough, MA, USA). In addition, the number of antibodies coated per particle was calculated using the equation below [30, 114]. The characterization of NCs is described in Section 4.2.1.

Antibody Molecules per NC = $[(CPM_{NC} / \text{Specific Activity}) / MW_{Ab}] * N_{avo}$

where CPM_{NC} are the ^{125}I counts-per-minute per NC, Specific Activity is the CPM/μg protein obtained using the protocol described in Section 3.3, MW_{Ab} is the antibody molecular weight, and N_{avo} is Avogadro's number.

Polystyrene particles were selected as a NC model because this material is not biodegradable and, hence, it allows us to evaluate degradation or protection of the antibody counterpart in extracellular conditions or during transport, without confounding effects of polymer degradation. Our previous works have shown that this model displays similar ICAM-1-mediated binding, endocytosis, intracellular trafficking, and *in vivo* circulation

and biodistribution as NCs composed of biocompatible poly(lactic-*co*-glycolic acid) [39, 40]. With regard to the antibody coat, surface adsorption of antibodies on polystyrene particles is believed to preferentially render an outward display of antibody variable regions, owing to hydrophobicity of the Fc region and the antibody concentration used [115], although a random orientation is conceivable. This is not conceptually different from covalent conjugation of antibodies, which also yields a random antibody orientation because the conjugation occurs at any of the available antibody residues. Extensive characterization of this formulation has shown negligible coating with serum proteins (albumin), presumably due to saturation of the NC surface with antibodies, with no apparent changes in aggregation or antibody detachment (whether in storage, physiological media, serum, or under varying temperature and pH), or fluorescence intensity at physiological pH [12-15, 27, 30, 31, 37, 86, 87, 93, 112, 116, 117]. In these reports, the antibody coating, hydrodynamic size, polydispersity index, and ζ-potential were also highly reproducible across independent formulations and batches, which is further supported by similar observations in binding, uptake, intracellular trafficking, and *in vivo* biodistribution [12-15, 27, 30, 31, 37, 86, 87, 93, 112, 116, 117].

3.5 Preparation of Multimeric Antibody Conjugates

An alternative multimeric model lacking a polymer particle consisted of anti-ICAM protein conjugates. For this purpose, anti-ICAM was biotinylated at a 1:5 antibody-to-biotin molar ratio using 6-biotinylaminocaproic acid N-hydroxysuccinimide ester, as previously described [118]. Conjugation was performed by incubating biotinylated anti-ICAM with

(green) Alexa Fluor 488-labeled streptavidin at 1:1 molar ratio for 1 h at 4°C. The hydrodynamic diameter, polydispersity index, and ζ-potential were determined using DLS.

3.6 Preparation of Monomeric Antibody-Enzyme (HRP) Conjugates

Following the manufacturer's instructions (Lightning Link® HRP Conjugation Kit by Innova Biosciences; Cambridge, UK), anti-ICAM or non-specific IgG (13 μmol/L) were incubated with LL-Modifier reagent® (1 μl/μl of antibody) and lyophilized HRP (21 μmol/L) for ~ 3 h at room temperature before quenching with LL-Quencher reagent® (1 μl/μl of antibody). This reaction covalently links primary amine groups of the antibody to lysine residues of HRP, and theoretically yields conjugates with a 1:2 antibody-to enzyme molar ratio. Verification of the molecular weight and presence of antibody-enzyme conjugates were performed using separation by SDS-PAGE followed by Coomassie blue staining of the resulting protein bands and, in parallel, Western blot analysis to immunodetect either the antibody or enzyme counterparts, as described in the Results section. Unconjugated HRP and antibodies served as controls.

In addition, antibody-enzyme conjugates or control unconjugated counterparts were fractionated using Asymmetrical Flow Field-Flow Fractionation (AF4) with Multi-Angle Light Scattering (MALS) and Quasi-Elastic Light Scattering (QELS) detection (Wyatt Technology, Santa Barbara, CA). An Agilent UV detector (wavelength set at 280 nm) and a Wyatt Optilab T-rEX differential refractive index (RI) (Wyatt Technology, Santa Barbara, CA, USA) detectors were connected sequentially to the channel outlet to monitor sample elution. A vendor-supplied spacer (350 μm thickness) was used to house a 10 kDa

molar mass cut-off regenerated cellulose membrane (Microdyn, Raleigh, NC) for the separation inside a short channel. Flow was controlled using Eclipse software (Wyatt Technology). The AF4 carrier liquid was 10 mmol/L phosphate buffered saline at pH 7.4. Samples were injected while focusing at 2.2 mL/min for 2 min. The injection step was followed by a second focusing step of 2.2 mL/min for 2 min. The crossflow was kept constant at 1.4 mL/min for 24 min while eluting the injected samples at 0.6 mL/min. UV, RI, and MALS data were obtained followed by conversion into molar mass, particle size, and size distributions using vendor-supplied software (ASTRA® 6.1.2.84). MALS intensity (wavelength of 690 nm) was measured at 15 angles simultaneously. MALS data were collected at 1 s intervals and QELS data at 5 s intervals. The QELS data were fitted to a single-mode exponential decay model to measure the translational diffusion coefficient with the hydrodynamic radii of the particles calculated via Stokes-Einstein equations. The apparent molar mass was calculated from the collected UV, RI, and MALS data using Zimm formalism with molar extinction coefficient of 1.4 mL/g·cm, which is that of antibodies in aqueous solutions, and a specific refractive index value (dn/dc) of 0.18 mL/g. In addition to this characterization of the conjugate mixture by AF4, the eluted conjugate species were separated into two major fractions (233 kDa and 686 kDa), as described in Section 6.2.1.

3.7 Preparation of Alginate and Chitosan-Alginate Microspheres and Beads

The following protocols for alginate microsphere and bead formation were adapted from [48, 105, 107, 119, 120], which were optimized to produce the desired physical and loading characteristics for this study. Sodium alginate (3% w/v aqueous) was used alone or

vortexed with antibody-coated NCs (16% and 32% v/v NCs to alginate for microspheres and beads, respectively; 2.7×10^{11} NCs/g alginate) to yield a homogenous suspension. As shown in Fig. 3.2, alginate solution was pumped at 5 µl/min by a peristaltic syringe pump through 100 µm inner diameter polyether ether ketone (PEEK) capillary tubing (SGE Analytical Science; Austin, TX, USA) for microspheres or a 20 G, 0.6 mm inner diameter needle for larger beads, from a height of 4 cm into a crosslinking medium of 2% $CaCl_2$. In the case of microspheres, polymer droplets were extruded by co-axial air flow (5 psi). To additionally coat alginate microspheres/beads with chitosan, chitosan was first dissolved in 1% v/v aqueous acetic acid at a concentration of 0.25 or 1% w/v , and adjusted to pH 5 using NaOH. Alginate microspheres/beads, with or without antibody-coated NCs, were incubated with the chitosan solution for 1 h at room temperature under gentle agitation, and then washed with 2% $CaCl_2$ [119, 121]. When indicated, rhodamine-labeled chitosan was used to confirm the presence and location of this coating using fluorescence microscopy. To crosslink the chitosan coat, an aqueous solution of genipin (1 mg/ml) was incubated with 1% chitosan-alginate microspheres for 24 h at room temperature, and washed with 2% $CaCl_2$ [119]. All formulations were stored in 2% $CaCl_2$ at 4 °C.

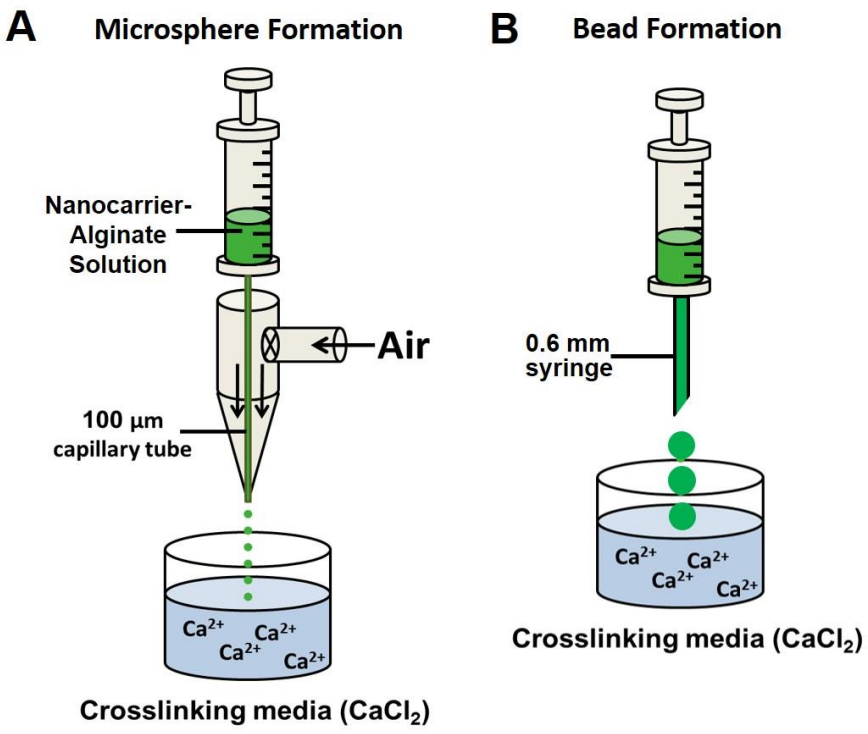

Figure 3.2. Encapsulation methods. (A) Method for formulating alginate microspheres ~180 µm in diameter, or (B) larger alginate beads ~2.8 mm in diameter.

3.8 Characterization of the Antibody-Coated Nanocarrier Loading in Microspheres

Radioisotope quantification of ^{125}I-antibody-coated NCs was also used to calculate the number of NCs per alginate or chitosan-alginate microsphere, the percent (%) loading, and the encapsulation efficiency (EE%), using the following equations:

$$\textbf{NCs per microsphere} = CPM_{microsphere} / CPM_{NC}$$

$$\textbf{\% Loading} = (\text{NCs per microsphere} / \text{NC Concentration}) / V_{microsphere} \times 100\%$$

$$\textbf{EE\%} = (\text{Measured NCs per microsphere} / \text{Added NCs per microsphere}) \times 100\%$$

where CPM are the ^{125}I counts-per-minute per microsphere ($CPM_{microsphere}$) or per NC (CPM_{NC}), and V is the theoretical volume of each microsphere ($V_{microsphere}$), as derived from their mean diameter. In parallel with radioisotope tracing, fluorescence microscopy was used to verify the presence of NCs within microspheres (settings described in Section 3.26).

3.9 Microsphere Stability and Release in Storage Conditions

To evaluate stability in storage conditions, alginate or chitosan-alginate microspheres loaded with antibody-coated, fluorescent NCs were incubated in 2% $CaCl_2$ at 4 °C over the period of 4 weeks. At the indicated time intervals, small aliquots were removed and analyzed by several means. First, fluorescence microscopy (10x objective) was used to image sample aliquots, from which the size and number of microspheres that were visualized as apparently intact were quantified, as well as their sum and mean fluorescence intensity. These parameters indicate potential changes in the microsphere size, their degradation, and relative changes in loading over time, as compared to the initial time of encapsulation (Day 1).

In addition, release of ^{125}I-antibody-coated, fluorescent NCs from microspheres was quantified by removing aliquots at the indicated time intervals, followed by centrifugation at 1000 × g for 1 min to separate the released (supernatant) and encapsulated (pellet) fractions. The radioisotope content and fluorescence intensity of each fraction, corresponding to the ^{125}I-antibody coat and fluorescent NC counterparts, were quantified using a gamma counter and a microplate spectrofluorometer, respectively. The percent

release was expressed as radioisotope or fluorescence content in the released fraction with respect to the total content (the sum of the released fraction and the encapsulated fraction).

3.10 Status of Microsphere-Encapsulated Antibody-Coated Nanocarriers in Storage Conditions

Since no significant release of antibody-coated NCs 4.2.4 was observed under storage conditions (2% $CaCl_2$, 4 °C), after 24 h in storage, we incubated microspheres for 4 h at 37 °C in 50 mM EDTA in dH_2O with shaking (150 rpm). Given that EDTA serves to extract Ca^{2+} (the reversible crosslinking agent) from the alginate matrix, this provides a means to induce the release of encapsulated NCs, enabling us to study their status while in storage.

To examine the status of the antibody moiety of encapsulated NCs, which is responsible for their targeting ability, ^{125}I-antibody counterparts were used in the NC formulation. Antibody degradation was assessed by quantifying the free ^{125}Iodine present in the released NC fraction, as determined by a trichloroacetic acid (TCA) precipitation assay [30, 114]. This was expressed as a percentage of the total radioisotope content in said released fraction.

In parallel, the ability of released NCs to bind to a surface-immobilized model target (a secondary antibody that recognizes the primary antibody on the NC coat) was evaluated using an in vitro binding assay in 24-well plates. For this purpose, wells were coated with 1 μg/ml goat anti-mouse IgG for 1 h at room temperature, then washed to remove unbound secondary antibody, and blocked with 1% BSA-PBS for 2 h at room temperature. Wells were then washed and incubated for 16 h at 4 ºC with antibody-coated

NCs that had been released from microspheres. NCs that bound to immobilized antibodies as well as non-bound NCs were collected and measured using a gamma counter. The percentage of NCs bound with respect to the total NCs added to wells, as well as the absolute number of NCs bound per well were obtained.

As controls, we incubated antibody-coated NCs that were not encapsulated within microspheres in the same conditions as encapsulated counterparts.

3.11 Microsphere Stability and Release in Simulated Gastrointestinal Fluids

The stability of microspheres loaded with antibody-coated NCs and the release of this content from microspheres were also evaluated in conditions mimicking the physiological pH of the GI, using methods and reagents adopted from U.S. Pharmacopeia (USP). NC-loaded microspheres were incubated under agitation (150 rpm) for 2 h at 37 °C in simulated gastric fluid (SGF; pH 1.2). Then, the microspheres were transferred to simulated intestinal fluid (SIF; pH 6.8), where they were incubated under agitation (150 rpm) for 4 h at 37 °C. Aliquots from the SGF and SIF solutions were removed at the indicated time points, from which we evaluated microsphere size, number of microspheres that appeared visibly intact (per field), and their fluorescence loading by fluorescence microscopy, as described for assays in storage conditions.

In parallel, release of ^{125}I-antibody NCs from the microspheres was addressed using radioisotope tracing, also as described above for the case of microsphere in storage conditions.

3.12 Status of Encapsulated and Released Antibody-Coated Nanocarriers in Simulated Gastrointestinal Conditions

Microspheres were first incubated up to 2 h at 37 ºC in SGF with or without pepsin, then analyzed or transferred to SIF with or without pancreatin for additional 4 h at 37 °C. As in the case of microspheres in storage conditions, those incubated for 2 h in SGF showed no significant release and, hence, release of antibody-coated NCs was induced by EDTA treatment as described above, to assess their status. For other cases, NC release resulted from pH-triggered microsphere dissolution, and this step was not necessary. In cases where incubations had been conducted in the presence of enzymes, a protease inhibitor cocktail was added to the samples at the time of evaluation, to preclude further proteolysis.

Degradation of antibodies comprising the NC coat was assessed by quantifying the free ^{125}Iodine content vs. the total ^{125}Iodine content in the released NC fraction (to obtain the percent degradation), as described above for storage conditions. Also, the ability of the released NCs to bind a surface-immobilized target (secondary antibody) was pursued, following the procedures described above for microspheres in storage conditions. The percentage of NCs bound with respect to the total NCs added to wells, as well as the absolute number of NCs bound per well, were calculated.

Non-encapsulated antibody-coated NCs incubated in the same conditions as those encapsulated within microspheres, served as controls.

3.13 Specific Cell Targeting of Antibody-Coated Nanocarriers after Release from Microspheres

Fluorescent non-specific IgG NCs or anti-ICAM NCs were encapsulated within alginate microspheres or 0.25% chitosan-alginate microspheres, and then incubated in SGF and, subsequently, SIF (in the presence of pepsin and pancreatin, respectively), as described above. At the indicated time points, NCs released from microspheres were incubated for 2 h at room temperature with ICAM-1-expressing Caco-2 cells and HUVEC (see Section 3.2). Cells were imaged by fluorescence microscopy (60x objective), and the number of NCs bound per cell was quantified using algorithms generated for this purpose, as described in previous works [15, 36, 37] and in Section 3.26. Binding was compared to that of anti-ICAM NCs that were not encapsulated but subjected to the same GI-mimicking conditions.

3.14 Oral Gavage in Mice

C57BL/6 wild type mice (Jackson Laboratory, Bar Harbor, ME) were first fasted for 2-4 hours [20]. Then, mice underwent oral gavage with 0.25% chitosan-alginate microspheres (~1.5×10^4 microspheres/animal) loaded with ^{125}I-anti-ICAM NCs or non-specific ^{125}I-IgG NCs vs. non-encapsulated ^{125}I-anti-ICAM NCs. In all cases, the administered doses were similar: ~1.1 mg antibody/kg, equivalent to 1.5×10^{13} NCs/kg. After 1 h from oral gavage, mice were sacrificed and the stomach, small intestine (duodenum, jejunum, ileum) and large intestine (cecum and colon) were isolated, from which the ^{125}I content, percent free ^{125}I of the sample, and the weight were measured [15, 30]. These data were used to calculate percentage of the total gavaged dose per gram (% dose/g) accumulated in said GI compartments, as well as the degradation of the antibody (labile) counterpart of NCs using a TCA precipitation assay, as described in Section 3.2 [30]. Studies were performed under

protocol R-13-15, which is in accordance with IACUC and University of Maryland regulations.

3.15 ICAM-1 Distribution and Recycling in the Absence of Ligands

To examine potential transit of ICAM-1 between the cell-surface and intracellular vesicles, TNF-α-activated HUVECs were incubated with 10 μg/ml cyclohexamide to inhibit *de novo* protein synthesis which may confound results. After 1 h, cells were fixed and ICAM-1 expressed on the cell-surface was immunostained in red using anti-ICAM followed by TxR-labeled goat anti-mouse IgG. Cells were then permeabilized and total cell-associated ICAM-1 (surface + intracellular) was labeled using anti-ICAM followed by green FITC goat anti-mouse IgG. Using this method, the percentage of green, single-labeled ICAM-1 that does not colocalize with double-labeled (FITC+TxR) ICAM-1 represents the intracellular fraction, which was quantified by fluorescence microscopy, as described in Section 3.26.

3.16 Intracellular Trafficking of ICAM-1 in the Absence of Ligands

To assess endocytosis of ICAM-1 in the absence of ligands, TNF-α-activated HUVECs were incubated continuously for 30 min, 1 h, 3 h, or 5 h at 37°C with 20 μg/ml TxR-labeled tomato lectin to stain the cell surface. After different periods of time, cells were washed and fixed, and ICAM-1 located on the cell surface was stained in blue using anti-ICAM

followed by blue Alexa Flour 350-goat anti-mouse IgG. Cells were then permeabilized and total cell-associated anti-ICAM was labeled in green with anti-ICAM and FITC goat anti-mouse IgG. Using this method, surface-located ICAM-1 should colocalize with lectin and appear white (green FITC + red TxR + blue Alexa Fluor 350), while intracellular ICAM-1 that was endocytosed from the cell surface should colocalize with lectin and appear yellow (green FITC + red TxR). Cell-surface ICAM-1 which did not colocalize with lectin should appear turquoise (blue Alexa Fluor 350 + green FITC) and intracellular ICAM-1 which does not colocalize with lectin should be green (FITC). Tracking these different fractions and their ratios over time, it is possible to discern potential trafficking of ICAM-1 between the cell surface and internal compartments by fluorescence microscopy. The mechanism of such a transport was also tested in the presence of 3 mM amiloride (inhibited in CAM-mediated endocytosis and macropinocytosis) or 0.5 μM wortmannin (inhibited in macropinocytosis, not CAM-mediated endocytosis).

3.17 Binding of Monomeric Anti-ICAM Assessed by Fluorescence Immunostaining

Control or TNFα-activated Caco-2 cells cultured on coverslips or transwell inserts were incubated continuously at 37 °C from 30 min to 5 h with complete cell medium containing 75 pM anti-ICAM or non-specific IgG. Cells were washed to remove non-bound antibodies, then fixed for 15 min at room temperature with 2% paraformaldehyde and permeabilized for 15 min with 0.2% Triton X-100. Total antibody molecules associated

with cells were immunostained using green FITC-labeled goat anti-mouse IgG for 1 h at room temperature, followed by visualization by fluorescence microscopy, as described in Section 3.26 [114].

3.18 Verification of Targeting and Enzyme Activity upon Targeting of Anti-ICAM-HRP Conjugates

Control Caco-2 cells were fixed to preclude uptake and permit only binding, and then incubated for 1 h at room temperature with either anti-ICAM-HRP conjugates or control IgG-HRP conjugates (75 pM antibody and 150 pM HRP, as per the 233 kDa conjugate observed in the Results section), vs. non-conjugated HRP (150 pM; 43 kDa) or anti-ICAM (75 pM; 155 kDa). Other controls consisted of incubation with anti-ICAM-HRP conjugates in the presence of 75 pM anti-ICAM, a specific competitor for ICAM-1 binding, or non-specific IgG. Total cell-bound antibody counterparts were immunostained using green FITC-labeled goat anti-mouse IgG, while total cell-bound HRP (naked or conjugated to antibodies) was immunostained with rabbit anti-HRP followed by TxR-goat anti-rabbit IgG. Binding was assessed by quantifying in micrographs the mean green or red fluorescence intensity (in arbitrary units, A.U.) for anti-ICAM or HRP, respectively, which also allowed us to determine the percentage of antibody colocalization with HRP, or vice versa, as dual-labeled (yellow) fluorescence [36, 114].

In addition to fluorescence quantification by microscopy, we also measured HRP activity that remained bound on cells after washing. This was conducted by incubating the cell samples for 5 minutes at room temperature with the HRP substrate, TMB, as per the

vendor instructions, followed by quenching with 2 M sulfuric acid. Absorbance at 450 nm was then quantified by spectrophotometry and the amount of HRP was derived from standard curves correlating absorbance and HRP activity (for unconjugated and conjugated forms) under the same reaction conditions.

3.19 Degree and Mechanism of Uptake of Monomeric vs. Multimeric Anti-ICAM

HUVEC (TNF-α-activated) or Caco-2 cells (control or TNF-α-activated) were incubated with monomeric anti-ICAM (140 pM), multimeric anti-ICAM NCs (36 pM antibody, since this formulation has greater avidity vs. anti-ICAM [86]), or multimeric anti-ICAM conjugates (214 pM antibody) for 30 min in 1% BSA-supplemented cell medium to allow their binding to the cell surface (pulse period). Control experiments were performed using either non-specific IgG or IgG NCs, or by incubating anti-ICAM conjugates in the presence of competing anti-ICAM vs. non-specific IgG. After this time, cell medium containing non-bound counterparts was removed, and cells were washed and incubated at 37ºC with fresh medium for 30 min to 4.5 h to allow internalization of surface-bound materials (chase period). In parallel, incubation at 4ºC served as a negative control for energy-dependent uptake. Alternatively, to evaluate the mechanism of uptake, incubations were performed in the presence of either 3 mM amiloride (an inhibitor of macropinocytosis and CAM-mediated endocytosis), 50 μM monodansylcadaverine (MDC; inhibitor of clathrin-mediated endocytosis), 1 μg/ml filipin (inhibitor of caveolar endocytosis), or 0.5 μM wortmannin (inhibitor of phosphatidylinositol 3 kinase (PI3K), involved in macropinocytosis) [12]. The specificity of these inhibitors was previously confirmed using ligands or markers of these pathways as controls [12].

All cell samples were then fixed with 2% paraformaldehyde for 15 min at room temperature. Surface-bound anti-ICAM, anti-ICAM NCs, or anti-ICAM conjugates were immunostained with TxR-labeled goat anti-mouse IgG for 1 h. Since polymer particles and streptavidin contain a green fluorescent label, all cell-associated anti-ICAM NCs and anti-ICAM conjugates are visible in the green channel while only surface-located counterparts fluoresce in the red channel, thus enabling differential visualization and quantification, as described [12, 114]. In the case of monomeric anti-ICAM, after similarly immunostaining cell-surface counterparts in red, cells were permeabilized with 0.2% Triton X-100, followed by incubation with green FITC-labeled goat anti-mouse IgG, which would label all cell-associated anti-ICAM in green, thereby enabling similar distinction and quantification of cell-surface bound vs. internalized counterparts by fluorescence microscopy. In both cases, in addition to endocytosis, the localization of anti-ICAM, anti-ICAM NCs, and anti-ICAM conjugates within 5 μm of the cell nucleus (perinuclear) or within 5 μm from the cell border (herein called periphery) was also quantified.

3.20 Cellular Uptake of Anti-ICAM-HRP Conjugates

Anti-ICAM-HRP conjugates were either non-separated (control mixture) or separated by AF4 into the 233 kDa and 686 kDa fractions described above (to distinguish uptake upon monomeric vs. multimeric binding) and their uptake was assessed by fluorescence immunostaining. For this purpose, control Caco-2 cells were incubated with non-separated and separated anti-ICAM conjugates or IgG-HRP conjugates (75 pM antibody and 150 pM HRP) for a pulse period of 30 min at 37 °C, followed washing and incubation at 37 °C with fresh medium for the indicated time intervals. Incubations were performed in the absence

vs. presence of 3 mM amiloride, to verify CAM-mediated uptake. Cells were fixed and the antibody counterpart of surface-bound conjugates was immunostained in red using TxR-goat anti-mouse IgG. Cells were then permeabilized and incubated with green FITC-goat anti-mouse IgG, to label all bound and internalized antibody molecules. In parallel experiments, a similar procedure was used to immunodetect surface-bound vs. internalized HRP counterpart. Hence, in both cases, the cell-surface bound fraction was double-labeled in green and red (yellow) while internalized counterparts were single-labeled in green. Using the methods noted above, cell samples were analyzed by fluorescence microscopy to quantify the absolute internalized fluorescence and the percentage of internalized fluorescence corresponding either to the antibody or the enzyme [36, 114].

In addition to microscopy analysis, internalized enzyme activity was evaluated by incubating Caco-2 cells for 30 min at 37 °C with non-conjugated anti-ICAM or HRP vs. anti-ICAM-HRP conjugates or IgG-HRP conjugates (same concentrations as noted above), in the absence vs. presence of 3 mM amiloride, which inhibits CAM-mediated endocytosis. Cells were washed and tested for HRP activity without permeabilization, which would primarily render activity bound on the cell surface. In parallel, cells treated similarly were washed and permeabilized to gain access to the cell interior and obtain the total surface-bound and internalized enzyme activity. In both cases, HRP activity was assessed by incubation with TMB for 20 minutes at room temperature and spectrophotometric measurement, from which the HRP amount was derived using activity standard curves, as described above.

3.21 Intracellular Trafficking of Monomeric vs. Multimeric Anti-ICAM

TNF-α-activated HUVECs or control Caco-2 cells cultured on coverslips were incubated with either green FITC-labeled anti-ICAM, non-specific IgG, anti-ICAM coated onto green Fluoresbrite® NCs, or green Alexa Fluor 488-labeled anti-ICAM conjugates for a pulse of 30 min, as described above. Cells were then washed and incubated for up to 1 h, 3 h, or 5 h (37°C) in the absence of a ligand, as described above. Cells were subsequently fixed and permeabilized, and lysosomes or recycling compartments were immunostained with anti-LAMP-1 or anti-Rab11a, respectively, followed by TxR-labeled secondary antibodies. In the case of anti-ICAM conjugates, an additional lysosomal labeling method was used to avoid cell permeabilization and subsequent leakage of the fluorescent dye from degraded conjugates. Here, cells were pre-treated with 10 kDa TxR dextran for 45 min at 37°C, washed, and incubated with fresh medium for another 45 min at 37ºC prior to addition of anti-ICAM conjugates [122]. This protocol enables lysosomal trafficking of dextran, which allows visualization of this compartment due to lack of dextran degradation by mammalian cells, as previously verified [122]. Colocalization of green-labeled anti-ICAM, anti-ICAM NCs, or anti-ICAM conjugates with each one of these red-labeled compartments (lysosomes or recycling endosomes) was calculated from fluorescence micrographs, as described in Section 3.26 [122]. The number of endocytic vesicles containing monomeric or multimeric anti-ICAM and the number of LAMP-1 and dextran-labeled compartments was additionally quantified (Section 3.26).

3.22 Intracellular Degradation of Monomeric vs. Multimeric Anti-ICAM

Using the protocol described above, degradation of naked green FITC-labeled anti-ICAM or green Alexa Fluor 488-labeled anti-ICAM conjugates was estimated by comparing the

total fluorescence remaining over time (chase incubation) to the cell-associated fluorescence achieved after the first 30 min pulse incubation. Agents that have been previously shown to inhibit lysosomal trafficking, nocodazole (20 μM) [122], or to inhibit activation of lysosomal hydrolases, chloroquine (300 μM) [122], were used as controls for degradation. These agents were incubated with cells during the chase period only to preclude potential effects on uptake. In the case of green anti-ICAM NCs, cells were incubated with TxR goat anti-mouse IgG after permeabilization, to immunodetect anti-ICAM on the surface of internalized particles. Hence, lack of antibody degradation was visualized as colocalization of TxR-labeled anti-ICAM with green fluorescent particles, while degradation was observed as single-labeled green-particles. Time-dependent degradation of anti-ICAM on NCs was calculated by comparing the number of antibody-free particles to the total number of cell-associated particles, as described [122].

3.23 Transepithelial Transport of Anti-ICAM in Epithelial Cell Monolayers

To track total binding and transport of anti-ICAM vs. control IgG in live Caco-2 monolayers, antibodies were labeled with ^{125}-Iodine [13]. The radioisotope content of ^{125}I-antibodies was measured using a gamma counter and protein concentration was determined by a Bradford assay. Control ^{125}I-IgG or ^{125}I-anti-ICAM (70 pM; 56 nCi/ml) was added to the chamber above Caco-2 cells and incubated at 37°C for the indicated time intervals. The radioisotope content in the chamber above the cells (non-bound antibodies), the chamber below the cells (transported antibodies), and the cell fraction (bound and internalized antibodies) was measured using a gamma counter. Free ^{125}Iodine released from antibodies (i.e., from degradation) was determined by TCA precipitation of each fraction, and this value was subtracted from the total (precipitated + free, non-precipitated) amount of

antibodies present in the samples. After subtraction, the number of molecules bound to the epithelial monolayer, the number of molecules transported across the monolayer, the percentage of molecules transported with respect to the total number associated to cells, and the apparent permeability coefficient (P_{app}) were determined using the following equations,

$$\textbf{Molecules bound/cell} = [(CPM_{cell\ fraction} / \text{Specific Activity}) / MW \times N_{avo}] / 150{,}000 \text{ cells}$$

$$\textbf{Molecules transported/mm}^2 = [(CPM_{basolateral} / \text{Specific Activity}) / MW \times N_{avo}] / 0.32\ mm^2$$

$$\textbf{\% Transported} = 100 \times [CPM_{basolateral} / (CPM_{basolateral} + CPM_{cell\ fraction})]$$

$$\textbf{P}_{\textbf{app}}\ \textbf{(cm/s)} = (CPM_{basolateral} \times Vol.) / (A \times t \times CPM_{added})$$

where CPM are the ^{125}Iodine counts-per-minute added to the upper chamber (CPM_{added}), the cell fraction ($CPM_{cell\ fraction}$), or the lower chamber ($CPM_{basolateral}$), and Specific Activity is the CPM/g of protein, MW is molecular weight (g/mol), N_{avo} is Avogadro's number, A is the surface area of the filter membrane (cm^2), Vol. is volume of medium in the upper chamber (ml), and t is time of incubation (s).

3.24 Mechanism of Transepithelial Transport of Anti-ICAM

Transcellular transport of ^{125}I-anti-ICAM by a vesicular mechanism was assessed in 20 µmol/L 5-(N-ethyl-N-isopropyl) amiloride (EIPA), which inhibits the exchanger protein, NHE-1, involved in macropinocytosis and CAM-mediated transport [91]. Paracellular transport was assessed by evaluating leakage to the bottom chamber of ^{125}I-BSA (^{125}I-

albumin) added above Caco-2 cells, in the presence of anti-ICAM. This was compared to ^{125}I-albumin transport in the absence of anti-ICAM or in 5 mM H_2O_2 known to disrupt cell junctions. In all experiments, TEER was monitored before and after all incubations to evaluate the status of the permeability barrier.

3.25 Transport of Anti-ICAM-HRP Conjugates in Epithelial Monolayers

Anti-ICAM-HRP conjugates were either non-separated (control mixture) or separated by AF4 into the 233 kDa and 686 kDa fractions described above (to distinguish uptake upon monomeric vs. multimeric binding), and 70 pM of control vs. separated conjugates were incubated with Caco-2 monolayers cultured on transwell inserts for 24 h at 37 °C. To assess the specificity of transport, Caco-2 monolayers were incubated for the indicated time intervals at 37°C with 70 pM HRP, anti-ICAM, non-specific IgG-HRP conjugates, or anti-ICAM-HRP conjugates in the presence or absence of anti-ICAM or IgG competitors. The apical, cell, and basolateral fractions were collected and measured for HRP activity by a spectrophotometric enzyme assay in phenol red-free cell culture media. Absorbance at 450 nm was then converted to the amount of active HRP (pM) using standard curves conducted in experimental reaction conditions, as described above.

To assess the mechanism of transepithelial transport of anti-ICAM-HRP conjugates, the above experiment was conducted in the presence of 20 µM EIPA, as described above. Paracellular transport was evaluated by monitoring TEER during transport of conjugates.

3.26 Microscopy Visualization and Image Analysis

Samples were analyzed using a 10x or 60× PlanApo objective, as indicated, and the Olympus IX81 inverted 3-axe automatic fluorescence microscope (Olympus Inc., Center Valley, PA). Samples were observed by phase contrast and fluorescence using filters from Semrock (Rochester, NY) in the red channel (excitation BP360–370 nm, dichroic DM570 nm, emission BA590–800+ nm), green channel (excitation BP460–490 nm, dichroic DM505 nm, emission BA515–550 nm), or blue channel (excitation BP380–400 nm, dichroic DM410 nm, emission BA415–480 nm). Micrographs were taken using Orca-ER camera from Hamamatsu (Bridgewater, NJ) and SlideBook 4.2 software from Intelligent Imaging Innovations (Denver, CO). Images were analyzed using Image-Pro 6.3 from Media Cybernetics Inc. (Bethesda, MD). Algorithms programmed for automatic image analysis were used to quantify diameter of objects, sum and mean fluorescence, number of NCs or objects ~100-300 nm, and colocalization of objects labeled with different fluorophores [12, 36, 92, 122].

3.27 Statistical Analysis

Data were calculated as mean ± standard error of the mean (S.E.M). For in vitro and animal studies the number of independent samples was ≥ 6. For cell culture assays conducted on coverslips (for fluorescence microscopy), the number of independent samples was ≥ 2. For cell culture assays conducted in transwell inserts, the number of independent wells was ≥ 4. Statistical significance was determined by Student's unpaired *t*-tests for comparisons between two groups, and one-way ANOVA followed by Tukey test for comparisons among more than two groups. Differences were considered significant at $p < 0.05$.

Chapter 4: Encapsulation of ICAM-1 Targeted Nanocarriers into Chitosan-Alginate Hydrogels for Gastric Protection and Intestinal Release

4.1 Introduction

As described in Chapter 2, active targeting of therapeutics to specific markers within the body may enhance biodistribution to sites of disease, minimizing the effective dose required for therapy and hence, the associated toxicity [7, 52, 123]. Targeting ligands may be directly conjugated to a therapeutic of interest or coupled to the surface of drug-bearing NCs to further improve drug solubility, stability, biodistribution, metabolism, and clearance [7, 8].

As said, active targeting is not only employed to improve drug biodistribution toward selected cells, but may also trigger receptor-mediated endocytosis, which in some cases leads to transcytosis [7, 52, 123]. This allows for transport of targeted drugs and their carriers across cells that control the passage of substances between body compartments, e.g. the endothelial lining that separates the bloodstream from underlying tissue or epithelial barriers at other interfaces [7, 52, 123].

To this end, active targeting and transport is valuable in the context of oral drug delivery, since targeted attachment to GI epithelial cells or uptake within these cells may improve treatment of GI disorders, while induced transport across this lining may enhance absorption into the circulation [2, 6, 54-58]. However, this strategy is limited by degradation or deactivation of labile targeting molecules (particularly protein-based ones) in the acidic and proteolytic environment of the stomach, which curtails targeting of drug

delivery systems to the intestine, the main site of drug absorption [53]. Hence, there is a need for protection of targeted drug carriers from degradation in gastric conditions as well as site-specific release in intestinal conditions, while preserving the activity of their targeting moieties.

As an example, the work in this chapter looked into improving GI targeting upon oral delivery of NCs addressed to ICAM-1. As described in Chapter 2, targeting to ICAM-1, e.g. using NCs coated with anti-ICAM antibodies or peptides, induces transport into and across cells via a CAM-mediated pathway that is clathin- and caveolae-independent [12-14, 93, 112]. This strategy has demonstrated enhanced delivery of therapeutic enzymes into and across GI epithelial monolayers in culture [13]. *In vivo* implementation of this strategy via oral gavage in mice has also shown promise, as specific targeting was observed vs. non-specific IgG-coated NCs [15]. Yet, intestinal biodistribution was largely restricted by retention of anti-ICAM NCs in the stomach, as well as substantial degradation [15]. Therefore, anti-ICAM NCs, and other targeted formulations, could benefit from protection and site-specific release in the GI tract.

Among the various polymers employed to satisfy these requirements [4], we selected alginate in light of numerous advantages, including low cost, low toxicity, biocompatibility, and biodegradability, as well as its effective encapsulation of active biological agents for protection and pH-sensitive release in GI conditions [16, 17, 48, 49, 105-107, 109, 119, 121, 124]. Dropwise addition of alginate to an aqueous crosslinking solution of polyvalent or divalent cations, such as Ca^{2+}, forms solid gel beads [16, 17]. The size of beads can range from a sub-millimeter (microspheres) to sub-centimeter scale depending on the method and diameter of extrusion, among other factors [48, 49, 105, 107].

In addition, alginate beads are often optimized by reinforcement with a chitosan coat during or after bead formation, providing greater mechanical stability as well as reduced drug leaching and burst release from alginate beads [16]. Chitosan is also a mucoadhesive agent, which prolongs residence time in the intestine [16, 124-126]. Despite the popularity of this strategy for encapsulation of therapeutics, encapsulation of targeted (ligand-coated) NCs in alginate and chitosan-alginate matrices for oral delivery has yet to be examined. Using the example of ICAM-1-targeted NCs, the work herein aimed at exploring this strategy. Our results demonstrate potential to improve ligand-mediated targeting for drug delivery systems to be administered via the oral route.

4.2 Results

4.2.1 Characterization of Antibody-Coated Nanocarriers

Our overall goal is to enable the study of ICAM-1-targeted NCs administered via the oral route, which requires encapsulation of said NCs within controlled release vehicles, to protect their labile targeting moiety from premature gastric degradation and provide intestinal release. As a NC model, we used polystyrene nanoparticles labeled with a pH-independent fluorophore, which were coated by surface adsorption with non-specific IgG or anti-ICAM (see Section 3.4). As shown in Table 4.1, this protocol rendered similar hydrodynamic diameter, polydispersity index, ζ-potential, and number of antibody molecules per NC for IgG NCs and anti-ICAM NCs. Antibody coating was also verified by an increase in NC diameter and more positive ζ-potential with respect to non-coated NCs. For cellular targeting experiments and *in vivo* oral gavage in mice, we used anti-

ICAM NCs compared to non-specific IgG NCs. For microsphere encapsulation and characterization of their stability, release, and protection against degradation we used IgG NCs, since this antibody is less costly and the properties of microspheres encapsulating IgG NCs should reflect those encapsulating anti-ICAM NCs, given that anti-ICAM is an IgG with similar molecular characteristics.

Table 4.1. Nanocarrier characterization.

	Size (nm)	Polydispersity	Z-potential (mV)	Antibody molecules/NC
Non-coated NCs	109 ± 2	0.06 ± 0.01	-39 ± 2	-
IgG NCs	158 ± 5	0.19 ± 0.03	-31 ± 2	176 ± 8
Anti-ICAM NCs	156 ± 2	0.22 ± 0.05	-27 ± 5	208 ± 43

NCs = nanocarriers. Data are shown as means ± S.E.M. ($n \geq 3$).

4.2.2 Preparation of Nanocarrier-Loaded Alginate and Chitosan-Alginate Microspheres

Alginate was selected based on its biocompatibility and gentle formulation [16, 17]. We employed a previously established co-axial air flow technique (see Materials and Methods), which renders homogeneous alginate microspheres with diameter <400 μm [107], a suitable size for oral gavage in mice. These microbeads are crosslinked by Ca^{2+} to efficiently entrap loaded contents [107]. Whereas this and other alginate microencapsulation methods have been extensively used for various biological agents [47-49, 105-107, 109, 121], microencapsulation of antibody-coated NCs had not yet been assessed. To examine this aspect, we used the ^{125}I-IgG-coated fluorescent NCs described above for both radioisotope and fluorescence quantification. Initial studies involved encapsulation within alginate microspheres alone or with the addition of a 0.25% chitosan

coat to increase their stability (Table 4.2). Contrary to internal gelation techniques, surface modification with chitosan was performed after formation of alginate microspheres to minimize changes in size and loading.

Table 4.2. Size and loading of alginate and chitosan-alginate microsphere formulations.

Formulation:	Diameter (μm)	NCs/Microsphere	EE%	% Loading (v/v)
Alginate	181 ± 0.4	$1.95 \pm 0.01 \times 10^6$	96.7 ± 1.7	15.5 ± 0.3
0.25% Chitosan-Alginate	185 ± 0.4	$1.96 \pm 0.01 \times 10^6$	99.1 ± 0.9	15.9 ± 0.2
1% Chitosan-Alginate	178 ± 0.4	$1.82 \pm 0.01 \times 10^6$	99.6 ± 0.5	15.9 ± 0.1
Genipin-1% Chitosan-Alginate	178 ± 0.5	$1.77 \pm 0.05 \times 10^6$	95.1 ± 1.7	15.2 ± 0.3

Theoretical Loading: 2.7×10^{11} NCs/g alginate; 16% v/v; 10% w/w.

As shown in Table 4.2, both preparations rendered a uniform microsphere size distribution of ~180 μm in diameter, and spherical shape, as observed by phase contrast microscopy as well as by fluorescence microscopy of fluorescence-labeled NCs (Fig. 4.1A). Fluorescence visualization also confirmed the presence of a chitosan coat (shown in red) for the corresponding microspheres, and NCs (shown in green) distributed within the alginate mesh (Fig. 4.1B). Quantification of entrapped NCs by fluorescence microscopy, which tracked the particle counterpart, revealed similar loading in both microspheres formulations (~1.2 x 10^8 A.U.; Fig. 4.1C). This corresponded to ~1.9 x 10^6 NCs per microsphere, as per quantification of the antibody counterpart by radioisotope tracing (Fig. 4.1C and Table 4.2). As such, % loading and EE% were similar for both alginate microspheres and chitosan-alginate microspheres (~15% loading and ~98 EE%;

Table 4.2). Therefore, these formulations contained equivalent physical and loading characteristics with or without a chitosan coat, and both radioisotope and fluorescence tracing are viable methods to examine these parameters.

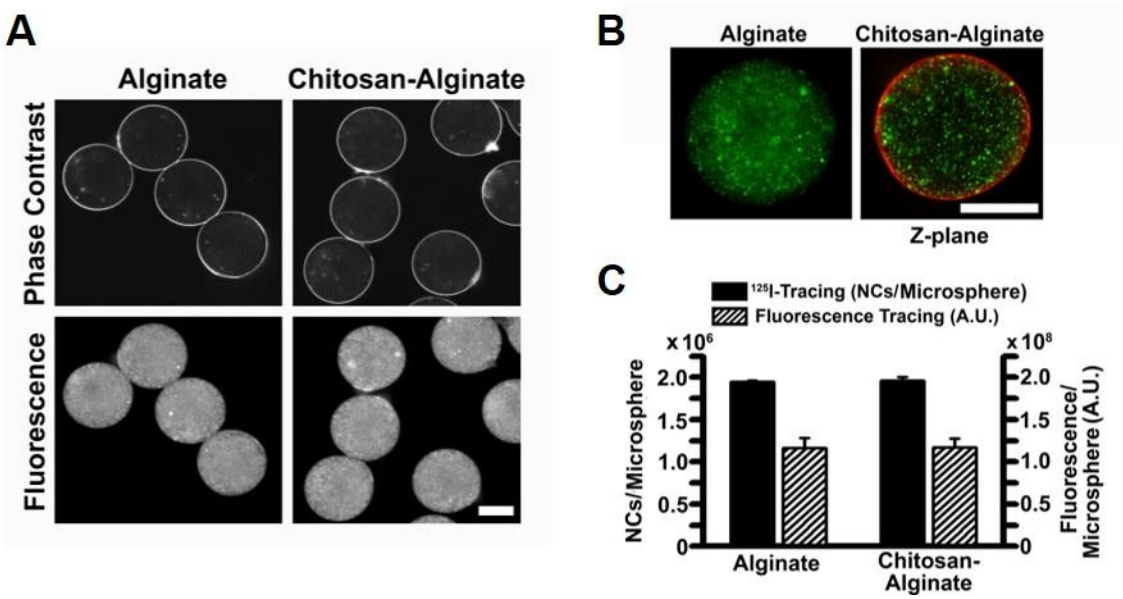

Figure 4.1. Encapsulation of antibody-coated nanocarriers into alginate or chitosan-alginate microspheres. ^{125}I-IgG-coated fluorescent NCs were encapsulated into alginate microspheres by co-axial air flow-driven extrusion through a 100 µm-diameter capillary needle into a crosslinking $CaCl_2$ solution. Chitosan-alginate microspheres were prepared by further incubation of alginate microspheres with 0.25% chitosan. (A) Phase contrast and fluorescence microscopy images of alginate microspheres and 0.25% chitosan-alginate microspheres. Scale bar = 100 µm. (B) Dual-fluorescence visualization of microspheres, with green NCs within the alginate core, in the presence (right) or absence (left) of a red rhodamine-labeled chitosan coat. Scale bar = 100 µm. (C) Loading assessed by radioisotope quantification of the antibody coat or fluorescence quantification (in arbitrary units, A.U.) of the NC counterpart. Data are Mean ± S.E.M. No statistically significant differences between alginate and chitosan-alginate formulations were observed.

In addition, alginate and chitosan-alginate beads ~2.8 mm in diameter were prepared for future *in vivo* studies in larger animals, including rats, by similar methods employed to formulate microspheres except polymer was extruded through a 0.6 mm-diameter needle. Coating with 0.25% chitosan was similarly performed following alginate bead formation. The presence of a chitosan shell (shown in red) and uniform distribution

of loaded fluorescent NCs (shown in green) within the alginate core was confirmed using confocal microscopy (Fig. 4.2A). Similar to microspheres, alginate beads were relatively homogenous in size and morphology, which was not altered with the addition of a chitosan shell following alginate bead formation (Table 4.3). Furthermore, we were capable of loading varying amounts of NCs into beads, as shown by UV illumination and fluorescence microscopy images (Fig. 4.2B). Radioisotope tracing of the ^{125}I-antibody counterpart of NCs also revealed efficient loading of alginate beads (23% loading and 70 EE%; Table 4.3), albeit lower than that of microspheres in terms of EE% (Table 4.2). This was equivalent to ~3.9×10^9 NCs/bead. The loading efficiency was not significantly altered with chitosan modification, as observed with microsphere formulations.

Table 4.3. Size and loading of alginate and chitosan-alginate beads.

Formulation:	Diameter (mm)	NCs/Bead	EE%	% Loading (v/v)
Alginate	2.8 ± 0.03	$3.9 \pm 0.1 \times 10^9$	70.8 ± 1.3	22.7 ± 0.4
0.25% Chitosan-Alginate	2.9 ± 0.04	$4.0 \pm 0.2 \times 10^9$	76.4 ± 3.9	24.4 ± 1.2

Theoretical Loading: 2.7×10^{11} NCs/g alginate; 32% v/v; 20% w/w.

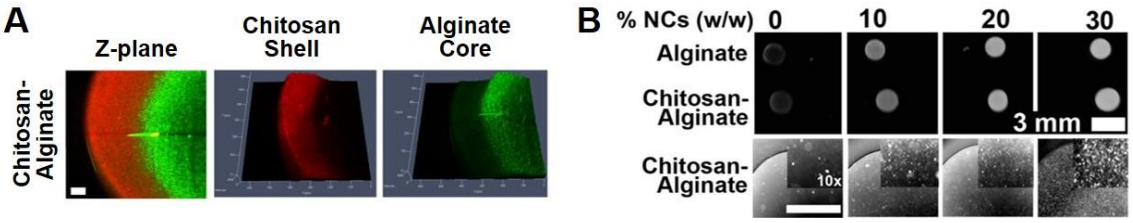

Figure 4.2. Formulation and loading of alginate and chitosan-alginate beads. Alginate was extruded through a 0.6 mm needle and crosslinked with Ca^{2+} to produce beads ~2.8 mm. Chitosan-alginate beads were formulated by incubating alginate beads in a 0.25% chitosan solution. (A) Confocal visualization of microspheres, with green NCs within the alginate core and a red rhodamine-labeled chitosan coat (left) and fluorescence intensity plots (middle and right). Bar = 100 µm. (B) Fluorescence imaging of alginate or chitosan-alginate capsules with various loads of FITC-labeled IgG NCs (0-30% w/w) using UV illumination (top panel) and fluorescence microscopy (bottom panel, bar = 1 mm).

Nevertheless, the following studies were conducted using 180 µm-diameter microspheres, given that they suit the size requirements for oral gavage in mice. Mice were selected for *in vivo* studies to provide a comparison with previous literature on GI biodistribution of non-encapsulated ICAM-1 targeted NCs [15].

4.2.3 Stability of Nanocarriers-Loaded Microspheres in Storage Conditions

To assess the stability of these formulations in storage conditions ($CaCl_2$ at 4 °C), we first examined the release of ^{125}I-IgG-coated fluorescent NCs from alginate microspheres or 0.25% chitosan-alginate microspheres over time. Radioisotope tracing revealed minimal (<10%) release of encapsulated contents for both microsphere formulations over 28 days (Fig. 4.3A). This was in agreement with the low level (also <10%) of release observed by spectrofluorometry (Fig. 4.4A), indicating sufficient stability of these two formulations in storage. The similar release pattern determined by tracing the antibody vs. NC counterparts suggest that they exist as antibody-coated NCs within either microsphere type, given that their size difference would otherwise account for a different release rate from the alginate network. In fact, when release of antibody-coated NCs from microspheres was induced by incubation with EDTA (after 24 h in storage), and the released NCs were tested for their ability to bind surface-immobilized secondary antibodies, we observed similar binding (~90%) to that of antibody-coated NCs which were not encapsulated in microspheres (Fig. 4.3B). Also, minimal amounts (<5%) of free ^{125}Iodine, which is released upon antibody degradation, were found upon EDTA-induced release of NCs from the either microsphere type (Fig. 4.3C).

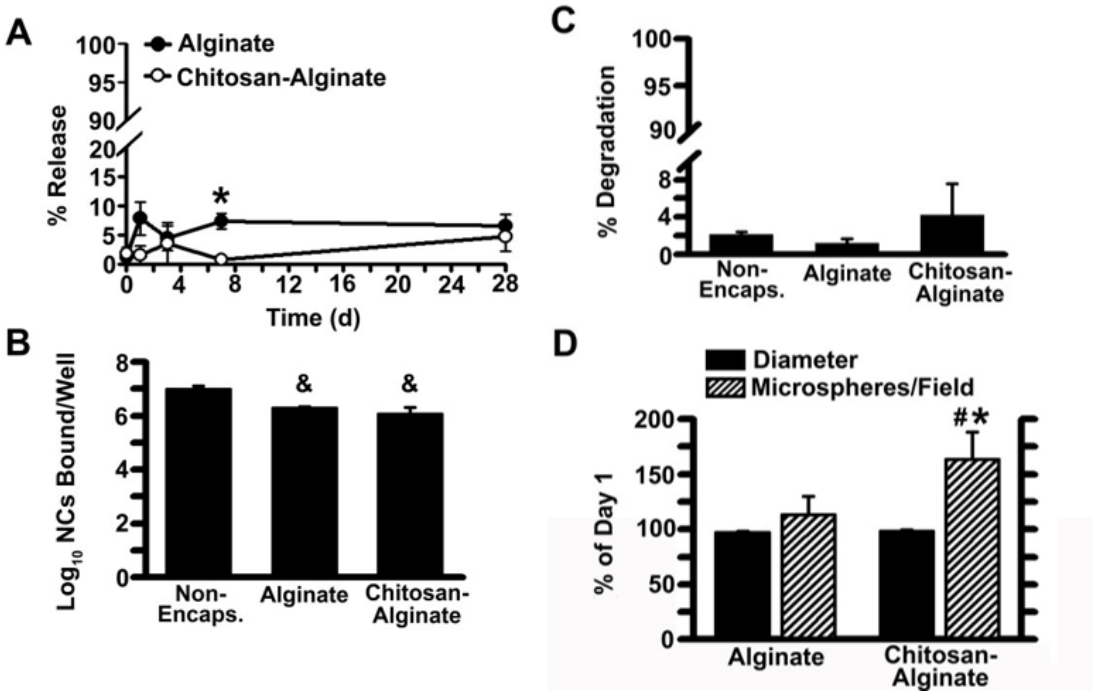

Figure 4.3. Stability of nanocarrier-loaded microspheres in storage conditions. Alginate vs. 0.25% chitosan-alginate microspheres loaded with ^{125}I-IgG-coated fluorescent NCs were incubated in storage conditions ($CaCl_2$, 4 °C). (A) At the indicated times, the radioisotope content of the released and encapsulated fractions were measured to calculate the percent release. (B) The encapsulated ^{125}I-IgG-coated NCs were extracted from microspheres using EDTA and their ability to bind to surface-immobilized secondary antibody was assessed using radioisotope tracing. (C) The percentage of free ^{125}Iodine, reflective of antibody degradation, was evaluated using ^{125}I-antibody-coated NCs extracted from microspheres as in (B). Non-encapsulated (non-encaps.) NCs were used as controls in (B) and (C). (D) After 28 days in storage, the diameter and number of microspheres per microscopy field were analyzed from fluorescence images, and expressed as the percentage of respective values at day 1. Data are Mean ± S.E.M. * Compares alginate vs. chitosan-alginate formulations; & compares values between microsphere-encapsulated and non-encapsulated NCs; # compares values at day 28 vs. day 1 ($p<0.05$, Student's *t* test).

Furthermore, the size, number, and loaded fluorescence content of alginate microspheres or chitosan-alginate counterparts, as measured by fluorescence microscopy, did not differ between the two formulations nor decreased over 28 days in storage (Fig. 4.3D and 4.4B). Hence, encapsulated antibody-coated NCs are not degraded and retain their binding capacity during encapsulation and incubation in storage, concurrent with observed microsphere stability under proper storage conditions.

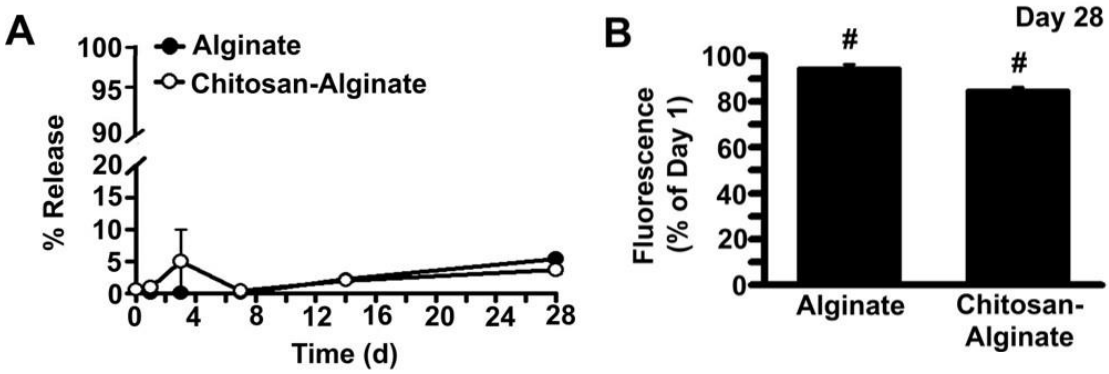

Figure 4.4. Release of fluorescent nanocarriers from microspheres in storage conditions. Alginate vs. 0.25% chitosan-alginate microspheres containing IgG-coated fluorescent NCs were incubated in storage conditions. (A) At the indicated times, aliquots were removed to assess the fluorescent NC content in the released vs. encapsulated fraction by spectrofluorometry, to determine percent release. (B) At day 28 in storage conditions, the sum fluorescence (in A.U.) per microsphere was quantified by fluorescence microscopy and expressed as a percentage of the fluorescence measured at day 1. Data are Mean ± S.E.M. No statistically significant differences were observed between alginate and chitosan-alginate formulations. # Compares values at day 28 vs. day 1 ($p<0.05$, Student's *t* test).

4.2.4 pH-Dependent Release of Antibody-Coated Nanocarriers from Microspheres

Next, we examined whether encapsulation within microspheres provided the intended release pattern at intestinal pH conditions, while precluding premature release at gastric pH. For this purpose, alginate microspheres and 0.25% chitosan-alginate microspheres (both containing similar loads of ^{125}I-IgG fluorescent NCs) were first incubated in SGF (pH 1.2) for 2 h followed by SIF (pH 7.8) for 4 h. These experiments were first conducted without GI enzymes to assess the effect of pH transitions on release, while subsequent experiments examined microsphere behavior in the presence of GI enzymes.

As seen in Fig. 4.5A, radioisotope tracing indicated that microspheres exhibited negligible release of antibody-coated NCs in SGF, with a slightly lower (but not significant) release in the absence of the chitosan coat (1% vs. 5% for alginate alone). Accordingly, the number of visibly intact microspheres as well as their size and

fluorescence content did not markedly vary upon incubation at gastric pH: ~85-95% of microspheres appeared to be intact (Fig. 4.5B), their size was slightly reduced by ~20-30% (Fig. 4.5C), and they retained ~95% of the initial sum fluorescence content while the mean fluorescence per area increased ~40% (Fig. 4.6). This suggests that in gastric pH, microspheres shrank to a modest degree, yet did not release NCs and may, hence, protect NCs in this environment.

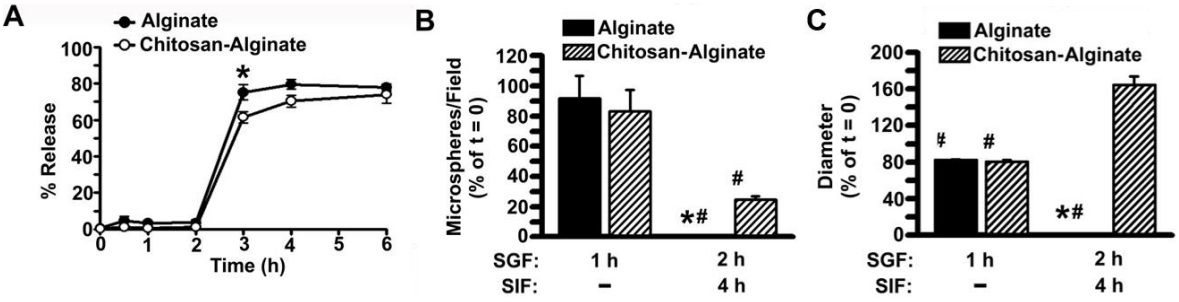

Figure 4.5. pH-dependent release of nanocarriers from microspheres. Alginate and 0.25% chitosan-alginate microspheres loaded with ^{125}I-IgG fluorescent NCs were incubated for 2 h at 37 ˚C in SGF at pH 1.2, and then transferred for 4 h at 37 ˚C to SIF at pH 7.8. (A) At the indicated times, aliquots were removed to assess the release of encapsulated NCs using radioisotope tracing. Aliquots were also removed after 1 h in SGF and 4 h in SIF (total incubation = 6 h) to quantify: (B) the number and (C) diameter of visibly intact microspheres from fluorescence microscopy images, expressed as the percentage of control values measured prior to GI incubations (t = 0). Data are Mean ± S.E.M. * Compares alginate vs. chitosan-alginate formulations; # compares values at each time point against those at t = 0 ($p<0.05$, Student's *t* test).

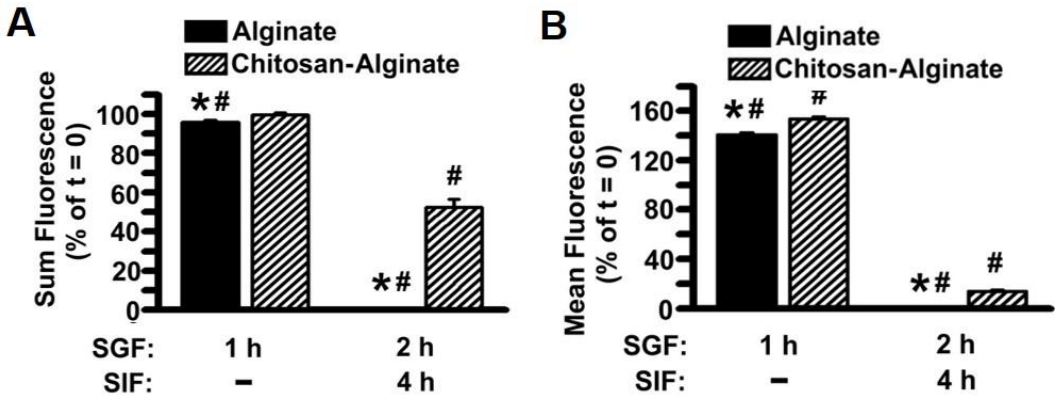

Figure 4.6. pH-dependent release of fluorescent nanocarriers from microspheres. Alginate and 0.25% chitosan-alginate microspheres loaded with IgG-coated fluorescent NCs were incubated for 2 h in SGF (pH 1.2) followed by a 4 h incubation in SIF (pH 7.8), as described in Fig. 4.5. At the indicated times, the: (A) sum fluorescence and (B) mean fluorescence intensity (sum / area) of visibly intact microspheres were quantified from fluorescence microscopy images. Values were expressed as a percentage of those measured prior to incubations (t = 0). Data are Mean ± S.E.M. * Compares alginate vs. chitosan-alginate formulations; # compares values at each time point against those at t = 0 ($p<0.05$, Student's *t* test).

Upon transferring microspheres to SIF, both formulations displayed burst release of antibody-coated NCs within the first hour (60-75% release), albeit to a lower extent for chitosan-coated microspheres (20% lower release; Fig. 4.5A). Whereas alginate microspheres reached the maximum level of release by this time, release from chitosan-alginate microspheres did not appear to plateau until 4 h in SIF (Fig. 4.5A). Therefore, the chitosan coat may help modulate burst release from microspheres, as expected. In agreement with these results, alginate microspheres fully dissolved by 4 h in SIF, as revealed by microscopy (Fig. 4.5B and 4.5C). Hence, no fluorescent content could be measured (Fig. 4.6). Meanwhile, 25% of the initial amount of chitosan-alginate microspheres remained (Fig. 4.5B), which swelled to ~160% of their initial size in this milieu (Fig. 4.5C) and retained only 50% of their initial fluorescence content (Fig. 4.6A). As a result, the mean fluorescence per area of chitosan-alginate microspheres considerably decreased (by 86%; Fig. 4.6B). Hence, both types of microspheres showed release at intestinal, but not gastric pH, and chitosan-coated formulations may be more amenable to control burst release in this environment.

4.2.5 Effect of Chitosan Concentration and Crosslinking on Microsphere Release

Given the results obtained by coating alginate microspheres with chitosan, we then evaluated the effects of increasing the concentration of the chitosan coat from 0.25% to

1%, and also that of crosslinking this coat with 1 mg/ml genipin. Genipin is a natural compound that provides a gentle, non-toxic method for crosslinking polymers, in contrast to synthetic crosslinking reagents, such as glutaraldehyde [119, 127]. As shown in Table 4.2, these modifications produced nearly equivalent characteristics as the former microsphere formulations, with a similar size distribution of ~180 µm, high encapsulation efficiency of ~95% and loading capacity of ~15% (w/w; NCs/alginate), corresponding to ~1.8 x 10^6 NCs/bead.

Similarly negligible (<4%) release of antibody-coated NCs was observed for all formulations in SGF at pH 1.2 (Fig. 4.7A), in agreement with minimal changes in this condition regarding the number of microspheres per field (Fig. 4.7B) and the total fluorescence content per microsphere (Fig. 4.8A). As seen above, all formulations showed a comparable (~20%) decrease in diameter in SGF (Fig. 4.7C), with a concomitant increase (~30-50%) in the mean fluorescence per area (Fig. 4.8A).

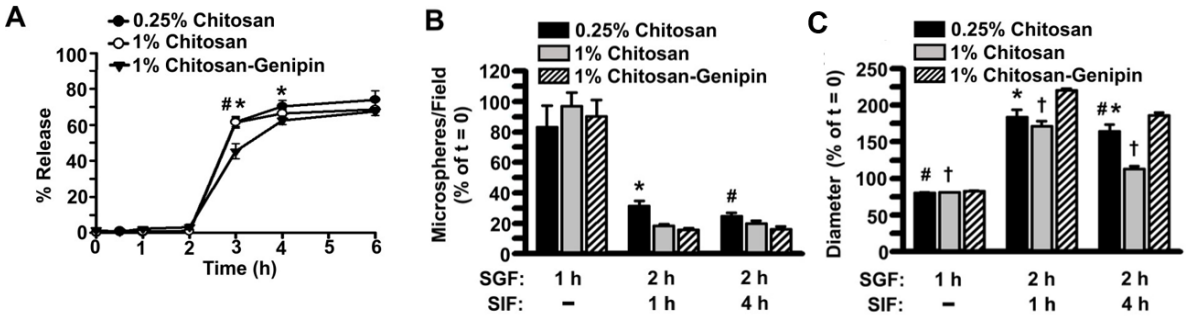

Figure 4.7. Effect of chitosan concentration and crosslinking on pH-dependent release from microspheres. Alginate microspheres containing ^{125}I-IgG fluorescent NCs were coated with either 0.25%, 1%, or genipin-crosslinked 1% chitosan, and incubated for 2 h in SGF at pH 1.2 followed by 4 h incubation in SIF at pH 7.8 (total incubation = 6 h). (A) NCs released from microspheres was assessed by radioisotope tracing of the released and encapsulated fractions, expressed a percentage of the total radioisotope content. In parallel, the (B) number and (C) diameter of visibly intact microspheres were quantified from fluorescence microscopy images, and expressed as the percentage of values measured prior to incubations (t = 0). Data are Mean ± S.E.M. * Compares 0.25% vs. 1% chitosan formulations; # compares 0.25% vs. 1% chitosan-genipin formulations; † compares 1% vs. 1% chitosan-genipin formulations ($p<0.05$, Student's *t* test).

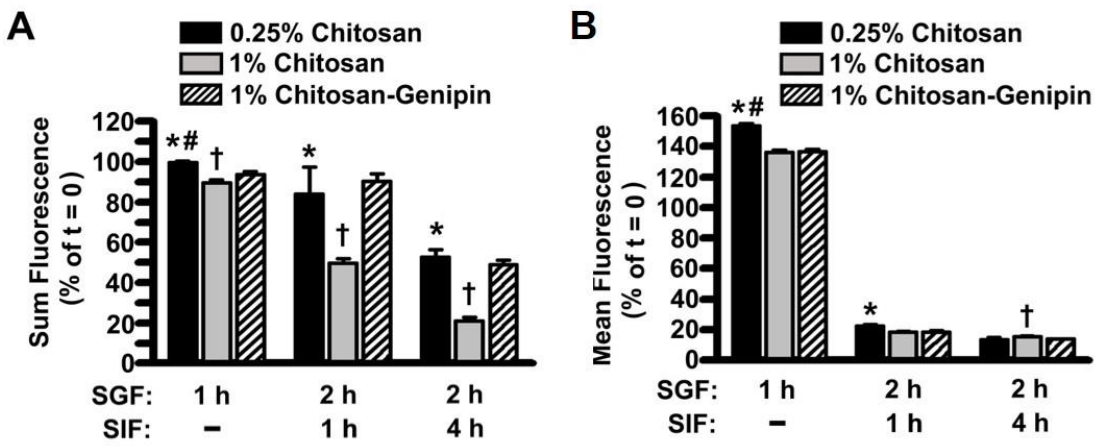

Figure 4.8. Effect of chitosan concentration and crosslinking on the pH-dependent release of fluorescent nanocarriers. Alginate microspheres loaded with ^{125}I-IgG fluorescent NCs were coated with 0.25% chitosan, 1% chitosan, or genipin-crosslinked 1% chitosan, and incubated in for 2 h in SGF (pH 1.2) followed by 4 h in SIF (pH 7.8) (6 h total incubation). At the indicated times, the (A) sum fluorescence and (B) mean fluorescence intensity (sum / area) of visibly intact microspheres were quantified from fluorescence microscopy images. Values were expressed as the percentage of those measured prior to incubations (t = 0). Data are Mean ± S.E.M. * Compares 0.25% vs. 1% chitosan formulations; # compares 0.25% vs. 1% chitosan-genipin formulations; †, compares 1% vs. 1% chitosan-genipin formulations ($p<0.05$, Student's *t* test).

Upon incubation in SIF at pH 7.8, microspheres with 1% chitosan coat displayed a similar release profile as 0.25% chitosan-alginate microspheres, with 61% release by 1 h after their transfer into SIF and 69% release by 4 h (Fig. 4.7A). Crosslinking of the 1% chitosan coat with genipin curtailed release by 25% after 1 h and 11% by 2 h in SIF (Fig. 4.7A), indicating that this formulation may better help control burst release. In parallel, when examining microspheres by microscopy, all formulations showed dissolution in SIF (Fig. 4.7B), swelling (Fig. 4.7C), and reduction of fluorescent content (Fig. 4.8). However, interesting differences were observed among these formulations. For instance, the diameter of 1% chitosan-coated microspheres was lower in intestinal conditions than that of 0.25% chitosan-coated microspheres (113 vs. 164% of t = 0 by 4 h in SIF; Fig. 4.7C). Hence, increasing the chitosan concentration altered the morphology of intact microspheres in SIF.

Although we had observed similar release of the ^{125}I-antibody counterpart (Fig. 4.7A), the lower sum fluorescence per microsphere of the 1% vs. 0.25% chitosan coat (e.g., 21 vs. 53% of t = 0 by 4 h in SIF; Fig. 4.8A), may indicate that NCs (not antibodies that may have detached from the NC coat) are better retained in the latter preparation. Crosslinking the 1% chitosan coat with genipin resulted in similar behavior as 0.25% chitosan microspheres, e.g., it increased the diameter by 39% at 4 h in SIF with respect to 1% chitosan microspheres (Fig. 4.7C), and also increased the retention of NCs by 57% at this time (Fig. 4.8A).

4.2.6 Microsphere Protection and Release of Nanocarriers in Gastrointestinal Conditions

In addition to examining the pH-dependent release of ^{125}I-IgG NCs from microspheres in fluids mimicking GI pH, we evaluated this aspect as well as the status of encapsulated NCs in the presence of GI enzymes, to infer the protection provided by microspheres. First, we examined whether all four formulations of alginate and chitosan-alginate microspheres would protect encapsulated antibody-coated NCs (only the antibody counterpart is labile) from premature gastric degradation. For this purpose, microspheres were incubated for 2 h in SGF in the presence vs. absence of pepsin (Fig. 4.9A). Since microspheres remained intact in gastric pH, we used EDTA to induce their release after incubation in these milieus. The level of free ^{125}Iodine (indicative of antibody degradation) in the released NC fraction was then quantified. In the absence of pepsin, the contents in all formulations, as well as non-encapsulated IgG NCs, displayed <10% degradation (Fig. 4.9A), which is expected since low pH should not result in antibody proteolysis. Most importantly, in the presence of pepsin, non-encapsulated IgG NCs was subjected to ~70% degradation, which was

largely attenuated by encapsulation within all microsphere formulations (<15% degradation) (Fig. 4.9A). Although all microspheres performed similarly in this regard, alginate microspheres showed statistically lower protection than chitosan-alginate formulations.

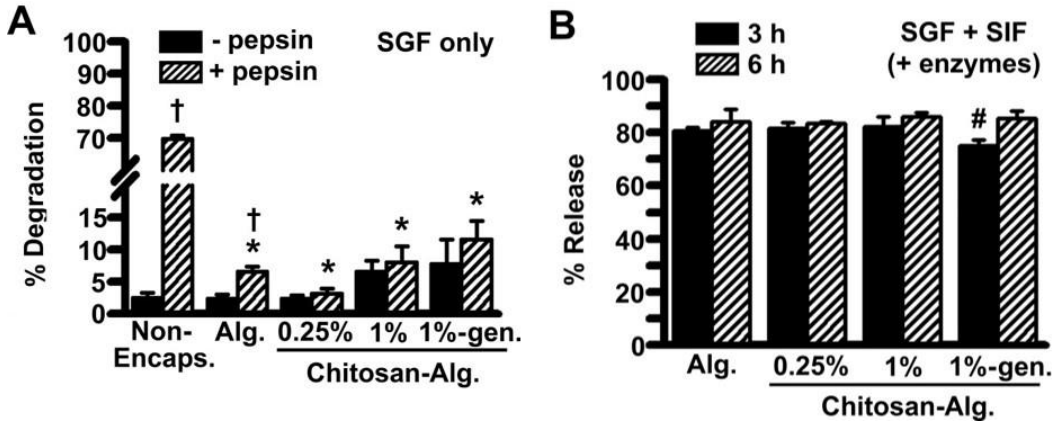

Figure 4.9. Microsphere protection and release of nanocarriers in gastrointestinal conditions. (A) Non-encapsulated ^{125}I-IgG NCs vs. ^{125}I-IgG NCs encapsulated in alginate microspheres with or without a 0.25%, 1%, or genipin-crosslinked 1% chitosan coat, were incubated for 2 h at 37 ˚C in SGF (pH 1.2) in the presence or absence of pepsin. Due to lack of NC release at this pH, microspheres were dissolved in EDTA to release the NC content. Content degradation was assessed by radioisotope quantification of free ^{125}Iodine (indicative of antibody degradation), expressed as a percentage of the total radioisotope content. (B) Microspheres were incubated in SGF containing pepsin as in (A) followed by a 4 h incubation at 37 ˚C in SIF containing pancreatin (pH 7.8). The percentage of ^{125}I-IgG NCs released from microspheres was determined by radioisotope tracing. Data are Mean ± S.E.M. * Compares non-encapsulated NCs vs. other formulations; no statistically significant difference was observed between other groups ($p<0.05$, one-way ANOVA followed by Tukey test). † Compares the presence vs. absence of pepsin; # compares 3 h vs 6 h ($p<0.05$, Student's *t* test).

Then, we examined NC release after a 2 h incubation in pepsin-containing SGF, followed by a 4 h incubation in pancreatin-containing SIF. Significant release (75-80%) of encapsulated NCs occurred by 1 h in enzyme-containing SIF (Fig. 4.9B), similar to the

level of release that had been observed in the absence of enzymes. Hence, this more physiologically relevant condition indicated that encapsulation within alginate and, primarily, chitosan-alginate microspheres, prevents premature gastric degradation of the antibody counterpart, in addition to release in intestinal conditions.

4.2.7 Receptor Targeting by Nanocarriers Released from Microspheres under Gastrointestinal Conditions

Given the above results, we next examined if antibody-coated NCs can bind an immobilized target (secondary antibody, as described above), when released from microspheres after incubation in enzyme-containing SGF and SIF. First, to provide a baseline for the subsequent comparison to GI conditions, we measured the extent of binding after EDTA-induced release from microspheres in storage. As shown in Fig. 4.10, NCs that had been encapsulated displayed substantial binding, with 10^6 – 10^7 NCs bound per well, with greater binding observed for 1% chitosan microspheres and the non-encapsulated control. Incubation of non-encapsulated antibody-coated NCs with enzyme-containing SGF, or SGF followed by SIF, resulted in a significant reduction in their binding ability: 10^2 NCs/well in SGF alone (95% reduced binding compared with storage conditions) and no detectable binding in SGF followed by SIF incubation (Fig. 4.11A). This parallels the high degradation observed for non-encapsulated counterparts (Fig. 4.11A).

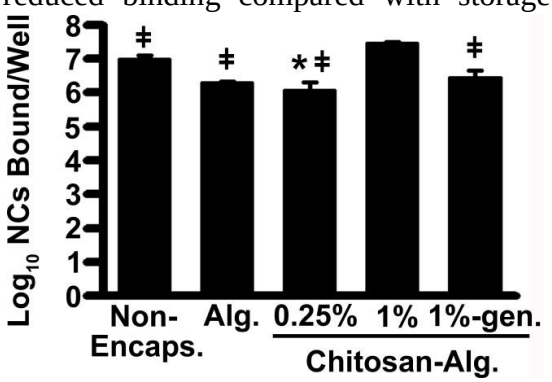

In contrast, NCs encapsulated within microspheres retained their targeting ability after incubation in SGF, or SGF followed by SIF: 10^5 – 10^7 NCs bound/well (Fig. 4.11A). This suggests that the protection and controlled release afforded by encapsulation may render sufficient receptor-targeting of antibody-coated NCs when administered via the oral route.

Figure 4.10. Binding of fluorescent nanocarriers released from microspheres in storage conditions. The binding ability of non-encapsulated ^{125}I-IgG NCs vs. ^{125}I-IgG NCs encapsulated in alginate, 0.25% chitosan-, 1% chitosan-, or genipin-1% chitosan-alginate microspheres was assessed after 1 day in control storage conditions, serving as a comparison to binding of respective formulations in GI conditions. This required release of NCs by EDTA-induced dissolution of microspheres, since no natural release occurs in storage. IgG NCs were incubated with secondary antibody-coated wells to allow binding, as described in Fig. 2. Wells were washed to remove non-bound counterparts, and radioisotope tracing was used to quantify the number of NCs bound per well. Data are Mean ± S.E.M. * Compares non-encapsulated NCs vs. other formulations; ǂ, compares 1% chitosan microspheres vs. other formulations ($p<0.05$, one-way ANOVA followed by Tukey test).

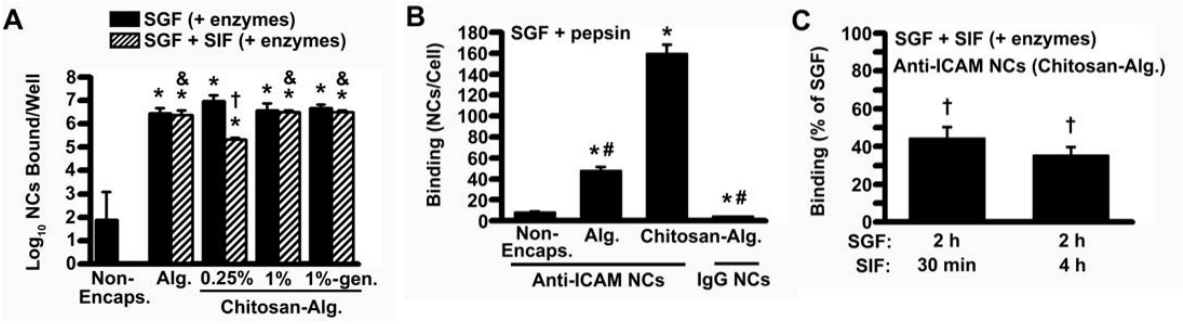

Figure 4.11. Receptor targeting by nanocarriers released from microspheres in gastrointestinal conditions. Non-encapsulated ^{125}I-IgG NCs vs. ^{125}I-IgG NCs encapsulated in alginate microspheres with or without a 0.25%, 1%, or genipin-crosslinked 1% chitosan coat, were incubated in enzyme-containing SGF, or SGF followed by SIF as in Fig. 5. NCs that were released by EDTA in the case of SGF incubation, or those naturally released after SGF + SIF incubation, were tested. (A) Binding of non-encapsulated vs. microsphere-released ^{125}I-IgG NCs onto secondary antibody-coated wells, measured by radioisotope tracing. (B) Anti-ICAM NCs (non-encapsulated vs. loaded into alginate or 0.25% chitosan-alginate microspheres) vs. non-specific IgG NCs loaded into 0.25% chitosan-alginate microspheres, were incubated in pepsin-containing SGF as in (A). Due to lack of release in this condition, NCs were released by EDTA and their ability to bind to cells (reflective of microsphere protection under gastric conditions) was tested. Binding was assessed by incubation for 2 h at room temperature with ICAM-1-expressing, fixed HUVECs. The number of NCs bound per cell was quantified by fluorescence microscopy after washing non-bound NCs. (C) Cell binding of non-encapsulated vs. anti-ICAM NCs naturally released from microspheres after incubation with enzyme-containing SGF followed by SIF was examined by fluorescence microscopy, and normalized to their binding prior to reaching intestinal conditions (where they were protected). Data are Mean ± S.E.M. * Compares binding of non-

encapsulated vs. microsphere-encapsulated NCs; # compares binding to that of anti-ICAM NCs within chitosan-alginate microspheres; † compares binding in SGF vs. SGF followed by SIF; ($p<0.05$, Student's *t* test). & compares 0.25% chitosan microspheres vs. other formulations ($p<0.05$, one-way ANOVA followed by Tukey test).

To further verify this hypothesis, we examined the targeting potential of antibody (anti-ICAM)-coated NCs to its receptor (ICAM-1) expressed on cells, after release from microspheres. First, we tested binding on HUVEC (vascular endothelial cells), which serve as a comparison to extensive literature on targeting to these cells [9, 37, 86, 117, 128, 129]. Since no major differences had been observed among the three chitosan-alginate formulations tested, we selected the simplest formulation composed of 0.25% chitosan-alginate to compare with alginate alone. As shown in Fig. 4.12B, after 2 h in pepsin-containing SGF, minimal binding (8 NCs bound/cell) was observed for control anti-ICAM NCs that had not been encapsulated in microspheres, as expected due to considerable degradation (Fig. 4.9A). In contrast, anti-ICAM NCs retained within microspheres and then released by EDTA (since there is no release in SGF) revealed significant binding: 48 NCs/cell and 159 NCs/cell for alginate and chitosan-alginate formulations, respectively. This reflected specific targeting by anti-ICAM NCs, since non-specific IgG NCs loaded into chitosan-alginate microspheres only resulted in 4 NCs bound/cell, signifying 49-fold enhanced targeting for anti-ICAM NCs vs. IgG NCs. Further transfer of anti-ICAM NC-loaded microspheres from pepsin-containing SGF to pancreatin-containing SIF caused a reduction in NC binding on cells (~60% reduction), yet considerable binding was still detected: 60-70 NCs/cell. Hence, it seems possible to achieve receptor-mediated targeting of NCs via the oral route when encapsulated within protective, controlled release vehicles.

We then similarly evaluated ICAM-1 targeting of encapsulated vs. non-encapsulated antibody-coated NCs in Caco-2 cells, a prevalent GI epithelial cell model [130]. This will allow us to evaluate potential binding to the GI epithelium, which may differ from binding to endothelial cells as a result of varying morphology (e.g., endothelial cells are large and flat, while GI epithelial cells are narrow, columnar, and villous), ICAM-1 expression, and the presence of brush border enzymes [13]. As shown in Fig. 4.12, after 2 h in pepsin-containing SGF, minimal binding (3 NCs bound/cell) was observed for non-encapsulated anti-ICAM NCs, similar to our findings in endothelial cells (Fig. 4.11B). Anti-ICAM NCs protected by chitosan-alginate microspheres, on the other hand, revealed significantly greater binding: 20 NCs/cell, yet lower than levels observed in endothelial cells. This discrepancy was previously observed for anti-ICAM NCs in storage conditions, suggesting that lower binding can be attributed to differences between these cell types, as described above. The specificity of targeting was demonstrated by the comparatively low binding of non-specific IgG NCs loaded into chitosan-alginate microspheres (6 NCs bound/cell).

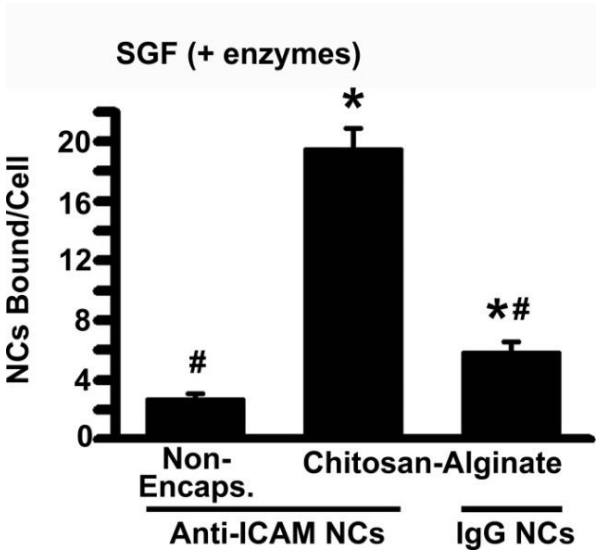

Figure 4.12. Nanocarrier targeting to GI epithelial cells after release from microspheres in gastrointestinal conditions. Anti-ICAM NCs (non-encapsulated vs. loaded into 0.25% chitosan-alginate microspheres) vs. non-specific IgG NCs loaded into 0.25% chitosan-alginate microspheres, were incubated in pepsin-containing SGF. NCs were released by EDTA, and their binding was assessed by incubation for 2 h at room temperature with ICAM-1-expressing, fixed Caco-2 cells. The number of NCs bound per cell was quantified by fluorescence microscopy after washing non-bound NCs. Data are Mean ± S.E.M. * Compares binding of non-encapsulated vs. microsphere-

encapsulated NCs; # compares binding to that of anti-ICAM NCs within chitosan-alginate microspheres; ($p<0.05$, Student's *t* test).

4.2.8 Oral Gavage of Encapsulated ICAM-1-Targeted Nanocarriers in Mice

Following verification of protection and release afforded by microspheres, and the resulting targeting to ICAM-1-expressing cells, we examined the degradation and biodistribution of encapsulated anti-ICAM NCs following *in vivo* administration in mice. For these studies, ^{125}I-anti-ICAM NCs were encapsulated in 0.25% chitosan-alginate microspheres. This formulation was administered to mice via oral gavage and compared to oral gavage of non-encapsulated ^{125}I-anti-ICAM NCs.

We first evaluated whether microspheres conferred protection against anti-ICAM degradation by quantifying the level of free ^{125}Iodine with respect to the total ^{125}Iodine content in each section of the GI tract (Fig. 4.13A). In agreement with observations *in vitro*, encapsulation in chitosan-alginate microspheres resulted in significant protection, with 60-70% of the total antibody content being preserved, while only 20-40% of the non-encapsulated control was preserved. This represented a 2-3-fold enhancement in protection for encapsulated anti-ICAM NCs as compared to non-encapsulated formulations. Importantly, anti-ICAM NC encapsulation within microspheres rendered lower retention in the stomach vs. non-encapsulated counterparts (36% vs. 59% ID/g), which is important for minimizing degradation (Fig. 4.13B). Instead, encapsulation enhanced NC biodistribution in the small intestine (22% vs. 6% ID/g) and the large intestine (8 vs. 0.9 %ID/g; Fig. 4.13B), desirable for treatment of pathologies in these regions or absorption into the circulation. In fact, additional experiments examining different sections of the

small intestine showed that enhanced intestinal biodistribution conferred by encapsulation was attributed to 9-fold greater localization in the duodenum.

Figure 4.13. Protection and biodistribution of microsphere-encapsulated ICAM-1-targeted nanocarriers in the GI tract of mice. Mice were orally gavaged with ^{125}I-anti-ICAM NCs (non-encapsulated vs. encapsulated in 0.25% chitosan-alginate microspheres) or non-specific ^{125}I-IgG NCs encapsulated in 0.25% chitosan-alginate microspheres. One hour after administration, the indicated sections of the GI tract were harvested and subjected to TCA precipitation to determine: (A) the percentage of free ^{125}Iodine (reflective of degradation) with respect to the total ^{125}Iodine content, (B-C) the ^{125}I-content and tissue weight, to calculate the percent gavaged dose per gram. Data are Mean ± S.E.M. * Compares non-encapsulated and encapsulated groups. # compares encapsulated anti-ICAM NCs vs. encapsulated IgG NCs. ($p<0.05$, Student's *t* test).

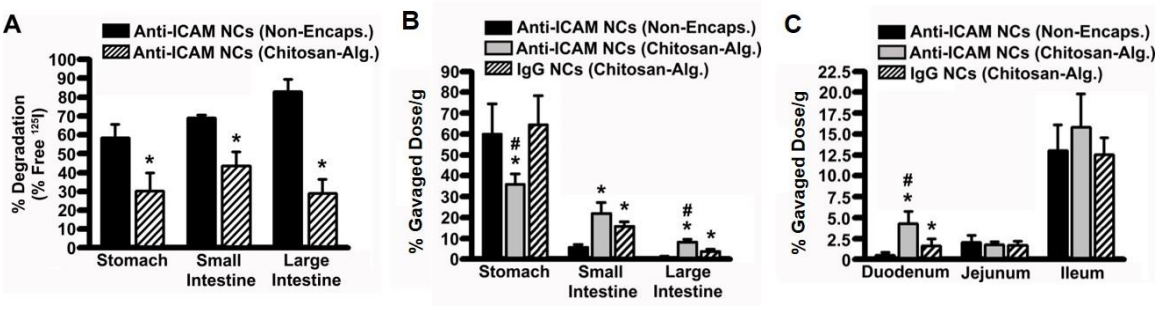

Finally, to assess targeting specificity, we compared anti-ICAM NCs to IgG NCs, both of which were encapsulated within 0.25% chitosan-alginate microspheres. Similar to targeted counterparts, IgG NCs showed a similar decrease in retention in the stomach (64 %ID/g) and enhanced accumulation in the small and large intestine (16 and 4 %ID/g) with respect to the non-encapsulated control (Fig. 4.13B). However, intestinal accumulation was reduced compared to that of anti-ICAM NCs, suggesting specific targeting. In fact, duodenal biodistribution of IgG NCs was significantly lower (3-fold) than that of anti-ICAM NCs (Fig. 4.13C). Taken together, ICAM-1-targeted NCs encapsulated in chitosan-alginate microspheres provide enhanced protection in the stomach, and site-specific accumulation in the small intestine, specifically the duodenum.

4.3 Discussion

Receptor-mediated targeting of drug carriers offers an opportunity to enhance their biodistribution as well as transport within or across cells [7, 52, 123]. These advantages also apply to oral delivery of drugs [2, 6, 53-58]. However, most targeting moieties are labile molecules (antibodies, peptides, aptamers, etc.) susceptible to premature inactivation and degradation *en* route to the intestine, an important target for therapeutic intervention and primary site of drug absorption [53]. Although encapsulation of drugs, biologicals, and carriers within controlled release hydrogels has been extensively studied [4, 16, 17, 48, 49, 105, 107, 109, 119, 121, 124], this approach remains largely unexplored in the case of receptor-targeted NCs. Using the example of ICAM-1 targeting by model antibody-coated polystyrene NCs, we have examined whether encapsulation within controlled released hydrogels provides protection against degradation in gastric conditions and intestinal release for specific targeting, and demonstrated this in *in vitro*, cell culture, and mice studies.

As described, we selected alginate microspheres as a model based on its biocompatibility and gentle formulation [17, 48, 49, 105, 107, 109, 121, 124]. The method employed produced uniform microspheres, in terms of size and shape, with a suitable size for oral gavage in mice (~180 μm in diameter). The encapsulation efficiency was very high (97%), with minimal release (<10%) over 28 days in storage conditions. These parameters did not vary when alginate microspheres were modified with different chitosan coatings, as expected since these modifications were conducted after, not during, encapsulation into the alginate core, as shown in other cases [107]. This high encapsulation efficiency varies

from other works that observed drug leaching from alginate beads [16, 17]. Similar, yet still lower, encapsulation efficiency has been seen for antibodies (~80%) [48]. This suggests that the porosity and mesh-pore size of the alginate matrix does not prevent leaching of small contents and water-soluble drugs [16, 17, 48], but it can prevent diffusion of encapsulated antibody-coated NCs, likely because of their greater size. Hence, this may be a viable application for alginate hydrogels. In fact, the stability of microspheres and minimal release of encapsulated NCs over 28 days in storage contrasts that of other alginate microspheres with similar size: this is the case for <300 μm diameter formulations which showed compromised microsphere stability, particularly when bulky loads (e.g., mammalian cells) occupied a large volume within the polymer [107].

Whereas microspheres suit the size requirements for oral gavage in mice, we have also formulated ~2.8 mm-diameter alginate and chitosan-alginate beads for future *in vivo* studies in larger animals, such as rats. The encapsulation strategy is similar to that used to create microspheres, except that alginate was extruded through a larger diameter needle, as in [48]. Similar to the microsphere formulations, larger beads exhibited a uniform size and spherical shape, even distribution of encapsulated NCs throughout the alginate core, and relatively efficient loading (70-80 EE%), which did not significantly differ in the presence of a chitosan shell. However, the encapsulation efficiency was considerably lower than that observed for microspheres, and paralleled that shown for previously reported beads of this size [48]. We speculate that higher percent loading of NCs in these beads (32 vs. 16%, v/v) may have compromised the strength of the alginate network, given the large volume occupied by NCs. Moreover, the distinct processing conditions used to create larger beads, including mechanical vs. air flow-driven extrusion, may give rise to a generally lower

encapsulation efficiency for larger beads [48, 49]. Hence, future optimization of these conditions may be required for higher loading. Nevertheless, these beads serve as a viable alternative to microspheres for *in vivo* experiments.

With regard to encapsulation of biological agents in alginate beads, we observed minimal degradation (<5%) of the antibody coat within microspheres, which did not seem to result from the encapsulation procedure itself, since the level of degradation was similar to that of non-encapsulated counterparts in storage conditions. In addition, encapsulated NCs retained ~90% of their targeting ability with respect to non-encapsulated counterparts, indicating that encapsulation is not detrimental to this function and, once released, the polymer does not interfere with binding. These results are key in pursuing these formulations for receptor-targeted applications, and agree with previous reports documenting the binding ability of IgY antibodies following encapsulation in chitosan-alginate beads [48].

Yet, a prevailing requirement of encapsulation strategies for oral therapies containing labile targeting agents, particularly proteins, is to provide protection from low gastric pH as well as proteases present in the stomach [4]. In agreement with previous literature, alginate microspheres remained insoluble at a low pH characteristic of the stomach and retained encapsulated NCs, as observed by tracking both the antibody and NC counterparts. Microspheres also appeared to shrink in gastric buffer, which may be a result of displacement of Ca^{2+} by monovalent H^{+} ions prevalent in a low pH environment, causing the gel network to collapse [17]. It appears that the chitosan shell is permeable to this ion exchange, as all chitosan-alginate formulations decreased in diameter to a similar degree as alginate alone.

As expected, alginate microspheres solubilized within 1 h of incubation at intestinal pH, likely due to Ca^{2+} displacement and the negative charge of carboxylic groups acquired at neutral pH. Coating with 0.25% chitosan reduced the level of burst release to some extent, confirming previous reports [48, 49]. Observations by fluorescence microscopy indicated that while the alginate core may have dissolved, the chitosan shell allowed some, but not all, microspheres to remain visible. Consequently, these "visible" chitosan-alginate microspheres could be traced, allowing us to observe a significant degree of swelling. Importantly, these microspheres retained the majority of the encapsulated fluorescent content (the NC counterpart) by 1 h in intestinal pH, which was then slowly released to ~50% of the initial content by 4 h at this pH. Radioisotope tracing of the antibody counterpart revealed faster release, suggesting that some antibodies may detach from the NC coat during this process and diffuse through the chitosan coat. Nevertheless, binding of released NCs onto cells indicated that a sufficient degree of antibodies remained on NCs to provide specific targeting.

The results described above suggest that the combination of burst release and swelling contribute to the mechanism of release from chitosan-alginate microspheres. Increasing the concentration of chitosan from 0.25% to 1% did not significantly alter the degree or mechanism of release. However, crosslinking the chitosan shell with genipin further curtailed the initial burst release, in agreement with previous work [119, 127]. Yet, while this was observed when tracking antibody release by radioisotope tracing, such crosslinking did not increase the number of intact microspheres or fluorescence content per microsphere compared to non-crosslinked formulations. As such, it can be speculated that burst release (as more accurately measured by radioisotope tracing of the bulk solution)

has a larger contribution to overall release than release from intact microspheres. Alternatively, it is possible that genipin crosslinking helps to retain the fraction of antibodies which may detach from the NC surface, suggesting that genipin crosslinking may not exert an advantage for NC formulations where targeting antibodies are covalently attached on their surface. Nevertheless, the microspheres studied herein exhibited pH-sensitive release, which holds significance for oral formulations requiring protection from gastric conditions and release in intestinal conditions.

Moreover, in agreement with minimal release from microspheres at gastric pH, encapsulated NCs showed minimal degradation and considerable targeting after exposure to SGF, which was also the case in the presence of gastric enzymes. Non-encapsulated NCs, on the other hand, were degraded to a great extent and showed little binding after incubation in these conditions. Hence, the mesh pore size of microspheres is seemingly small enough to prevent penetration of enzymes into the alginate core. Counterintuitively, increasing the chitosan concentration and crosslinking chitosan resulted in a modest, yet increase in degradation, which was unexpected. However, it is plausible that these changes are merely due to restricted release through the chitosan coat of NCs bearing degraded antibody. In support of this, degradation and loss of targeting ability of NCs encapsulated in 1% chitosan and crosslinked 1% chitosan microspheres did not increase in the presence of gastric enzymes, indicating that the increase in degradation was not due to greater penetration of enzymes but rather, greater retention of degraded products within the microsphere, which could then be measured. In addition to encapsulated NCs retaining binding ability after incubation in gastric conditions, significant targeting was also verified upon release in SIF in presence of pancreatin, while binding of non-encapsulated

counterparts was abolished. Therefore, encapsulation affords protection of targeted NCs in gastric and intestinal conditions in the presence of digestive enzymes, preserving functional activity of targeting moieties to a considerable extent.

An application that could benefit from this encapsulation strategy is targeting to ICAM-1, a molecule expressed on the GI and other tissues, involved in GI (among other) pathologies associated with inflammation, including infections, immune alterations, cancers, genetic conditions, etc. [10, 113]. NCs and conjugates directed by ICAM-1-targeted ligands have shown promising results regarding delivery of therapeutic and imaging agents in numerous disease applications [9, 27, 30-32, 37, 131-138]. Moreover, in GI epithelial monolayers, anti-ICAM NCs facilitated intra- and transepithelial delivery of a model therapeutic enzyme (α-Galactosidase, deficient in Fabry disease [139]), revealing particular promise for oral delivery [13]. However, oral delivery *in vivo* was limited by premature degradation of ICAM-1 targeted antibodies in the stomach [15]. Our results hereby indicate that encapsulation in chitosan-alginate microspheres could overcome these obstacles for oral delivery of ICAM-1 targeted systems. In fact, after incubation in GI-mimicking buffers containing digestive enzymes, encapsulated NCs demonstrated a significant degree of specific binding to ICAM-1 expressing cells, including both vascular endothelial and GI epithelial cells, relative to both control IgG NCs loaded into chitosan-alginate microspheres and non-encapsulated anti-ICAM NCs. Importantly, relative to non-encapsulated counterparts, microspheres revealed substantial protection of anti-ICAM NCs against degradation in all sections of the GI tract upon oral gavage in mice. Encapsulation also lowered retention in the stomach and enhanced biodistribution in the small and large intestine, specifically in the duodenum. In this segment, the specificity of ICAM-1

targeting was apparent compared to that of encapsulated IgG NCs. Therefore, enhanced intestinal biodistribution of anti-ICAM NCs loaded within chitosan-alginate microspheres, particularly in the duodenum, is a result of both pH-dependent release from microspheres and ICAM-1 targeting.

4.4 Conclusion

Alginate and chitosan-alginate microspheres formulated in the present study provided protection of antibody-targeted NCs in storage and gastric conditions (including pH and digestive proteases), with pH-sensitive release in intestinal conditions. Following transit in gastric and intestinal conditions, NCs released from microspheres retained a significant degree of targeting ability, as measured in *vitro*, cell culture, and animal models. Therefore, this encapsulation strategy may be valuable for implementing oral delivery of targeted drug carriers, where protection from harsh gastric conditions and intestinal bioavailability is required. Whereas this encapsulation strategy was hereby illustrated for ICAM-1 targeting and antibody-coated polymer NCs, similar approaches may benefit other targeted systems which employ labile targeting moieties against this and other GI surface markers.

Chapter 5: Distinct Endocytic Routing of Monomeric ICAM-1 Targeted Ligands Enables Transport Into and Across Gastrointestinal Epithelial Cells

5.1 Introduction

In Chapter 4, we demonstrated that encapsulation of anti-ICAM NCs in chitosan-alginate microspheres affords them with protection in gastric conditions, pH-triggered release in intestinal conditions, and targeting to ICAM-1-expressing cells following release. It is therefore conceivable that following release from microspheres and subsequent binding to cells, anti-ICAM NCs will induce CAM-mediated uptake and transport across cultured GI epithelial cells, as previously demonstrated [13]. Moving forward, the goal of Chapter 5 was to evaluate whether these phenomena also hold for targeted carriers that bind to ICAM-1 in a monomeric fashion (e.g., anti-ICAM antibodies). Cellular transport of monomeric ICAM-1 ligands may provide an opportunity for direct conjugation of these ligands to therapeutic or imaging agents for oral delivery. This holds significance because, in contrast to multimeric targeting strategies, direct conjugation may offer a simpler formulation from a manufacturing perspective and may lead to distinct characteristics regarding biodistribution, cellular trafficking, metabolism, clearance, etc., expanding the range of future oral applications of ICAM-1 targeting beyond existing multimeric strategies.

Following release from encapsulation vehicles, targeted delivery systems must be capable of binding to absorptive cells in the GI epithelium, which triggers transport into and/or across these cells, e.g., by endocytic mechanisms. As described in Chapter 2, receptor-targeted conjugates and carriers may significantly differ in their ligand-receptor

interactions and subsequent endocytic fates [7]. For example, a small drug conjugate typically involves interaction of one ligand with one receptor (or two if a divalent antibody is used), while larger drug conjugates and NCs employ multiple copies of a ligand to engage multiple copies of a cell surface receptor [7]. In nature, receptors typically bind to either monomeric or multimeric ligands, but rarely both [140]. As a consequence, drug targeting to endocytic receptors does not guarantee a similar uptake efficacy or mechanism to that of natural, unmodified ligands of said receptors, as observed in several studies [37, 141-143]. This is also the case with regard to intracellular routing after endocytosis: some receptors may follow more than one itinerary (e.g., to lysosomes, recycling compartments, transcytosis, etc.), which further depends on whether they are bound by natural or artificial ligands, or by monomeric vs. multimeric counterparts, as observed for receptors of immunoglobulins, transferrin, and folate, for instance [141, 142, 144-146]. Therefore, understanding the endocytic fate of ligands employed for targeted drug delivery is important in order to determine the efficacy of these strategies and the selection of suitable therapeutic applications. Our knowledge of endocytic events not only benefits the translation of targeted systems exploiting these pathways [52], but also provides insight on the biological regulation of cell surface receptors: endocytosis of cell surface receptors mediates a wide range of physiological functions, including cellular uptake of nutrients, signal transduction, recycling of membrane components, and clearance of foreign or pathogenic elements [140, 147].

Most previous studies comparing the endocytic fates of drug targeting platforms against natural ligands have examined receptors whose said natural ligands are monomeric (transferrin, folate, aminopeptidase A, etc.) [141-143]. There are fewer studies available

regarding receptors whose natural ligands are multimeric. Perhaps one of the examples where more mechanistic information is available is that of drug targeting to ICAM-1 [12, 87, 92, 93, 117]. Previous studies on ICAM-1 targeting in vascular endothelial and GI epithelial cells revealed that this molecule undergoes efficient uptake by CAM-mediated endocytosis when bound in a multimeric manner [9, 12, 37]. This pairs well with the fact that natural ligands of ICAM-1 bind this molecule in a multimeric fashion, including leukocytes, apoptotic bodies, plasmodium-infected erythrocytes, and pathogens such as major class rhinoviruses, etc. [148-152]. As a result of such prominent uptake, CAM-mediated endocytosis and the subsequent intracellular itinerary of multimeric ICAM-1 conjugates and carriers has been well documented, using vascular endothelial cells as a model, allowing us to exploit this pathway for intracellular drug delivery [9, 25-28, 31-35]. In addition to providing intracellular delivery, CAM-mediated uptake of multimeric carriers leads to transcytosis across GI epithelial cells, enabling delivery of therapeutics across this barrier [13]. Therefore, ICAM-1 mediated transport provides a valuable gateway for oral therapies aimed at entering GI epithelial cells, for local interventions, or traversing these cells for entry into the systemic circulation.

While endocytosis of monomeric ligands targeting ICAM-1 did not seem prominent a priori [9], their pathway of uptake has not been examined. In addition, certain plasmalemma receptors can be internalized in the absence of ligand binding and their intracellular itinerary can differ from that of the ligand-receptor complex [146, 153, 154], yet potential endocytosis of unbound ICAM-1 also remains largely unexplored. Indeed, ICAM-1 has been observed to recycle back to the cell surface after separating from ligands in endocytic compartments [92], a phenomenon which seems reminiscent of the continuous

redistribution of ICAM-1 between the cell surface and an intracellular pool in certain immune cells [155]. Hence, the first portion of this chapter seeks to evaluate the endocytic regulation of ICAM-1 itself and its monomeric vs. multimeric ligands, to shed light on the biological regulation of ICAM-1 and its utility for diverse therapeutic applications. This was performed in vascular endothelial cells, where fundamental knowledge on multimeric ICAM-1 ligands was previously characterized [12, 87, 92, 93, 117].

As described in Section 2.3.2, CAM-mediated endocytosis induced by targeting ICAM-1 leads to transcytosis across cellular barriers, as previously shown for ICAM-1-targeted NCs in cultured GI epithelial and brain microvascular endothelial cell monolayers [13, 14]. Such transport enabled intracellular and transcellular delivery of a model therapeutic enzyme in cultured GI epithelial monolayers, valuable in the context of therapies aimed at either treating gastrointestinal disorders or reaching the systemic circulation via the oral route [13]. Moreover, no apparent paracellular leakage of a luminal marker was observed during transport, suggesting that CAM-mediated transcytosis may preserve the integrity of cellular barriers [13]. These findings also agree with delivery of ICAM-1 targeted NCs into systemic organs upon intravenous injection in mice, without any apparent side effects compromising safety [27]. Therefore, ICAM-1 targeting holds promise for drug delivery into cells for the treatment of intracellular pathologies, as well as across cellular barriers for access to the circulation (e.g., relevant for oral delivery) or tissues beyond the systemic circulation.

Nevertheless, the potential of monomeric ICAM-1 targeting strategies for oral delivery has yet to be elucidated. Therefore, the second portion of this chapter explores whether the novel knowledge gained on endocytosis of monomeric ICAM-1 ligands in

endothelial cells can be exploited for oral delivery in GI epithelial cells. In doing so, we first evaluated whether (A) the pathway of uptake and intracellular trafficking observed for monomeric anti-ICAM in endothelial cells also occurs in GI epithelial cells. We then determined whether (B) such uptake leads to transcytosis across GI epithelial cells, as it does for multimeric anti-ICAM NCs [13]. Hence, this knowledge would provide a novel opportunity to utilize monomeric ICAM-1 ligands as an alternative vehicle for intracellular and transcellular delivery in the GI epithelium.

5.2 Results

5.2.1 Degree of Uptake of Monomeric vs. Multimeric ICAM-1 Ligands in Endothelial Cells

A well characterized monoclonal antibody to human ICAM-1 (R6.5) [156, 157] was used as a model ligand capable of specific binding to ICAM-1 on human endothelial cells. To provide monomeric vs. multimeric binding, the antibody was used either as a naked molecule in solution or as multiple copies coated on the surface of polymer nanoparticles (see the Sections 3.3 and 4.2.1 for details), both of which have been extensively characterized [12, 92, 93, 122]. As previously demonstrated, these two ICAM-1 binding entities showed specificity against ICAM-1 expressed on activated endothelial cells: 174 NCs/cell after a 60 min incubation (90-fold over non-specific IgG NCs) and 3.8×10^8 fluorescence units (38-fold over IgG) [9, 86].

Incubation of human endothelial cells with anti-ICAM vs. anti-ICAM NCs was conducted in a pulse-chase manner to track endocytosis without concomitant binding taking place. We used an established technique that allows differential visualization of cell-

surface-bound (yellow color in Fig. 5.1A) vs. internalized (green color) ligands by fluorescence microscopy [12, 25, 87, 92, 93, 117]. This allowed us to observe a significantly high uptake of multimeric anti-ICAM NCs, as expected: ~90% of total cell-associated carriers by 1 h (Fig. 5.1B). Negligible binding of control non-specific IgG or IgG NCs (described above) rendered uptake undetectable [9, 86]. Internalization of monomeric anti-ICAM was markedly lower at this time: ~10% of total cell-associated antibodies (9-fold below the level of uptake of anti-ICAM NCs), as observed previously [9]. Yet, uptake of anti-ICAM increased ~2.5-fold by 3 h, decreasing the difference against anti-ICAM NCs to 3.5-fold. Anti-ICAM reached a maximal uptake level of 25% vs. 100% for anti-ICAM NCs. Hence, although to a much lower extent than anti-ICAM NCs, internalized anti-ICAM still represented a considerable fraction with regard to the total amount of antibodies that initially bound to cells.

Interestingly, examination of the distribution of internalized anti-ICAM vs. anti-ICAM NCs (Fig. 5.1A) revealed that internalized anti-ICAM localized to the cell periphery, whereas anti-ICAM NCs resided in the perinuclear region of the cell, which has been previously shown to correspond to lysosomal compartments [122] and will be subsequently verified here. This may be due to a differential mechanism of uptake between the monomeric and multimeric ligands or a difference in the route of intracellular trafficking.

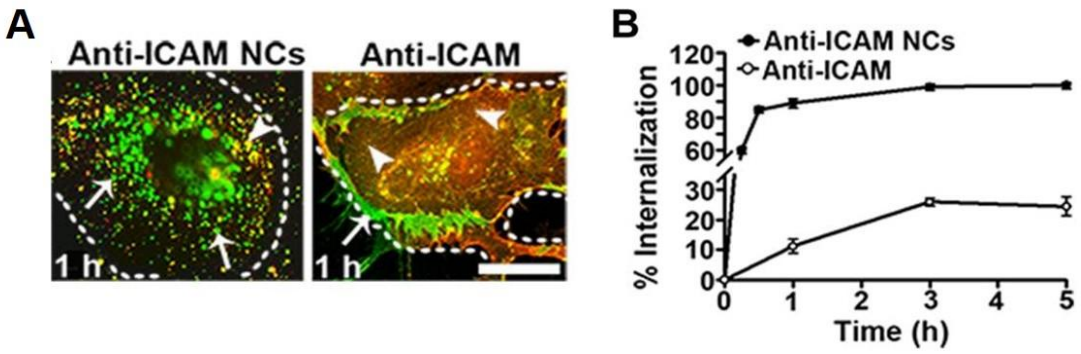

Figure 5.1. Comparative uptake of monomeric vs. multimeric ICAM-1 ligands in endothelial cells. (A) TNF-α-activated HUVECs were incubated with monomeric vs. multimeric ligands (anti-ICAM vs. anti-ICAM NCs) for 30 min to enable binding to cell-surface ICAM-1 (pulse period). After washing unbound materials, cells were incubated at 37 ºC for various time intervals to allow subsequent uptake (chase period). Samples were then fixed and cell-surface vs. internalized ligands were differentially stained (see Methods for details) so that the former appear yellow (green+red; arrowheads) while internalized materials appear green (arrows). Dashed lines mark the cell borders. Scale bar, 10 μm. (B) Internalization was calculated automatically by fluorescence image analysis as the percentage of internalized ligands relative to the total amount of cell-associated ligands. Percent internalization values are means ± S.E.M. Where not visible, S.E.M. bars are masked by the value symbol.

5.2.2 Mechanism of Uptake of Monomeric vs. Multimeric ICAM-1 Ligands in Endothelial Cells

Hence, we next examined the mechanism responsible for uptake of monomeric anti-ICAM by endothelial cells against that of multimeric anti-ICAM NCs, previously identified as clathrin- and caveolae-independent CAM-mediated endocytosis [12, 93].

As shown in Fig. 5.2A, internalization of both anti-ICAM and anti-ICAM NCs was driven by active means, since incubation at 4°C abolished this phenomenon: at this temperature uptake was lowered to 7% for anti-ICAM and 1% for anti-ICAM NCs (30 min), which is consistent with an endocytic event. However, given the different kinetics, maximal uptake levels, and subcellular distribution observed above for internalization of monomeric vs. multimeric ICAM-1 ligands, it would seem plausible that uptake of these counterparts operates via different mechanisms.

Surprisingly, this was not the case (Fig. 5.2B). Just as anti-ICAM NCs, uptake of anti-ICAM was not affected by MDC (83% of control) or filipin (88% of control), which are inhibitors of clathrin- and caveolin-mediated pathways, respectively. In addition, amiloride, an inhibitor of CAM-mediated endocytosis and macropinocytosis, markedly reduced uptake of anti-ICAM anti-to a similar extent to that inhibition of ICAM NCs (~50% by 1 h). Wortmannin, an inhibitor of phosphoinositide 3-kinase (PI3K) associated with macropinocytosis but not CAM-mediated endocytosis, did not significantly alter the degree of uptake of anti-ICAM (83% of control). This was also the case for anti-ICAM NCs (99% of control). Therefore, uptake of both monomeric and multimeric ICAM-1 ligands appears to be regulated by CAM-mediated endocytosis, despite the differences noted above.

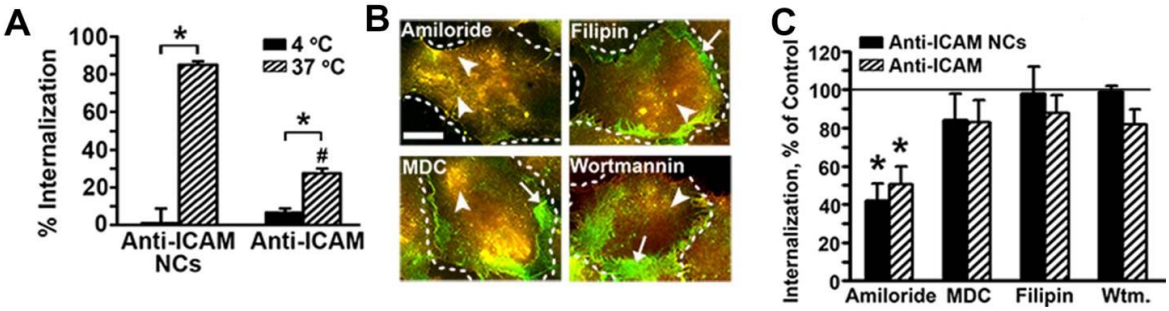

Figure 5.2. Mechanism of uptake of monomeric vs. multimeric ICAM-1 ligands. (A) TNF-α-activated HUVECs were incubated with monomeric anti-ICAM or multimeric anti-ICAM NCs for 30 min at 4ºC or at 37ºC. Cell-surface vs. internalized ligands were imaged and quantified as described in Fig. 5.1. Percent internalization values are means ± S.E.M. *: $p < 0.05$ comparing 4ºC vs. 37ºC. #: $p < 0.05$ comparing anti-ICAM vs. anti-ICAM NCs. (B) TNF-α-activated HUVECs were incubated with anti-ICAM or anti-ICAM NCs for 1 h at 37ºC in the absence (Control) or presence of inhibitors of CAM endocytosis and macropinocytosis (amiloride), macropinocytosis alone (wortmannin (wtm.)), clathrin-coated pits (monodansylcadaverine (MDC)), or caveoli (filipin). Cell-surface vs. internalized ligands were stained as indicated in Fig. 1. Dashed lines mark the cell borders. Scale bar, 10 μm. (C) The percent internalization was calculated as in Fig. 1 and normalized to that in Control cells. *: $p < 0.05$ comparing inhibitors to the control.

5.2.3 Lysosomal Trafficking and Degradation of Monomeric vs. Multimeric ICAM-1 Ligands in Endothelial Cells

Since monomeric anti-ICAM and multimeric anti-ICAM NCs seem to undergo the same mechanism of endocytosis, it is possible that their different levels of uptake may reflect different intracellular trafficking. Differential distribution of these ligands at the cell periphery vs. the perinuclear region after endocytosis, as observed above, seems to support this hypothesis. Hence, to examine this aspect in more detail, we tracked the potential colocalization of intracellular anti-ICAM to lysosomal compartments characterized by the presence of LAMP-1 (Fig. 5.3A), since this represents a predominant destination for anti-ICAM NCs [30, 122]. Indeed, 78% of all cell-associated anti-ICAM NCs colocalized with LAMP-1-positive compartments by 3 h (Fig. 5.3B). In contrast, minimal lysosomal colocalization was observed for anti-ICAM: <7.5% within this time frame.

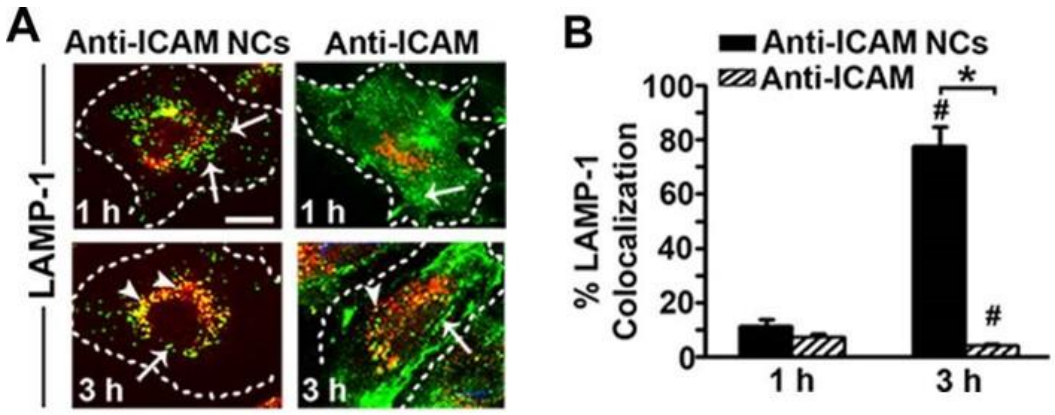

Figure 5.3. Lysosomal trafficking of monomeric vs. multimeric ICAM-1 ligands. (A) TNF-α-activated HUVECs were incubated with green-fluorescent anti-ICAM or anti-ICAM NCs for a 30 min pulse, washed, incubated for up to 1 h or 3 h at 37ºC, then fixed and permeabilized. Lysosomes were labeled with TxR anti-LAMP-1 (red). Yellow color represents green anti-ICAM or anti-ICAM NCs localized to the red-labeled lysosomes, marked by arrowheads. Arrows represent anti-ICAM or anti-ICAM NCs which do not colocalize with anti-LAMP-1. Dashed lines mark the cell borders. Scale bar, 10 μm. (B) The percent colocalization with LAMP-1 with respect to the total cell-associated anti-ICAM or anti-ICAM NCs was quantified by fluorescence image analysis. Data are means ± S.E.M. *: $p < 0.05$ comparing anti-ICAM vs. anti-ICAM NCs. #: $p < 0.05$ comparing 1 h vs. 3 h.

We must note that, in this experiment, fluorescent tracking of anti-ICAM NCs focuses on the polymeric component (fluorescent polystyrene), which is non-degradable. Instead, lysosomal colocalization of anti-ICAM may go unnoticed if the antibody was subjected to proteolytic degradation in lysosomes. Therefore, we examined potential changes over time in the level of immunodetectable anti-ICAM associated with cells, which would be indicative of its degradation (Fig. 5.4). In agreement with the lack of lysosomal colocalization observed above, only 15% of cell-associated anti-ICAM seemed to disappear over a period of 5 h. This was in contrast to anti-ICAM NCs. Immunodetection of anti-ICAM on the surface of green-fluorescent carriers using a red-labeled secondary antibody (which renders yellow color only when the antibody coat is present on green particles; Fig. 5.4A), showed considerable degradation of anti-ICAM on carriers over time: from 8% at 1 h, to 67% at 3 h, and 85% by 5 h (Fig. 5.4B), in agreement with their lysosomal trafficking (Fig. 5.3B).

To further ensure that degradation of monomeric anti-ICAM did not go unnoticed, similar experiments were performed in the presence of chloroquine, and agent that inhibits acidification and, hence, lysosomal degradation [122], or in the presence of nocodazole, an agent that disrupts lysosomal trafficking by altering the microtubular network [122]. Uptake was not affected in the presence of chloroquine or nocodazole (85 ± 15% and 120 ± 15% of control uptake at 3 h; not shown). Moreover, neither agent decreased degradation of anti-ICAM any further (10% and 15% degradation observed for chloroquine and nocodazole vs. 11% for the control at 1 h; not shown). In addition, if there was any trafficking of anti-ICAM to lysosomes, it would be expected that inhibition of lysosomal degradation would increase the number of anti-ICAM vesicles that remain visible over

time. However, as shown in Fig. 5.4C, this parameter remained nearly constant (~25-35 vesicles/cell) over 5 h and similar to the control.

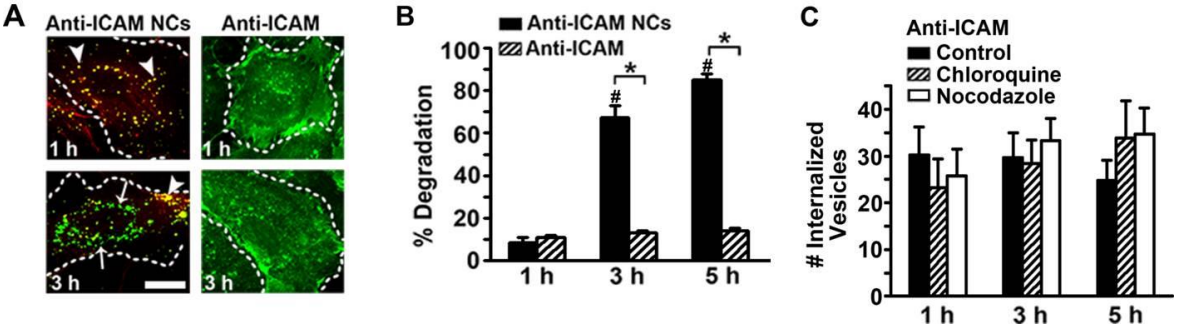

Figure 5.4. Degradation of monomeric vs. multimeric ICAM-1 ligands. (A) TNF-α-activated HUVECs were treated with green-fluorescent anti-ICAM or anti-ICAM NCs for a 30 min pulse to allow only binding, then washed and incubated for up to 1 h, 3 h, or 5 h at 37ºC to allow uptake. Cells were then fixed and permeabilized. For NCs, permeabilized cells were immunolabeled with TxR-goat anti-mouse IgG, which binds non-degraded anti-ICAM on the carrier surface to produce yellow, double-labeled particles (arrowheads). The green, single-labeled fraction represents NCs with a non-immunodetectable (herein called degraded) antibody coat (arrows). In the case of anti-ICAM, non-degraded antibody associated to cells is shown in green, which should diminish over time if there was degradation. Dashed lines mark the cell borders. Scale bar, 10 μm. (B) Percentage of NCs which lack immunodetectable anti-ICAM and percent of anti-ICAM compared to the initial anti-ICAM fluorescence at 4ºC. (C) Number of intracellular vesicles containing anti-ICAM after incubation in control cell medium vs. medium containing chloroquine or nocodazole during the chase period. Data are means ± S.E.M. *: $p < 0.05$ comparing anti-ICAM vs. anti-ICAM NCs. #: $p < 0.05$ with respect to degradation after 30 min.

5.2.4 Uptake and Intracellular Trafficking of Multimeric Anti-ICAM Conjugates in Endothelial Cells

To ascertain whether the differential trafficking of anti-ICAM NCs vs. monomeric anti-ICAM was due to chemical/physical factors associated with the polymer particle, we examined another multimeric ligand: biotinylated anti-ICAM conjugated with streptavidin. With respect to anti-ICAM NCs, which was characterized in Section 4.2.1, this model differed in size (320 nm vs. 150 nm in diameter) and charge (-4 vs. -30 mV), yet it similarly represents a multimeric entity. Cells incubated with anti-ICAM conjugates from 30 min to 5 h showed 94-99% colocalization between the streptavidin and anti-ICAM counterparts,

verifying that conjugate components remain linked throughout this time (not shown). Binding of anti-ICAM conjugates to cells was specific: 261 objects/cell at 30 min, which was reduced by 65% in the presence of anti-ICAM competitor (data not shown). Importantly, over time, anti-ICAM conjugates displayed a significant and increasing perinuclear localization (up to 77% at 5 h) and uptake (up to 72% at 5 h) as in the case of anti-ICAM NCs (compare Fig. 5.5A vs. Fig. 5.1A-B and Fig. 5.6C), suggesting that this is a general property of multimeric ICAM-1 ligands.

However, when we examined colocalization of anti-ICAM conjugates with LAMP-1-labeled lysosomes (Fig. 5.5B), we found poor colocalization (e.g., 15% at 5 h). Since LAMP-1 labeling requires permeabilization, this result may be due to lysosomal degradation of anti-ICAM conjugates and leaching of the fluorophore after permeabilization. Indeed, upon quantification of the total cell-associated fluorescence of anti-ICAM and streptavidin components of the conjugate over time (Fig. 5.5C), we found significant decay for both (53% and 58% degradation at 5 h, respectively), suggesting degradation. In addition, the number of perinuclear vesicles containing conjugates significantly decreased with permeabilization (13 vs. 33 vesicles at 1 h for permeabilized vs. non-permeabilized cells; Fig. 5.5B). This result implied escape of the fluorophore from these compartments, also indicative of conjugate degradation. Hence, to avoid permeabilization that precludes visualizing conjugates within degradative compartments, we pre-labeled lysosomes using TxR dextran as described [122]. To ensure consistency between the two methods, we revealed a similar quantity of intracellular vesicles labeled by anti-LAMP-1 antibodies and dextran (~65-70 vesicles/cell). Importantly, significant and increasing colocalization of anti-ICAM conjugates with dextran-labeled lysosomes

was observed (e.g., 65% at 5 h), which was similar to anti-ICAM NCs and different from monomeric anti-ICAM (Fig. 5.3).

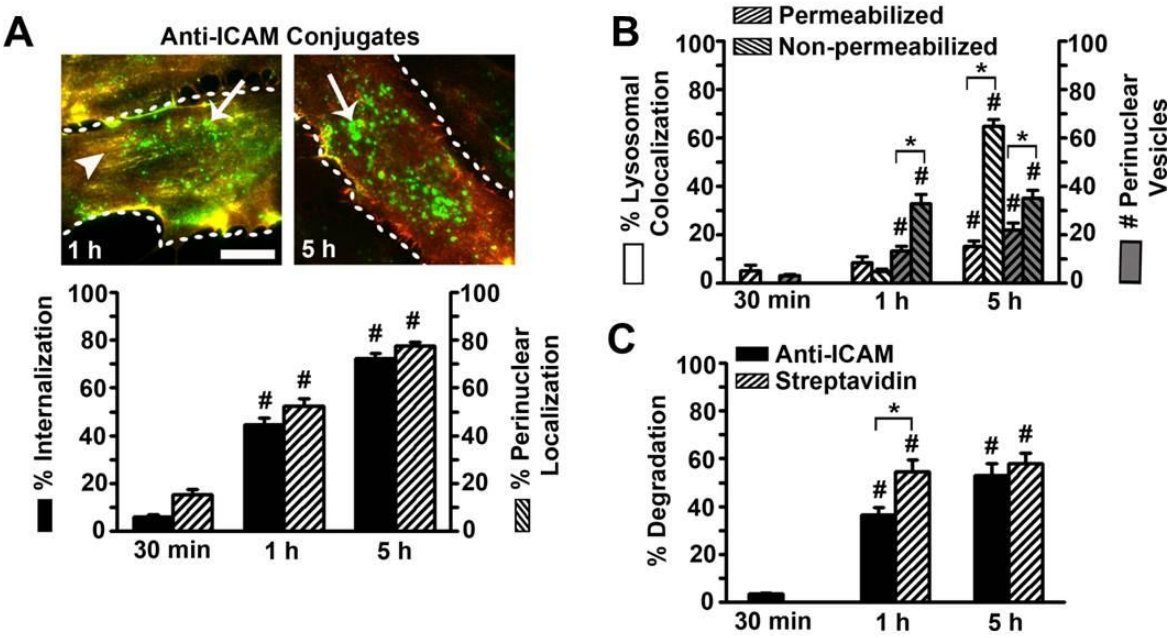

Figure 5.5. Uptake and intracellular trafficking of multimeric anti-ICAM conjugates. (A) TNF-α-activated HUVECs were treated with green-fluorescent anti-ICAM conjugates for a 30 min pulse to permit only binding, then washed and incubated for up to 1 h, 3 h, or 5 h at 37ºC to allow uptake. Cells were then fixed and surface-bound conjugates were immunolabeled with TxR-goat anti-mouse IgG (yellow; arrowheads). The green, single-labeled fraction represents internalized counterparts (arrows). Dashed lines mark the cell borders. Scale bar, 10 μm. The percentage of internalized conjugates relative to the total cell-associated fraction and the percentage of internalized, perinuclear conjugates relative to the total internalized fraction were quantified by fluorescence microscopy. (B) Percentage of green-labeled anti-ICAM conjugates colocalized with red lysosomes labeled by two methods: (1) permeabilization and staining with TxR anti-LAMP-1 vs. pre-labeling with TxR dextran prior to incubation with conjugates (non-permeabilized cells). The number of perinuclear vesicles containing conjugates was also quantified by fluorescence microscopy. (C) Percentage of anti-ICAM or streptavidin compared to the initial anti-ICAM fluorescence at 30 min. Data are means ± S.E.M. #: $p < 0.05$ with respect to data at the initial timepoint. *: $p < 0.05$ comparing permeabilized to non-permeabilized cells in (B) or anti-ICAM vs. streptavidin in (C).

5.2.5 Routing of Monomeric vs. Multimeric ICAM-1 Ligands to the Cell Periphery

The aforementioned results revealed that monomeric anti-ICAM, not multimeric counterparts, avoided lysosomal compartments and the associated degradation (Fig. 5.3 and Fig. 5.4). Also, internalized monomeric anti-ICAM, not multimeric forms, had been observed to localize to the cell periphery (Fig. 5.1A). This clearly indicates that, although exploiting the same endocytic pathway into cells, monomeric anti-ICAM follows a different intracellular routing from multimeric anti-ICAM NCs.

To complement these studies, we analyzed this differential subcellular distribution (Fig. 5.6A). In accord with lysosomal trafficking and degradation, the fraction of internalized anti-ICAM NCs detected at the cell periphery decreased with time (from ~40% at 30 min to ~15% at 5 h; Fig. 5.6B), while the fraction located at the perinuclear region increased (from ~25% at 30 min to ~85% at 5 h; Fig 5.6C), similar to anti-ICAM conjugates (Fig. 5.6A). In contrast, in agreement with its lack of lysosomal routing and degradation, the trafficking of anti-ICAM to the perinuclear region of cells remained very low over time (~8% at 30 min and ~12% at 5 h; Fig. 5.6C), while it remained stably located at the cell periphery (~68% at 30 min and ~77% at 5 h; Fig. 5.6B).

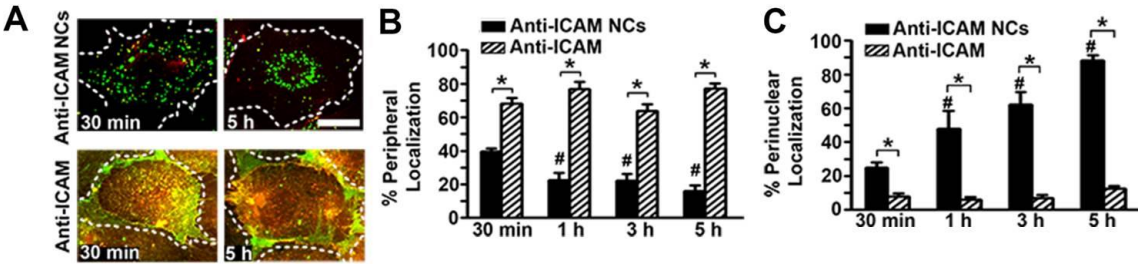

Figure 5.6. Peripheral and perinculear localization of monomeric vs. multimeric ICAM-1 ligands. (A) TNF-α-activated HUVECs were incubated with anti-ICAM or anti-ICAM NCs for a 30 min pulse to allow only binding, then washed and incubated for up to 30 min, 1 h, 3 h, or 5 h at 37 ºC to allow uptake. Cells were fixed and immunostained to differentially label surface-bound (yellow) vs. internalized (green) fractions. Dashed lines mark the cell borders. Scale bar, 10 μm. (B) Fluorescence image analysis was used to quantify the percentage of internalized anti-ICAM or anti-ICAM NCs localized to the cell periphery (within ~5 μm from the cell border) or (C) perinuclear region (within ~5 μm from the nucleus) relative to the total internalized fraction. Values

are means ± S.E.M. *, $p < 0.05$ comparing anti-ICAM vs. anti-ICAM NCs. #: $p < 0.05$ with respect to percent localization after the pulse (30 min).

5.2.6 Recycling of Monomeric vs. Multimeric ICAM-1 Ligands in Endothelial Cells

We next tested whether the peripheral localization observed for monomeric anti-ICAM may be associated with recycling from endocytic compartments to the plasma membrane. For this purpose, we comparatively examined the colocalization of anti-ICAM vs. anti-ICAM NCs (green in Fig. 5.7A) with Rab11a (red). This marker belongs to the small GTPase superfamily of proteins and has been well established for its role in the recycling of various ligands and/or their receptors, including transferrin, transferrin receptor, E-cadherin, LFA-1, GLUT4, etc. [153, 158-162]. Surprisingly, fluorescence microscopy revealed that both anti-ICAM and anti-ICAM NCs colocalized significantly with Rab11a-positive compartments after internalization (yellow color): ~75%-85% in the case of anti-ICAM and ~55%-60% for anti-ICAM NCs within the first hour (Fig. 5.7B). However, localization of anti-ICAM NCs with Rab11a decayed to 23% by 3 h and 13% by 5 h. Instead, this was not the case for anti-ICAM, a substantial fraction of which remained within this compartment even after 5 h (75%).

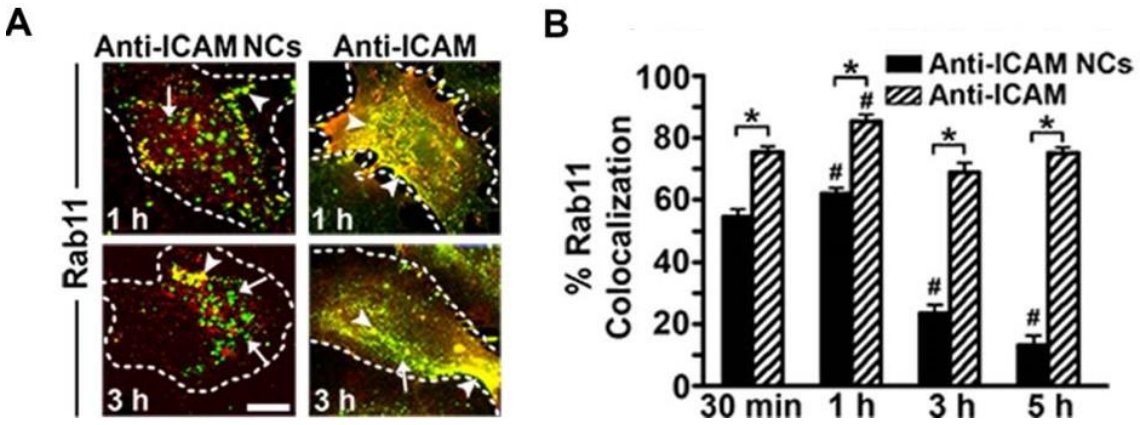

Figure 5.7. Colocalization of monomeric vs. multimeric ICAM-1 ligands with recycling compartments. (A) TNF-α-activated HUVECs were incubated with green fluorescent anti-ICAM for a 30 min pulse to allow only binding, then washed and incubated for up to 30 min, 1 h, 3 h, or 5 h at 37 ºC to allow uptake. Cells were then washed, fixed, and permeabilized. Recycling compartments were labeled with antibodies to Rab11a and a TxR secondary antibody. Arrowheads denote green anti-ICAM or anti-ICAM NCs localized to red-labeled compartments (yellow color) and arrows represent non-colocalized counterparts (green color). Dashed lines mark the cell borders. Scale bar, 10 μm. (B) The percent Rab11a colocalization with respect to total cell-associated anti-ICAM or anti-ICAM NCs was quantified by fluorescence image analysis. Data are means ± S.E.M. *: $p < 0.05$ comparing anti-ICAM vs. anti-ICAM NCs. #: $p < 0.05$ comparing Rab11a colocalization after the pulse (30 min).

Therefore, it appears that both anti-ICAM and anti-ICAM NCs enter cells via the same pathway and initially traffic to a similar membrane-proximal intracellular compartment, yet anti-ICAM recycles back to the plasmalemma while anti-ICAM NCs deviate to lysosomes. Supporting this, tracking the cell-surface vs. intracellular distribution of monomeric anti-ICAM over time revealed that, while the total cell-associated fraction remained constant (~90% of the original value at 30 min), the intracellular fraction cycled: this fraction decreased by 65% at 1 h, then increased to 83% of the original value by 3 h (Fig. 5.8). This result could be visualized by fluorescence microscopy in that the internalized "green" fraction of anti-ICAM at the cell periphery nearly disappeared (compare 30 min vs 1 h), then re-accumulated (compare 1 h vs 3 h).

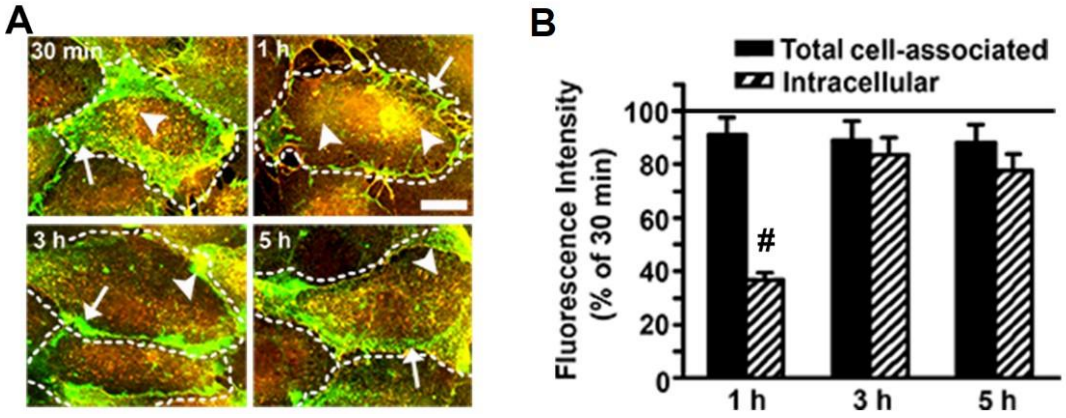

Figure 5.8. Recycling of monomeric anti-ICAM. (A) TNF-α-activated HUVECs were incubated with monomeric anti-ICAM for 30 min to enable binding to cell-surface ICAM-1 (pulse period), washed to remove unbound materials, and incubated for various time intervals at 37 ºC to allow subsequent uptake and/or recycling to the cell surface (chase period). Samples were then fixed and cell-surface vs. internalized ligands were differentially stained yellow (green+red; arrowheads) and green (arrows), respectively. Dashed lines mark the cell borders. Scale bar, 10 μm. (B) Fluorescence intensity of total cell-associated and intracellular anti-ICAM was quantified by fluorescence image analysis and expressed as a fraction of the respective amount after the pulse (30 min; solid line). Values are means ± S.E.M. #: $p<0.05$ with respect to the fluorescence intensity at 30 min.

5.2.7 Endocytic Recycling of Endothelial ICAM-1 in the Absence of Ligands

In a previous study it was observed that internalized multimeric anti-ICAM NCs trafficked to early endosomal compartments, from which the receptor, ICAM-1, recycled back to the cell surface while carriers trafficked to lysosomes [92]. Since it is known that Rab11a recycling compartments can arise from early endosomes, it seems that recycling of monomeric anti-ICAM observed in this study may simply be following the itinerary of its receptor after uptake. If this is the case, the question remains whether anti-ICAM induces endocytosis and recycling upon binding to ICAM-1, or whether ICAM-1 is constitutively endocytosed and recycled in activated endothelial cells whereby anti-ICAM simply remains bound to (and follows) its receptor.

To assess the latter possibility, we tracked the cellular location of ICAM-1 in the absence of ligands (Fig. 5.9A). We first labeled the cell surface using red-fluorescent lectin, which binds to glycoproteins on the plasma membrane, hence, allowing us to track intracellular compartments that may originate from the cell surface as red punctate structures (asterisks). At various times after labeling the plasmalemma, surface-located ICAM-1 was immunostained in blue and total (surface + intracellular) ICAM-1 was additionally immunostained in green (see Section 3.16 for details). As expected, this protocol revealed colocalization of cell surface ICAM-1 (blue+green) with lectin (red),

which appeared as triple labeled regions (white; denoted by arrowheads). The presence of white regions decreased with time (compare 30 min or 1 h with 5 h), as expected if ICAM-1 was endocytosed. Verifying this, intracellular ICAM-1 (green with no blue label) could be found to colocalize with punctate lectin-containing compartments (red), indicating that this pool had been endocytosed from the plasmalemma (yellow; denoted by arrows). This fraction represented ~16% of total ICAM-1 (Fig. 5.9B). Also, we found a fraction of intracellular ICAM-1 (green) that did not colocalize with lectin (red), which may originate from the biosynthetic route. Therefore, it appears that indeed surface-expressed ICAM-1 is endocytosed in the absence of ligands.

Interestingly, with time, there was an increase in the fraction of lectin that distributed to the perinuclear region of the cell (from 36% at 30 min to 75% at 5 h; Fig. 5.9C), and this coincided with a decrease in the colocalization of ICAM-1 and lectin (from 16% at 30 min to 6% by 5 h). This would be in agreement with endocytic transport of ICAM-1 away from perinuclear compartments, just as observed when studying endocytosis of anti-ICAM (Fig. 5.6).

Figure 5.9. ICAM-1 internalization in the absence of ligand binding. (A) TNF-α-activated HUVECs were incubated at 37ºC continuously for different time intervals with TxR tomato lectin (red) to label the cell surface and allow potential endocytosis. Cells were then fixed and immunostained to visualize surface-bound ICAM-1 in blue, followed by permeabilization and immunostaining of total ICAM-1 (surface and internal) in green. Colocalization of surface ICAM-1 with lectin appears in white (arrowheads). Colocalization of intracellular ICAM-1 with lectin (therefore, originating from the plasmalemma) appears in yellow (arrows). Asterisks indicate punctate lectin-containing compartments (red; generated from endocytosis), which do not colocalize with ICAM-1. Dashed lines mark the cell borders. Scale bar, 10 μm. (B) The extent of colocalization of ICAM-1 and lectin was quantified by fluorescence image analysis. (C) The percentage of lectin localized to the perinuclear region (within ~5 μm from the nucleus) relative to the total amount of cell-associated lectin is also shown. Data are means ± S.E.M. #: $p < 0.05$ against values at the initial time point (30 min).

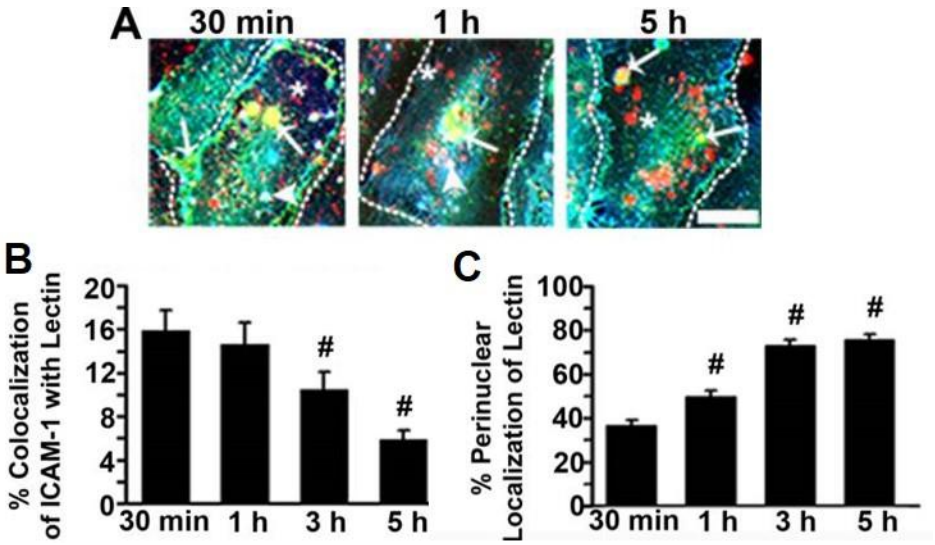

To verify this, we examined the fraction and location of intracellular ICAM-1 in the absence of ligands (sham), using cells that were previously treated with cyclohexamide to minimize the presence of intracellular ICAM-1 originating from the biosynthetic route (Fig. 5.10). These cells were fixed and cell surface vs. intracellular ICAM-1 were differentially immunostained (yellow and green, respectively; see Section 3.15 for details). This revealed the presence of intracellular ICAM-1 at the cell periphery (Fig. 5.10A), representing ~26% of total ICAM-1 (Fig. 5.10B). This is comparable to the location and fraction of anti-ICAM (29%) that is endocytosed by cells upon incubation with this ligand (Fig. 5.10B). Amiloride reduced the fraction of intracellular ICAM-1 by 68% (Fig. 5.10C), similar to the inhibition observed with regard to uptake of anti-ICAM shown in Fig. 5.2B. Also, in parallel to results obtained in the presence of these ligands, wortmannin did not reduce the level of intracellular ICAM-1 in the absence of ligands. This set of results indicates that ICAM-1 is endocytosed from the endothelial plasmalemma in the absence of ligands and is routed through similar peripheral compartments, via CAM-mediated endocytosis.

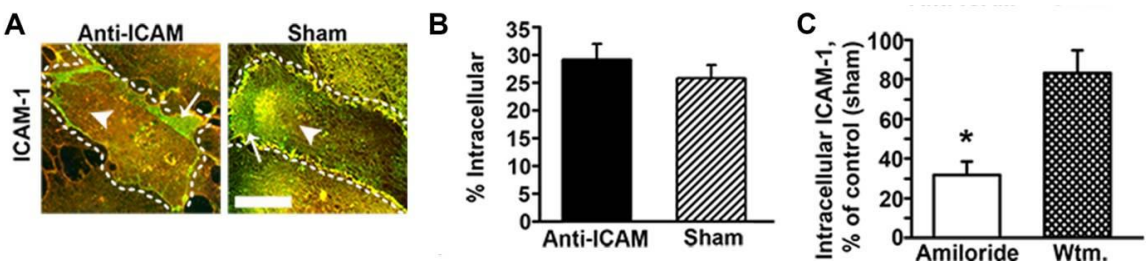

Figure 5.10. Presence of intracellular ICAM-1 in the absence of ligand binding. (A) TNF-α-activated HUVECs were incubated for 1 h at 37°C with anti-ICAM, for ligand-induced uptake. Alternatively (sham), cells were treated with cyclohexamide (to minimize intracellular ICAM-1 arising from *de novo* synthesis) and fixed before being incubated with anti-ICAM, so that there is no ligand-induced uptake. In both cases, samples were then incubated with a TxR-secondary antibody to label ICAM-1 at the cell surface, followed by permeabilization and staining of total ICAM-1 (surface + intracellular) with anti-ICAM and FITC-secondary antibody. This labels cell-surface ICAM-1 in yellow (red + green; arrowheads) vs. intracellular ICAM-1, which appears green only (arrows). Dashed lines mark the cell borders. Scale bar, 10 μm. (B) Images were scored by fluorescence analysis to quantify the percentage of intracellular ICAM-1 with respect to the total pool of cell-associated ICAM-1. (C) A similar analysis was performed comparing sham cells from (A-B) (Control) to sham cells treated with an inhibitor of CAM-endocytosis and macropinocytosis (amiloride) or an inhibitor of macropinocytosis only (wortmannin; wtm). Data are means ± S.E.M. and represent percent intracellular ICAM-1. *: $p < 0.05$ against control (sham) values.

The results shown thus far are depicted in Fig. 5.11. To summarize, monomeric ligands targeted to ICAM-1 in model endothelial cells induces uptake into cells by CAM-mediated endocytosis. The intracellular itinerary of anti-ICAM differed from that of multimeric entities: anti-ICAM appears to undergo recycling to the cell membrane, following the pathway of ICAM-1 in the absence of ligands, rather than lysosomal degradation.

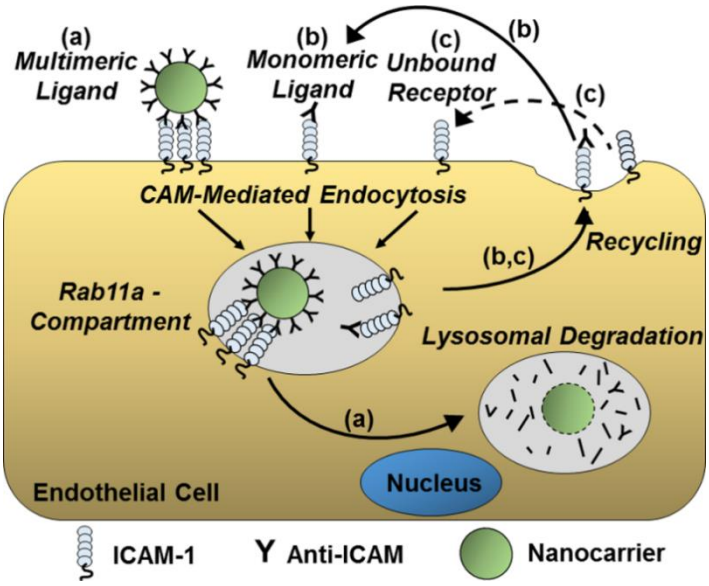

Figure 5.11. Distinct intracellular itineraries of ICAM-1 and monomeric vs. multimeric ICAM-1 ligands in vascular endothelial cells. Multimeric ligands to ICAM-1, such as anti-ICAM NCs (a) are internalized by cells via CAM-mediated endocytosis, and subsequently undergo lysosomal degradation. Monomeric ligands to ICAM-1, e.g. anti-ICAM (b), as well as ICAM-1 in the absence of ligand-binding (c) are also endocytosed by the CAM pathway, yet subsequently undergo Rab11-dependent recycling to the plasma membrane.

In continuation of these findings, the following section aims to exploit this knowledge for oral delivery. As such, we evaluated whether (A) uptake induced by monomeric ligands also holds for GI epithelial cells, and whether (B) such uptake leads to transcytosis, as it did for anti-ICAM NCs [13]. Hence, these studies will determine, for the first time, the potential of monomeric ICAM-1 targeting strategies for oral delivery into and across the GI epithelium.

5.2.8 Binding and Endocytosis of Monomeric Anti-ICAM by Model Gastrointestinal Epithelial Cells

In light of our observation that monomeric anti-ICAM does indeed undergo endocytosis via the CAM pathway, we then evaluated if this is also the case for GI epithelial cells,

which may offer the opportunity for targeting and uptake to this tissue upon oral delivery. With this in mind, we examined the behavior of Caco-2 cells, a well-established model of the GI epithelial cells [130], when exposed to monomeric anti-ICAM. Confirming previous results [13], we first verified binding of anti-ICAM on these cells by fluorescence microscopy (Fig. 5.12), which was: (a) specific vs. control IgG, a non-specific antibody with an isotype matching that of anti-ICAM (8-fold over IgG at 1 h); (b) similar for inflammation-mimicking (TNFα) vs. control conditions (99% of control at 1h); and (c) time-dependent (e.g., 1.8-fold greater at 3 h over 30 min).

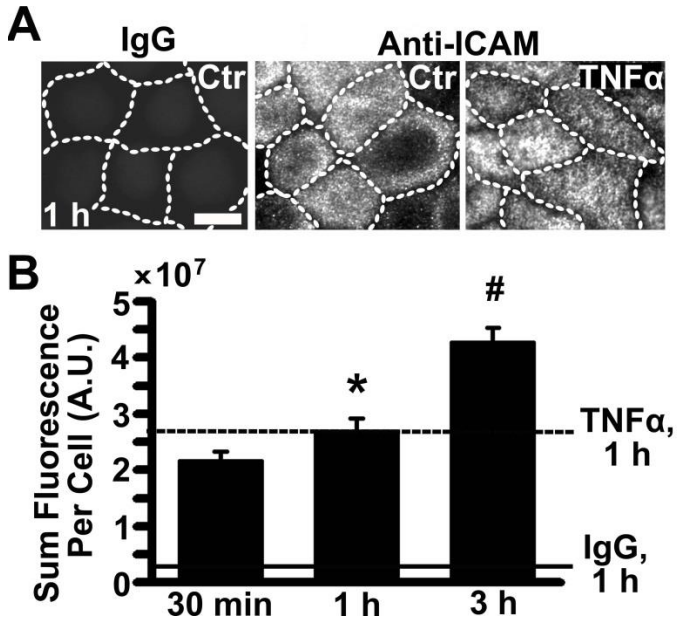

Figure 5.12. Binding specificity of anti-ICAM in model gastrointestinal epithelial cells. (A) Mouse anti-human ICAM-1 (anti-ICAM) vs. non-specific mouse IgG were incubated with control (Ctr) vs. TNFα-activated Caco-2 cells for 1h at 37 °C. Cells were washed, fixed and permeabilized, and total cell-associated anti-ICAM or IgG were immunostained with FITC-labeled goat anti-mouse IgG. Scale bar = 10 μm. Dashed lines mark the cell borders, as observed by phase-contrast microscopy. (B) Association of anti-ICAM to control cells was quantified by measuring the sum fluorescence intensity per cell, expressed in arbitrary units (A.U.), after subtracting the background fluorescence for the equivalent surface area of samples voided of cells. The horizontal continuous and dashed lines are association of non-specific IgG to control cells and anti-ICAM association to TNFα-treated cells, respectively, both at 1 h. Data are Mean ± S.E.M. No difference was observed between control and TNFα-treated cells;* compares anti-ICAM vs. IgG; # compares each time point to the preceding one ($p < 0.05$, Student's *t* test).

Then, uptake was assessed in these cells using a pulse-chase incubation method, in which antibody was allowed to bind to cells for 30 min and then removed from the cell medium in order to track internalization of the pre-bound fraction without the confounding effects of concomitant binding. Using differential immunostaining of surface-bound anti-ICAM (yellow color marked by arrowheads) from internalized anti-ICAM (green color marked by arrows), we observed that the total amount of antibody internalized per cell was highly specific for anti-ICAM vs. IgG (IgG displayed non-detectable uptake; Fig. 5.13A). In addition, uptake did not occur at 4 ºC (16% of 37 ºC at 1 h), indicating an energy-dependent mechanism (Fig. 5.13B). Uptake was also significant, since ~30% of all cell-associated anti-ICAM was internalized within 30 min and this increased to ~50% by 1 h, which was similar for both control and TNFα-treated cells (Fig. 5.13C). Interestingly, the percentage of uptake decreased after 1 h, e.g., to 24% by 5 h. In agreement with the percentage of uptake, anti-ICAM internalized in TNFα-activated and control cells similarly increased from 30 min to 1 h, and subsequently decreased by 5 h (Fig. 5.13B).

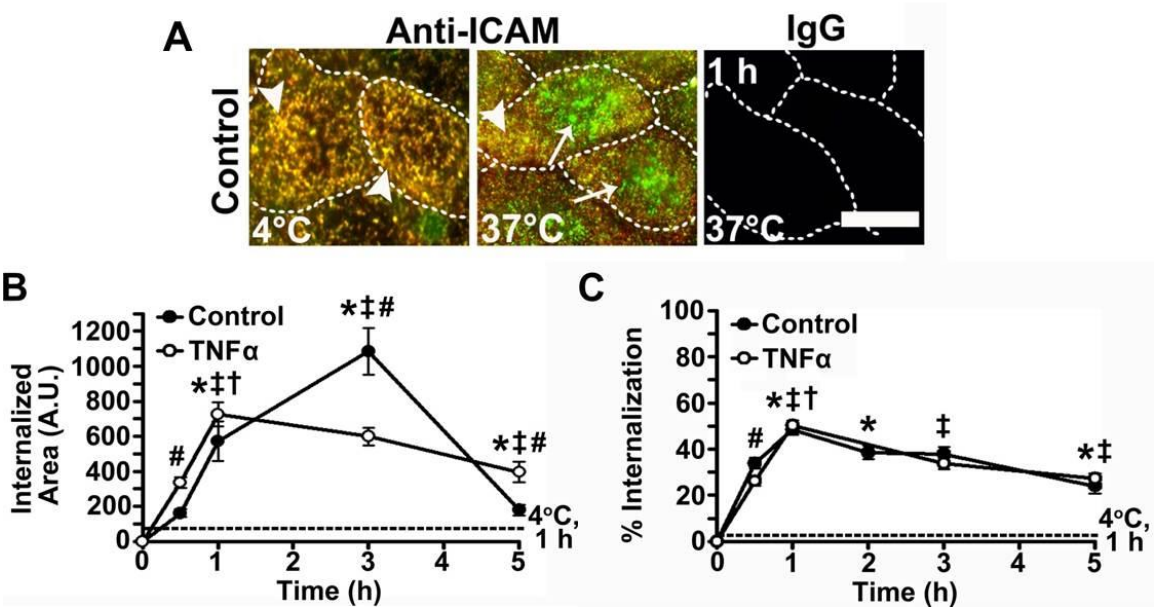

Figure 5.13. Uptake of anti-ICAM by gastrointestinal epithelial cells. (A) Anti-ICAM or non-specific IgG were incubated with control vs. TNFα-activated Caco-2 cells (only control is shown) at 37 °C for 30 min to allow binding (pulse period). Non-bound antibody was removed and cells were chase-incubated at 37 °C with fresh medium for additional time periods up to 5 h (only 1 h is shown) to allow endocytosis. Incubation at 4 °C served as a negative control for uptake. Cells were fixed and incubated with TxR-goat anti-mouse IgG, which is only accessible to surface-bound counterparts. Cells were then permeabilized in order to label total cell-surface and internalized antibody with FITC-goat anti-mouse IgG. This renders differential staining of cell-surface antibody (green + red = yellow; arrowheads) vs. internalized counterparts (green; arrows). Scale bar = 10 µm. Dashed lines mark the cell borders, observed by phase contrast microscopy. (B) Total internalized fluorescence (area occupied by green pixels) per cell was quantified using image analysis. (C) The percentage of internalization was assessed using the ratio of internalized antibody vs. total (surface-bound and internalized) antibody, as measured by fluorescence image analysis. The total time shown includes the 30 min pulse incubation. Internalization of IgG was undetectable. Data are Mean ± S.E.M. * Compares each time point to the preceding one, for control cells; ‡ compares each time point to the preceding one, for TNFα-activated cells; # compares control vs. TNFα at respective time points; † compares 1 h uptake in control cells at 37 °C vs. 4 °C; ($p < 0.05$, Student's *t* test).

However, this was not due to degradation of the internalized pool, since the total amount of antibody associated with cells did not change over this period of time (Fig. 5.14), and additional binding was precluded after the first 30 min pulse. As shown in Fig. 5.15, uptake of anti-ICAM in Caco-2 cells occurred by an endocytic pathway similar to that observed in endothelial cells: it was reduced to 49% of the control by amiloride, which

affects the Na^+/H^+ exchanger involved in the CAM pathway, but not filipin (88% of control) or MDC (99% of control), which affect caveolae- and clathrin-mediated endocytosis, respectively [12].

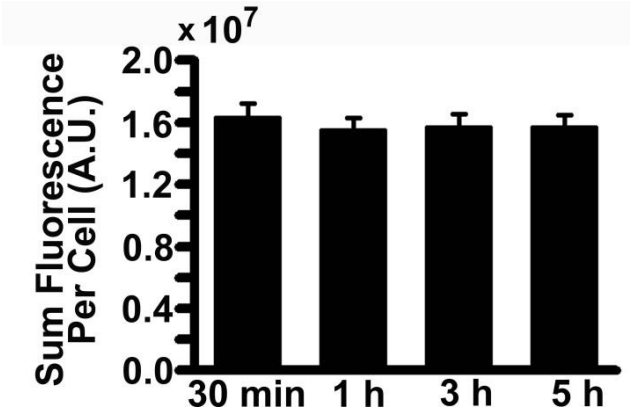

Figure 5.14. Total anti-ICAM associated to gastrointestinal epithelial cells. Control Caco-2 cells were incubated with anti-ICAM for a 30 min pulse period, washed, and incubated in fresh media for a total of 1, 3, and 5 h to permit uptake. Cells were fixed, permeabilized, and treated with FITC-goat anti-mouse IgG to label total cell-associated anti-ICAM in green. The sum fluorescence of anti-ICAM per cell was quantified using image analysis. The total incubation time is shown. Data are Mean ± S.E.M. No difference was observed between successive time points ($p < 0.05$, Student's *t* test).

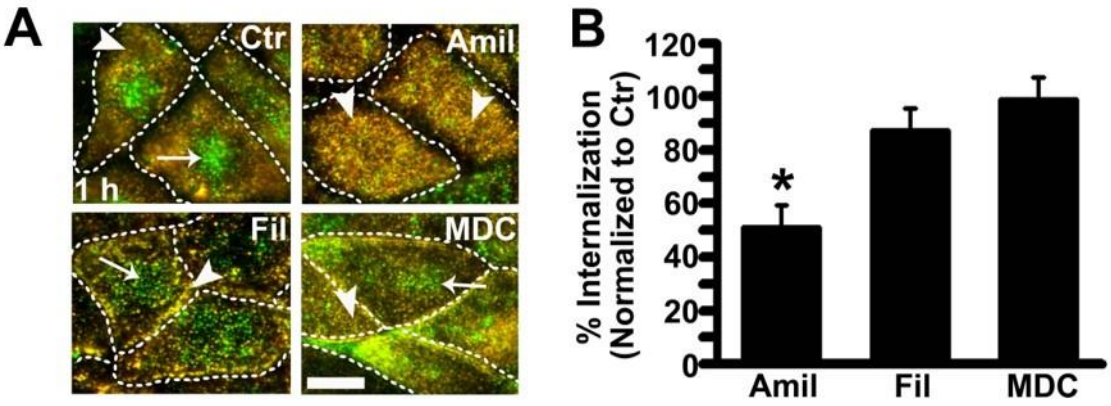

Figure 5.15. Mechanism of endocytosis of anti-ICAM by gastrointestinal epithelial cells. (A) Caco-2 cells were incubated for 1 h at 37 °C with anti-ICAM in the presence of control (Ctr) cell medium or medium containing amiloride (Amil), filipin (Fil), or MDC, which are inhibitors of CAM-, caveolae-, and clathrin-mediated endocytosis, respectively. Surface-bound vs. internalized anti-ICAM was differentially immunostained to appear yellow (arrowheads) vs. green (arrows). Scale bar = 10 μm. Dashed lines mark the cell borders, as observed from phase-contrast microscopy. (B) The percentage of internalized anti-ICAM with respect to total cell-associated anti-ICAM was quantified by image analysis, and normalized to control cells. Data are Mean ± S.E.M. * Compares inhibitor-treated vs. control cells ($p < 0.05$, Student's t test).

Following uptake in vascular endothelial cells, anti-ICAM had exhibited minimal lysosomal trafficking and degradation. To assess whether this is the case for GI epithelial cells, we examined the colocalization of anti-ICAM with a lysosomal marker, LAMP-1. As shown in Fig. 5.16, anti-ICAM exhibited modest trafficking to lysosomes, with 14 and 27% LAMP-1 colocalization between 1 h and 5 h. As expected, IgG exhibited no binding, uptake, or subsequent intracellular trafficking (Fig. 5.16A). We also examined trafficking in the presence of chloroquine, a weak base that diminishes lysosomal degradation. Interestingly, lysosomal colocalization of anti-ICAM decreased by 45 and 39% at 3 h and 5 h in the presence of chloroquine with respect to control cells (Fig. 5.16B).

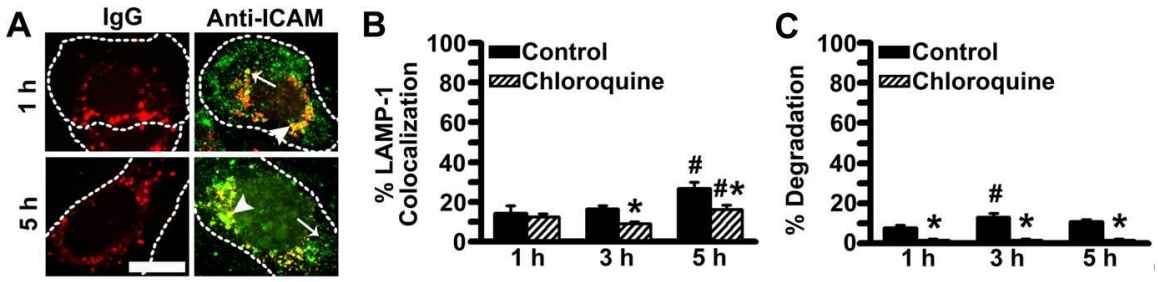

Figure 5.16. Lysosomal trafficking of anti-ICAM in gastrointestinal epithelial cells. (A) Caco-2 cells cultured on coverslips were treated with FITC-labeled anti-ICAM or non-specific IgG for 30 min at 37 ºC to allow binding to the cell surface, followed by washing non-bound antibodies and incubation at 37°C for the indicated time to allow uptake and intracellular trafficking. As a control for degradation, cells were incubated in the presence of chloroquine. Cells were fixed and permeabilized, and LAMP-1-positive lysosomes were then immunostained with TxR mouse anti-LAMP-1 for 1 h. This protocol renders antibodies colocalized with lysosomes double-labeled with TxR and FITC, rendering yellow fluorescence (arrowheads), while non-colocalized antibodies appear single-labeled in green (arrows). Scale bar = 10 μm. Dashed lines mark the cell borders, as observed by phase-contrast microscopy. (B) Colocalization of green objects with red-labeled lysosomes was calculated from fluorescence micrographs. (C) Degradation of FITC-labeled anti-ICAM was estimated by comparing the total fluorescence remaining over time to the cell-associated fluorescence achieved after the first 30 min incubation. Data are Mean ± S.E.M. * compares cells in the presence vs. absence of chloroquine; # compares each time point to the preceding one ($p < 0.05$, Student's *t* test).

It is possible that in the event of degradation of anti-ICAM by lysosomal proteases, colocalization with lysosomes may have gone unnoticed. Hence, using fluorescence

microscopy, we quantified the degree of immunodetectable anti-ICAM associated to cells over time, indicative of degradation. In agreement with minimal LAMP-1 colocalization, only 11% of total cell-associated anti-ICAM was degraded by 5 h (Fig. 5.16C). Chloroquine reduced degradation to 2% by 5 h, indicating that anti-ICAM undergoes a minor level of lysosomal trafficking and degradation. Given that the degree of lysosomal trafficking and degradation was similar to that in vascular endothelial cells, anti-ICAM may follow a similar intracellular fate in GI epithelial cells. In addition, minimal lysosomal trafficking may indicate that anti-ICAM is deferred to an alternative route in a cell barrier model, such as trafficking across the cell body for transcytosis.

5.2.9 Transport of Anti-ICAM Into and Across Gastrointestinal Epithelial Monolayers

The following section seeks to determine whether endocytosis of anti-ICAM leads to transport across GI epithelial cells, analogous to anti-ICAM NCs [13], in order to reveal the potential of this strategy for oral delivery across the GI epithelium. Whereas the studies conducted thus far utilized cells cultured on coverslips to enable characterization of uptake and intracellular trafficking by fluorescence microscopy, this cell culture model does not expose the basolateral surface of cells, precluding the possibility of transepithelial transport. Consequently, the following work utilized Caco-2 cells cultured on transwell inserts (Section 3.2; Fig. 3.1), which exposes both apical and basolateral membranes to the extracellular space. Cells cultured in this configuration serves as a prevalent model of the GI epithelium for studying transepithelial drug transport, and expresses ICAM-1 in both quiescent and disease-mimicking states [13, 130, 163]. Formation of a permeability barrier

in this model was previously validated by immunostaining of occludin-positive tight junctions, consistent with a rise and plateau of TEER, as shown in Fig. 5.17 [13].

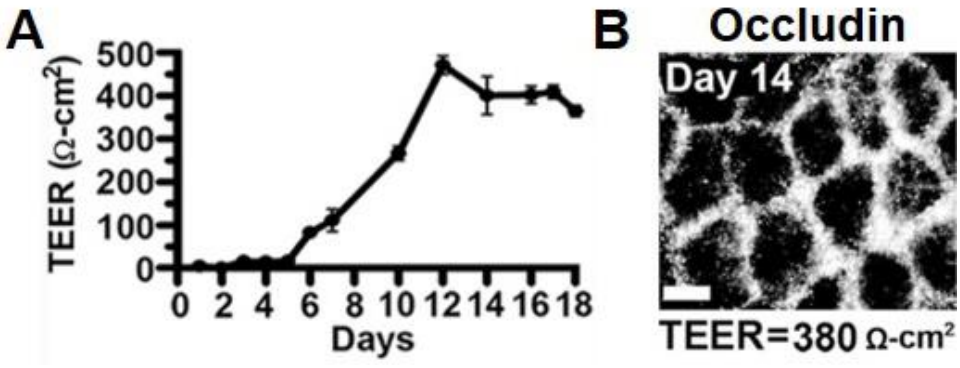

Figure 5.17. Validation of a gastrointestinal epithelial cell barrier model for studying transepithelial transport. (A) Cell barrier formation of Caco-2 monolayers cultured on transwell inserts was validated by transepithelial electrical resistance (TEER) and (B) the presence of occludin, a tight junction protein. Data are means ± S.E.M. Figure is reproduced from Ghaffarian, et al., 2012 [13].

Prior to evaluating transport in this transwell model, we first verified by fluorescence immunostaining that anti-ICAM binds specifically to ICAM-1 on the apical surface of fixed Caco-2 cells (Fig. 5.18A). This was not the case for mouse IgG, a non-specific control which lacks a variable domain targeting ICAM-1, ruling out any contribution of the Fc region in binding, e.g. to Fc receptors (Fig. 5.18A). Staining of bound anti-ICAM also revealed the presence of microvilli on these cells, giving rise to the appearance of small clusters on the apical surface. Specific, time-dependent binding was also demonstrated by radioisotope tracing of ^{125}I-labeled antibodies incubated with live cells: non-specific IgG displayed 12 and 4-fold lower association to cells after 3 h and 24 h (Fig. 5.18B). Despite negligible binding, non-specific uptake or leakage between cells may account for the minor presence of IgG in the cell fraction.

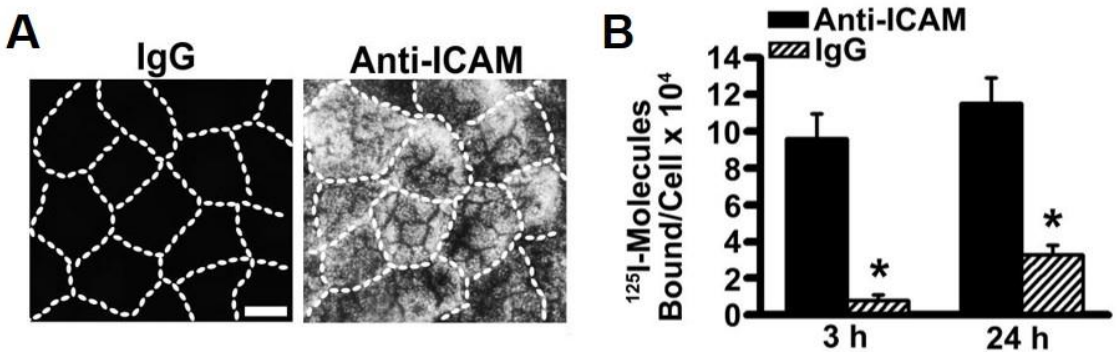

Figure 5.18. Specific binding of anti-ICAM in gastrointestinal epithelial cell monolayers. (A) Caco-2 cell monolayers cultured on transwell inserts were fixed (to prevent antibody internalization) and treated with anti-ICAM or control, non-targeted IgG for 1 h at room temperature to allow binding. FITC-labeled goat anti-mouse IgG was used to stain the total cell surface-bound fraction. Samples were imaged by fluorescence microscopy. Scale bar = 10 μm. Dashed lines mark the cell borders, as observed by phase-contrast microscopy. (B) Antibody binding and uptake in live caco-2 cell monolayers cultured on transwell inserts was assessed by incubation with ^{125}Iodine-labeled anti-ICAM or IgG for 3 h or 24 h at 37 ºC. The radioisotope content in the cell fraction was then quantified using a gamma counter to derive the number of antibody molecules associated to cells. Data are Mean ± S.E.M. * compares anti-ICAM vs. IgG ($p < 0.05$, Student's *t* test).

To assess the possibility that anti-ICAM traffics across cells for release at the basolateral side, analogous to the pathway triggered by anti-ICAM coated nanocarriers, we incubated ^{125}I-labeled anti-ICAM with Caco-2 monolayers cultured on transwell inserts to allow transport from the apical to basal compartment. Radioisotope tracing revealed that anti-ICAM is indeed transported across Caco-2 monolayers in a time-dependent manner, with an increase from 3×10^8 to 3×10^9 molecules transported per mm^2 of epithelium between 3 h and 24 h (Fig. 5.19A). Transport appeared to be ICAM-1-specific, considering that the apparent permeability coefficient (P_{app}), which signifies the rate of transport, was 4-fold greater than that of non-specific IgG antibodies at 24 h (Fig. 5.19C). Fig. 5.19B represents the efficiency of transport as the percentage transported with respect to the amount of total cell-associated anti-ICAM. In terms of this parameter, 25% of cell-associated anti-ICAM was transported at 1 h, which increased and plateaued at ~80%

transported by 5 h. Taken together, these findings verified that monomeric targeting to ICAM-1 may indeed provide oral delivery across the GI epithelial barrier.

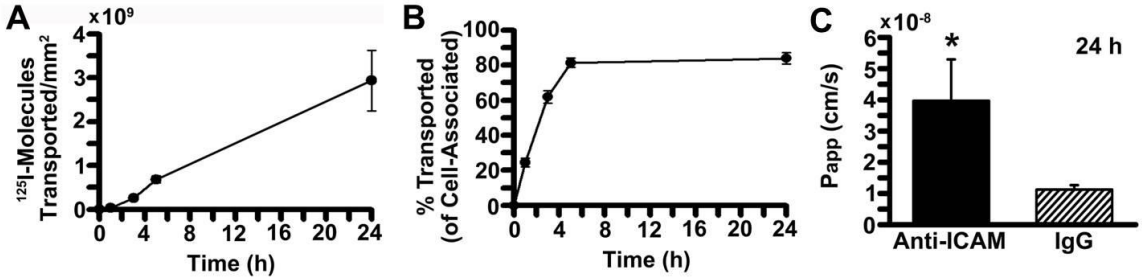

Figure 5.19. Transepithelial transport of anti-ICAM across gastrointestinal epithelial monolayers. ^{125}I-anti-ICAM or non-specific ^{125}I-IgG were added to the apical chamber above Caco-2 cell monolayers cultured on transwell inserts, and incubated at 37 ºC to permit transport into cells and/or across cells to the basolateral chamber. (A) ^{125}I content in the basolateral chamber was measured at the indicated time points, to calculate the amount of antibodies transported per mm^2. The dashed line represents the level of transported IgG after 24 h. (B) The percentage of transport was calculated as the ratio of radioisotope content found in the basolateral fraction to that in the combined basolateral and cell fractions. (C) The apparent permeability coefficients (P_{app}) were calculated as described in Methods to represent the rates of transport of ^{125}I-anti-ICAM or ^{125}I-IgG. Data are Mean ± S.E.M. * compares anti-ICAM vs. IgG; # compares each time point to the preceding one ($p < 0.05$, Student's *t* test).

5.2.10 Assessment of the Mechanism of Transport of Anti-ICAM

Given that anti-ICAM was transported across cells, and that such transport was substantially greater than that of non-targeted IgG, there is evidence to believe that ICAM-1 binding triggers either transcellular transcytosis, as previously shown for anti-ICAM nanocarriers, or opening of junctions leading to paracellular transport. First, to evaluate the role of transcytosis in the transepithelial transport of anti-ICAM, Caco-2 cells were treated with EIPA, an inhibitor of Na^+/H^+ exhanger-1 involved in CAM-mediated endocytosis [91]. As shown in Fig. 5.20A, EIPA significantly reduced transport of anti-ICAM in terms of molecules transported per mm^2 (3% of control, untreated cells) and P_{app} (50% of the control) at 5 h, consistent with previous observations on anti-ICAM NCs [13]. This likely

did not result from changes in monolayer permeability, as EIPA does not alter TEER values during transport [13].

Furthermore, to identify a possible contribution of paracellular transport between adjacent cells, TEER was monitored during transport of anti-ICAM, whereby a decrease in TEER would signify opening of intercellular junctions. Fig. 5.20 reveals that transepithelial passage of anti-ICAM over 24 h did not trigger substantial changes in TEER compared with control, untreated cells (TEER was 91 and 102% of the control between 30 min and 24 h). In contrast, treatment with H_2O_2, known to disrupt monolayer integrity, drastically decreased TEER values to 9% of the control by 24 h (Fig. 5.20A). In parallel with TEER, we also tested permeability of albumin, a tracer compound to identify changes in paracellular leakage. Transport of anti-ICAM over 24 h did not increase albumin permeability, as the P_{app} was 76% of untreated cells (Fig. 5.20A). On the other hand, H_2O_2 significantly increased leakage of albumin by 2-fold, in agreement with opening of intercellular junctions (Fig. 5.20A).

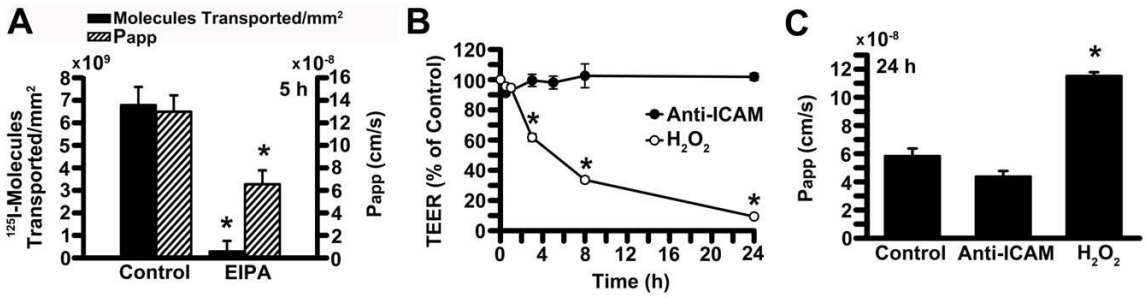

Figure 5.20. Mechanism of transport of anti-ICAM across gastrointestinal epithelial monolayers. (A) Transcellular transport of ^{125}I-anti-ICAM across Caco-2 cell monolayers was assessed at 5 h in the absence or presence of EIPA, an inhibitor of CAM-mediated endocytosis. Quantification of ^{125}I content in the basolateral chamber was used to calculate the amount of antibody molecules transported per mm^2 as well as the rate of transport (P_{app}). (B) TEER was measured during transport of ^{125}I-anti-ICAM across Caco-2 cells, to assess paracellular transport. Incubation with H_2O_2 is a positive control for opening of intercellular junctions. TEER was expressed as a percentage of values measured for untreated, control cells. (C) Paracellular protein leakage, measured as the P_{app} of ^{125}I-albumin crossing the cell monolayer in the absence or presence

of H_2O_2 or anti-ICAM. Data are Mean ± S.E.M. * compares values to control, untreated cells ($p < 0.05$, Student's *t* test).

5.3 Discussion

Many cell surface receptors undergo different endocytic outcomes when bound to ligands, e.g., monomeric vs. multimeric counterparts, compared to their unbound state. Yet, this is still a rather unexplored phenomenon, particularly in cases where natural ligands of a receptor represent multimeric engagement entities. The present study has examined these aspects in the case of endothelial ICAM-1, using monomeric anti-ICAM vs. multimeric anti-ICAM NCs and conjugates as representative ligands. Although previous investigations had deemed monomeric anti-ICAM unable to enter cells as multimeric anti-ICAM counterparts (NCs and conjugates) do [9, 12], to our surprise, a closer examination revealed appreciable uptake via a similar mechanism, CAM-mediated endocytosis. Lower apparent or steady-state levels of endocytosis of monomeric anti-ICAM resulted from a distinct intracellular itinerary. At initial time points, both anti-ICAM and anti-ICAM NCs localized to Rab11a compartments at the cell periphery. Yet, with time, multimeric anti-ICAM NCs and conjugates trafficked to perinuclear lysosomes with significant degradation of the antibody counterpart (as previously reported [122]), while monomeric anti-ICAM remained localized to Rab11a-compartments with little degradation and recycled back to the plasma membrane. Similar trafficking was found for ICAM-1 in the absence of ligand binding, suggesting that this molecule recycles between the plasmalemma and an endosomal-like subplasmalemma compartment. Hence, contrary to anti-ICAM NCs and conjugates that follow an endo-lysosomal pathway, anti-ICAM simply follows the route of the receptor.

These results demonstrate a clearly differential endocytic fate for monomeric vs. multimeric ligands against ICAM-1. The pattern observed for this cell surface marker held similarities and differences as compared to other receptors. For instance, greater uptake of multimeric anti-ICAM NCs with respect to monomeric anti-ICAM contrasted observations of slower internalization of an oligomer composed of ten transferrin molecules vs. monomeric transferrin [141]. Yet, greater intracellular retention of anti-ICAM NCs relative to anti-ICAM was somewhat similar to longer intracellular retention of transferrin oligomers vs. monomeric transferrin [141]. Nevertheless, multimeric ligands in these two cases resided in different sites, i.e. lysosomes for multimeric ICAM-1 ligands as opposed to pericentriolar recycling compartments for multimeric transferrin counterparts [141]. Another example is that of monomeric folate-drug conjugates vs. multivalent folate-decorated carriers [142]. Analogous to ICAM-1, multivalent folate carriers trafficked to lysosomes, whereas monomeric folate conjugates followed a recycling route to the plasma membrane [142]. However, distinct from ICAM-1, monomeric folate carriers followed the route of the natural ligand (folate)-receptor pair [142], whereas monomeric anti-ICAM followed the recycling route of naked ICAM-1. Antibody receptors have also shown different patterns of endocytic routing for different ligands, e.g. binding of an artificial monovalent ligand of macrophage Fc receptor (a modified Fab) resulted in recycling to the cell membrane, whereas a polyvalent immunoglobulin G complex triggered lysosomal trafficking and degradation [144, 145]. However, no difference in the final intracellular destination was found between these divalent and polyvalent Fc receptor ligands, while this was not the case for ICAM-1 (anti-ICAM shown here is divalent).

The differences observed between monomeric and multimeric anti-ICAM ligands are not due to physicochemical characteristics of the polymer particle in the case of anti-ICAM NCs, since a similar uptake, perinuclear distribution, lysosomal colocalization, and degradation was found for multivalent anti-ICAM conjugates formed by crosslinking biotinylated anti-ICAM with streptavidin. It is likely that different physicochemical properties of the carrier may further impact the intracellular behavior. Yet, the fact that multimeric ICAM-1-targeted entities with diverse composition and valency (anti-ICAM-coated PLGA particles, DNA-built dendrimers, liposomes, etc.) behave similarly in terms of intracellular trafficking [132, 164, 165], supports that this is a general feature of multimeric vs. monomeric targeting to ICAM-1. However, it is likely that intracellular trafficking to other receptors and pathways may be more sensitive to variations of the carrier formulation [132, 164, 165].

Importantly, our results indicate that intracellular trafficking of anti-ICAM reflects a pathway by which endothelial ICAM-1 seems to recycle between the cell surface and a subplasmmalema compartment in the absence of ligand binding, which was previously overlooked. This was supported by the fact that, in the absence of *de novo* protein synthesis or ICAM-1 ligands, ICAM-1 expressed on the cell surface was internalized, as observed by tracking the endothelial plasmalemma after lectin-labeling. Following uptake, ICAM-1 diverged from the perinuclear distribution of lectin-positive internalized compartments. This, along with lack of significant disappearance (reflective of degradation) of immunodetectable ICAM-1 with time and reappearance of this molecule at the cell surface suggest that endocytosed ICAM-1 is not destined for lysosomal degradation but recycling.

This may explain why endocytosis of monomeric anti-ICAM had been overlooked in the past [9, 12].

Given that the outcome and kinetics for all these events were similar upon ICAM-1 engagement by monomeric anti-ICAM, it is possible that this ligand does not induce endocytosis and rather passively follows the route of the receptor to which it is bound. Multimeric anti-ICAM NCs are also internalized via CAM-mediated endocytosis and localized at early time points to similar Rab11a compartments. However, from here this ligand did not follow subsequent recycling but lysosomal transport, as previously shown [31, 92]. Hence, multimeric engagement of the receptor may not provide the signal for CAM-endocytosis as previously believed [9, 12], but rather the signal to deviate the subsequent intracellular trafficking from the "constitutive" recycling route. In fact, a previous study had shown that, although anti-ICAM NCs traffic to endo-lysosomal compartments within cells, a significant fraction of ICAM-1 co-internalized with such carriers also recycles back to the plasmalemma [92]. The fact that higher uptake is observed for anti-ICAM NCs and conjugates vs. anti-ICAM may be due not to a greater endocytic efficiency but to cumulative retention of endocytosed carriers within the cell. Hence, anti-ICAM recycling, which leads to lower intracellular accumulation, would be misinterpreted as a lower degree of endocytosis.

From a biological standpoint, ICAM-1 uptake and recycling by endothelial cells in the absence of ligands is a new finding whose biological significance remains to be elucidated. However, recycling of membrane determinants is a common process, broadly involved in numerous cellular processes, such as cell-cell adhesion, migration, polarization, differentiation, and signaling [147, 158, 160, 166]. In fact, in antigen

presenting cells (APCs), ICAM-1 has been observed to undergo uptake and recycling at sites of T-cell contact, which was mediated by an amiloride-sensitive pathway [155], analogous to CAM endocytosis in endothelial cells. This uptake and recycling seemed to provide a continuous redistribution of ICAM-1 on the APC surface, which helped maintain the dynamic contact with T-cells and strengthen cell-cell signaling [155]. In addition, platelet-endothelial cell adhesion molecule 1 (PECAM-1), a surface molecule structurally and functionally related to ICAM-1, and also associated with CAM endocytosis, has been shown to undergo constant recycling through specialized submembrane compartments of endothelial cells, to guide transmigration of leukocytes across the endothelium [167]. It is possible that CAM-mediated endocytosis of ICAM-1 represents an analogous phenomenon. Indeed, ICAM-1 also contributes to extravasation of leukocytes, where ICAM-1 continuously redistributes on the endothelial surface toward the migrating fronts of leukocyte contacts [168].

From a translational perspective, the findings of this study significantly extend previous knowledge on the potential for targeted drug delivery via ICAM-1. As indicated in Chapter 1, ICAM-1 is being explored for targeted interventions against conditions involving inflammation, immune disorders, cardiovascular disease, genetic and metabolic syndromes, etc. [9, 24, 31, 112, 133, 134, 164, 169-172]. In most of these settings, multimeric targeting to ICAM-1 has been pursued, e.g. by coupling affinity moieties to liposomes, microbubbles, polymer particles, gold nanorods, iron oxide nanoparticles, and other NC formulations [9, 24, 31, 112, 133, 134, 164, 169-172]. By providing endocytosis and intraendothelial trafficking, said multimeric ICAM-1-targeting strategies are valuable for intracellular drug delivery to cope with these maladies. For instance, lysosomal

transport of multimeric ICAM-1-targeted carriers is ideal for delivery of lysosomal enzyme replacement therapies necessary to treat genetic deficiencies of these enzymes (i.e., lysosomal storage disorders) [31, 37, 39]. However, lysosomal trafficking is expected to result in premature degradation and/or entrapment of most other therapeutic agents [92, 122]. Therefore, delivery by conjugation to monomeric ICAM-1-targeting ligands may resolve this problem by avoiding lysosomal transport while retaining the therapeutic agent within cells via an uptake-recycling pathway, providing more sustained delivery. This is feasible since several ICAM-1 targeting monoclonal antibodies, their humanized counterparts, antibody fragments, and peptides, have shown efficient ICAM-1 targeting and significant safety in animal models and clinical trials [25, 31, 33, 37, 45, 173].

In light of our observations above, uptake of monomeric anti-ICAM in endothelial cells revealed an opportunity to use monomeric ICAM-1 ligands as vehicles for drug delivery via the oral route. In exploring this opportunity, we first validated that monomeric anti-ICAM binds specifically to ICAM-1 on cultured GI epithelial cells, in agreement with prior observations for both endothelial and epithelial cells [9, 13, 116]. As in our earlier work using Caco-2 cells [13] and contrary to endothelial cells [9, 116], anti-ICAM binding to Caco-2 cells did not significantly vary between control and disease-like conditions mimicked by TNFα activation. This may be due to the fact that this cell line is derived from cancer tissue and its basal state already reflects a disease condition [174]. In fact, this supports previous evidence indicating that ICAM-1 expression is up-regulated in many pathologies affecting the vasculature and GI tissues, including inflammatory disorders, pathogenic infections, and cancers [10, 113, 150, 174-176]. Interestingly, monomeric targeting to ICAM-1, enhanced in pathology in virtue of ICAM-1 overexpression, has

shown success in neutralizing the receptor's involvement in pathology [45, 173, 177]. As such, it has been proposed that ICAM-1 targeting may not only improve biodistribution of therapeutics to disease sites but may simultaneously serve as an ICAM-1-blocking agent to reduce its own involvement in pathology [113, 178].

More importantly for the focus of this study, our results demonstrate that internalization of monomeric anti-ICAM is not restricted to endothelial cells, but also occurs in model GI epithelial cells. In comparison to endothelial cells, uptake in Caco-2 cells was more efficient, reaching a maximum of ~50% internalization of all cell-associated anti-ICAM vs. 25-30% for endothelial cells. Considering that enterocytes have a high absorptive capacity, in line with their physiological function [174], it is possible that these cells may be better suited for said uptake. This difference may also be due to the fact that cancer derived cell lines, such as Caco-2 cells, generally have enhanced uptake capacity in support of their high metabolic, mitotic, and migratory activity [179]. Nevertheless, analogous to endothelial cells, internalization of anti-ICAM in GI epithelial cells occurred via active endocytosis, in particular, the CAM pathway. In light of this result, it is possible that CAM-mediated endocytosis is utilized for uptake of anti-ICAM in all cell types expressing ICAM-1, as previously shown in the case of multimeric ICAM-1-targeted formulations [12-14, 27, 164]. Given that in endothelial cells, ICAM-1 itself undergoes endocytic internalization via the CAM route in the absence of ligand binding, it is expected that anti-ICAM would follow a similar internalization pathway. As such, having reached a maximum between 1 h to 3 h, the level of anti-ICAM located intracellularly decayed over time, although no detectable decay was found in the total amount of anti-ICAM associated

to cells. This may be due to a continuous process encompassing uptake and surface recycling of internalized materials, which we demonstrated in the case of uptake of monomeric anti-ICAM by endothelial cells.

Interestingly, likely because of the above phenomenon, anti-ICAM associated to cells did not decay or traffic to lysosomes over 5 h, although uptake via endocytic mechanisms, including the CAM pathway, typically leads to lysosomal transport and degradation of biological molecules [92, 172]. This is in contrast to lysosomal degradation of anti-ICAM coated on multimeric NCs, which occurs between 3-5 h from their uptake [92], and similar to our previous finding on monomeric anti-ICAM in endothelial cells. Such enhanced intracellular stability associated with uptake of monomeric ICAM-1 targeted ligands may be a significant advantage for drug delivery.

In GI epithelial monolayers cultured on transwell inserts, which exposes the basolateral face of cells to the extracellular milieu, we observed substantial transepithelial transport of anti-ICAM. Whereas this phenomena was previously observed upon multimeric binding [13], the present work elucidates a novel role for ICAM-1 mediated transport upon monomeric binding. As such, monomeric ligands to ICAM-1 may serve as an alternative vehicle for transport across cellular barriers. Indeed, transepithelial transport of anti-ICAM appeared to be more efficient than anti-ICAM NCs in terms of the percentage of transport (84 vs 41% at 24 h) and P_{app} denoting the rate of transport (4×10^{-8} vs. 2×10^{-8} cm/s at 24 h) [13]. It can be speculated that anti-ICAM NCs are more likely to become retained in cells due to differences in intracellular routing, as observed for monomeric vs. multimeric ICAM-1-targeted systems in vascular endothelial cells; for example,

multimeric ICAM-1-targeted systems undergo greater endosomal accumulation as well as lysosomal trafficking and degradation [116]. On the other hand, lower intracellular retention of monomeric ligands may be more conducive to transepithelial transport. In light of minimal lysosomal trafficking, monomeric ligands may be deferred to the transcytosis route. In addition, while the coverslip model restricted recycling of endocytosed anti-ICAM to the apical membrane, it is possible that transport across cells in a transwell model is attributed to recycling to the basolateral membrane, yet this remains to be elucidated.

Despite differences in transport efficiency, both anti-ICAM and anti-ICAM NCs follow a CAM-mediated transcytotic pathway, in agreement with the fact that both systems are internalized into cells via CAM-mediated endocytosis [13]. Moreover, the paracellular pathway does not appear to contribute to transport, as no increase in albumin permeability or electrical conductivity was observed in the presence of anti-ICAM. Compared to paracellular mechanisms, transcytosis is preferred for drug delivery across cellular barriers considering that the permeability barrier regulating the passage of undesired substances is more likely to remain intact [6]. CAM-mediated transport may also provide for effective oral drug delivery in light of its flexibility compared with more restrictive vesicular pathways, such as clathrin- and caveolin-mediated transport; as described in Section 2.3.2, CAM-mediated endocytosis accommodates drugs and drug carriers with a wide range of size, shape, chemistry, and targeting valency [9, 12, 24-34]. Transport of a monomeric antibody, which varies in size and valency compared with previous multimeric systems utilized for CAM-mediated delivery, provides further support of the versatility of this pathway.

5.4 Conclusion

The first portion of this chapter has provided insight into the differential endocytic fates associated with bound (via monomeric vs. multimeric ligands) and unbound endothelial ICAM-1. This highlights the complex regulation of endocytic events, which at present still remains elusive, particularly for non-conventional clathrin- and caveolae-independent pathways such as CAM-mediated endocytosis. Our findings reveal that this pathway may be a constitutive process in activated endothelial cells, which provides a means to maintain a subplasmalemma pool of recycling ICAM-1 molecules. This pool may allow for rapid redistribution of ICAM-1 to the cell surface, e.g. at sites of adhesion by natural ligands (primarily leukocytes). ICAM-1-trafficking does not appear to be disrupted by binding of monomeric affinity molecules but by multimeric carriers, which traffic to lysosomes. These findings pair well with the biological function of ICAM-1 and provide new avenues for therapeutic targeting to this marker. For instance, monomeric delivery vehicles directed at ICAM-1 may allow more prolonged therapy without undergoing lysosomal degradation, contrary to multimeric formulations that are more amenable for delivery into endo-lysosomal compartments. Hence, these newly identified features are critical to the selection and optimization of formulations that tailor particular therapeutic needs.

In the second portion of this chapter, we revealed that in GI epithelial cells, monomeric ICAM-1-ligands (anti-ICAM) undergo CAM-mediated uptake and intracellular trafficking in a similar manner as endothelial cells, expanding the utility of this targeting strategy for oral delivery. We further demonstrated that, analogous to multimeric ICAM-1 ligands, monomeric ligands also elicited CAM-mediated, vesicular transport into and across a model GI epithelial barrier. This is significant because CAM-

mediated transport may provide a safe and effective avenue for oral delivery, given that it does not compromise GI barrier integrity and relative to classical vesicular pathways, it provides greater versatility in accommodating different drug delivery systems [9, 12, 24-34]. From a translational perspective, these results reveal a novel opportunity for using monomeric ICAM-1 ligands as drug carriers for oral delivery into and across the GI epithelium. From a biological standpoint, this knowledge also lends novel insight on regulation of such transport by ICAM-1 and other non-classical endocytic receptors.

Chapter 6: A Monomeric ICAM-1 Targeted Ligand Delivers Active Enzymes Into and Across Gastrointestinal Epithelial Cells

6.1 Introduction

In Chapter 5, we demonstrated that monomeric ICAM-1 ligands are transported into GI epithelial cells by CAM-mediated endocytosis, which led to CAM-mediated transcytosis across these cells. These findings revealed a novel opportunity for direct conjugation of these ligands to therapeutic or imaging agents for oral delivery, which may bypass the barriers in formulating a more complex, multimeric carrier system. In addition, Chapter 5 demonstrated that although transport is mediated by the same CAM-mediated pathway, monomeric vs. multimeric ICAM-1 binding leads differential cellular regulation in terms of efficiency of uptake, intracellular itinerary, and extent and rate of transepithelial transport. Therefore, monomeric vehicles may expand the range of future oral applications of ICAM-1 targeting beyond existing multimeric strategies.

In light of these results, the aim of Chapter 6 was to exploit the transport avenue triggered by monomeric targeting for delivery of a drug cargo into and across the GI epithelial barrier, as was shown for multimeric anti-ICAM-coated nanoparticles carrying α-Gal enzymes as a model drug cargo [13]. In addition, we examined the retention of drug activity after targeting and transport into and across GI epithelial cells. This holds significance, as the GI epithelium represents a valuable gateway for therapies aimed at either treating gastrointestinal disorders or reaching the systemic circulation via the oral route [1, 2]. As a proof-of-concept, we have conjugated anti-ICAM antibodies to a model enzyme, horseradish peroxidase (HRP). This is relevant in that ICAM-1-mediated delivery

of therapeutic enzymes has been extensively explored in the case of multimeric targeting [9, 13, 25, 27, 30, 31, 36, 37, 128, 178] and a monomeric delivery platform may offer alternative opportunities. Our results shown herein indicate that monomeric targeting to ICAM-1 indeed represents a valid alternative to multimeric targeting for delivery of therapeutics into and across the GI epithelium.

6.2 Results

6.2.1 Conjugation of a Model Enzyme to Anti-ICAM

The fact that anti-ICAM can bind to and be endocytosed by cells, such as model GI epithelial cells shown here, suggests that direct coupling of a cargo to anti-ICAM could be sufficient to achieve specific targeting and transport within cells, without the need of a multivalent strategy as previously thought. As a proof-of-concept to examine this, we conjugated anti-ICAM to a model cargo, horseradish peroxidase (HRP), an enzyme that is commercially available and well characterized in terms of molecular weight and activity. We used a commercial kit for conjugation, employing an antibody-to-enzyme molar ratio of 1:2 (see Section 3.6).

We initially verified the presence of a conjugate and its constituents by electrophoretic (SDS-PAGE) separation of the reaction mixture using denaturing, non-reducing conditions, followed by Coomassie blue staining and Western blot immunodetection (Fig. 6.1A). Coomassie blue staining showed protein bands at ~150 kDa for control unconjugated anti-ICAM (Lane 2) and ~40 kDa for control unconjugated HRP (Lane 3), in agreement with their theoretical molecular weights. In the case of the conjugate reaction, Coomassie blue staining marked a predominant band at ~230 kDa (arrow in Lane

1), which is the theoretical size of a conjugate carrying 2 HRP molecules per anti-ICAM molecule, as expected. This band was clearly positive for the presence of both antibody and HRP components by Western blot (arrows in Lanes 4 and 7), whose specificity was verified by differentially labeling control unconjugated anti-ICAM or HRP, respectively (Lanes 5-6 and 8-9). Apart from this predominant ~230 kDa conjugate band, faint bands of ~150 kDa and ~40 kDa were also present in the conjugate reaction (Lane 1), which were positive for either anti-ICAM or HRP, but not both (Lanes 4 and 7). This indicates traces of unconjugated antibody and enzyme in the reaction mixture. In addition, two bands above 230 kDa (Lane 1) were positive for both anti-ICAM and HRP (Lanes 4 and 7), suggesting the presence of larger conjugates. However, the Coomassie blue intensity of these lower and higher molecular weight bands was much lower than that of the predominant 230 kDa band (2.2-, 1.5-, and 1.7-fold lower for the 40 kDa, 150 kDa, and >230 kDa bands, respectively; Lane 1), indicating that only a minor fraction of these species is present in the conjugate mixture. These results indicate that the predominant conjugate species had a molecular weight of ~230 KDa, expected for a conjugate bearing anti-ICAM-to-HRP molar ratio of 1:2.

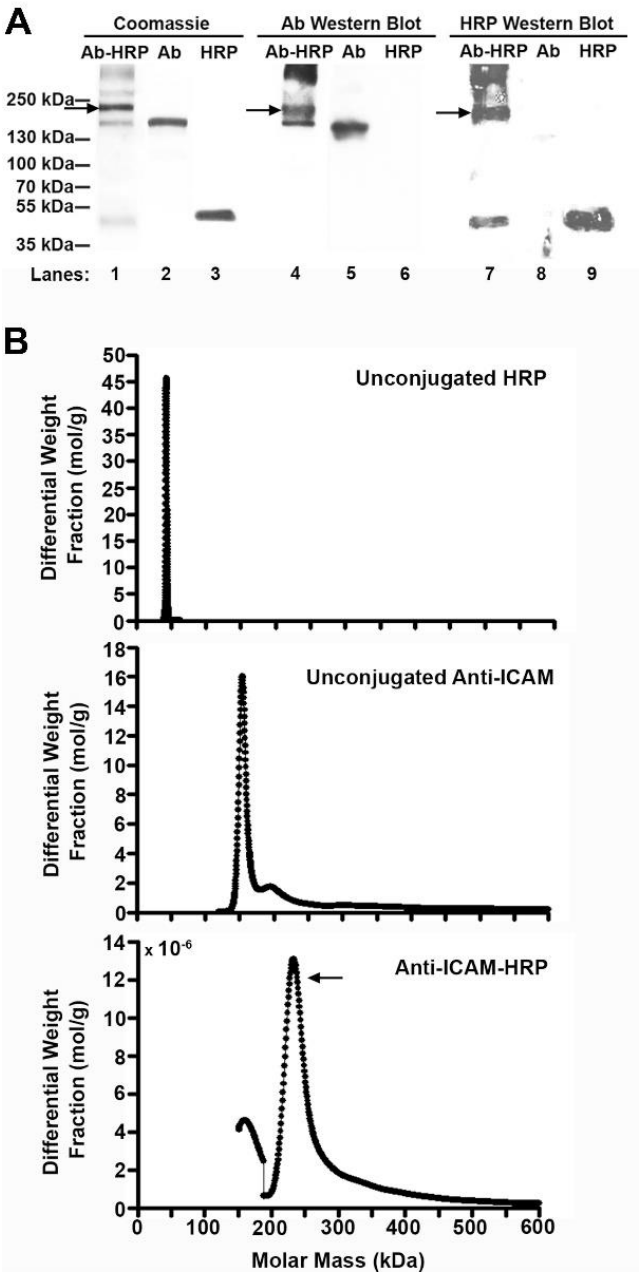

Figure 6.1. Characterization of anti-ICAM-HRP conjugates using SDS-PAGE and AF4. Horseradish peroxidase (HRP) was conjugated to anti-ICAM antibody (Ab) according to the manufacturer's instructions to yield a theoretical antibody-to-enzyme molar ratio of 1:2. (A) The anti-ICAM-HRP conjugate mixture vs. unconjugated anti-ICAM or HRP were separated by SDS-PAGE in denaturing, non-reducing conditions. Left: Coomassie blue staining was used to visualize protein bands. For Western blot, proteins were transferred to a PVDF membrane and immunostained with either goat anti-mouse IgG-HRP to visualize protein bands containing anti-ICAM (Lanes 4-6) or with rabbit anti-HRP followed by goat anti-rabbit IgG-HRP to visualize protein bands containing HRP (Lanes 7-9). Arrows designate a predominant ~230 kDa conjugate band. (B) HRP, anti-ICAM, and anti-ICAM-HRP were fractionated using AF4 connected with MALS, QELS, UV and RI detectors to characterize the differential weight fraction (mol/g) of

eluted samples as a function of molar mass (kDa). A predominant peak with an average molar mass of 233 kDa is observed for anti-ICAM-HRP (arrow).

We then characterized the conjugate population using AF4 coupled to MALS, RI, and UV absorbance detectors [180] to more accurately determine average molecular weight. The differential weight fraction vs. molecular weight represented in Fig. 6.1B shows that unconjugated HRP and anti-ICAM result in relatively monodisperse peaks with average molecular weights of 43 and 155 kDa, respectively, in agreement with the SDS-PAGE determination (Fig. 6.1A). The anti-ICAM-HRP reaction mixture contained a range of conjugate species. The major peak representing ~40% of the conjugate population contained conjugates ranging between ~190 – 340 kDa, which correspond to antibody-to-enzyme molar ratios of 1:1 – 1:4, therefore, all with the ability to bind ICAM-1 in a monomeric manner. Within this population, the average molecular weight was 233 kDa, indicating a predominant species of 1:2 antibody-to-enzyme molar ratios (just as in SDS-PAGE). This pick was preceded by a minor peak of 196 kDa representing ~10% of the population, which contained monomeric conjugates with a 1:1 antibody-to-enzyme molar ratio and a fraction of unconjugated anti-ICAM at 155 kDa. Unconjugated HRP was not detected. Finally, the higher molecular weight tail following the major conjugate peak represented ~40% of the population and an average molecular weight of 686 kDa. This fraction is presumably composed of large multimeric conjugates and/or aggregates, therefore, with the ability to bind ICAM-1 in a multimeric manner. In light of these results, the cellular uptake studies discussed below employ AF4 to separate conjugates into 233 kDa and 686 kDa fractions, in order to evaluate uptake from monomeric vs. multimeric binding.

6.2.2 Specific Binding of Active Anti-ICAM-Enzyme Conjugates to Model Gastrointestinal Epithelial Cells

Specific binding of monomeric anti-ICAM antibodies, as well as multimeric anti-ICAM conjugates and carriers, have been extensively demonstrated in previous work [9, 12, 24-34] and in this dissertation (Fig. 5.12). However, the question remaining is the induction of uptake by monomeric anti-ICAM. As such, in this study we simply verified the specificity of binding of the anti-ICAM-HRP conjugate mixture (Fig. 6.2 and Fig. 6.3). Using fixed Caco-2 cells to avoid concomitant uptake that may confound binding results, anti-ICAM and HRP were differentially immunostained in green and red, respectively, and both the fluorescence of these components as well as their colocalization were quantified by fluorescence microscopy.

Unconjugated anti-ICAM bound to cells (fluorescence intensity of 970 A.U.; Fig. 6.2A-B), yet as anticipated, did not exhibit significant HRP staining (136 A.U.; Fig. 6.2A-B) or colocalization (1.7%; Fig. 6.2C). Also as expected, unconjugated HRP did not bind to cells, as deduced from minimal staining for anti-ICAM (88 A.U.; Fig. 6.2A-B) and HRP (15 A.U.; Fig. 6.2A-B), and lack of colocalization of these components (0.5%; Fig. 6.2C). These results support that only trace amounts, if any, of unconjugated anti-ICAM and HRP are present in the conjugation reaction (as observed in Fig.6.1), and they will not interfere with targeting and activity studies to be subsequently conducted. In contrast, incubation of cells with anti-ICAM-HRP conjugates showed substantial binding to cells, with positive staining of both the anti-ICAM (907 A.U.; 6.2A-B) and HRP (1343 A.U.; Fig. 6.2A-B) counterparts. In fact, the degree of targeting by anti-ICAM-HRP conjugates was similar to that of unconjugated anti-ICAM (94% of anti-ICAM fluorescence; Fig. 6.2B), which

supports the predominant presence of conjugates bearing one antibody molecule. This binding was 88-fold above the binding level of unconjugated HRP (Fig. 6.2B), demonstrating that targeting is attributed to the anti-ICAM component of conjugates. In agreement with this, co-incubation of anti-ICAM-HRP conjugates in the presence of naked anti-ICAM, to compete for ICAM-1 binding sites, significantly reduced binding of HRP (e.g., 59% of fluorescence compared to control), while non-specific IgG did not compete for binding (e.g., 95% HRP fluorescence compared to control) (Fig. 6.2B and Fig. 6.3). Moreover, 100% of the anti-ICAM component of conjugates colocalized with the HRP component, and 96% of the HRP component colocalized with anti-ICAM (Fig. 6.2C). This confirms that we tracked conjugates rather than unconjugated species. Anti-ICAM-HRP conjugates also showed high binding specificity to cells when compared to control IgG-HRP conjugates (Fig. 6.2A), which represented only 1% of the antibody and HRP fluorescence displayed by anti-ICAM-HRP conjugates (Fig. 6.2B). This verifies the ability of anti-ICAM to specifically target a model enzyme (HRP) to ICAM-1 expressing cells after conjugation.

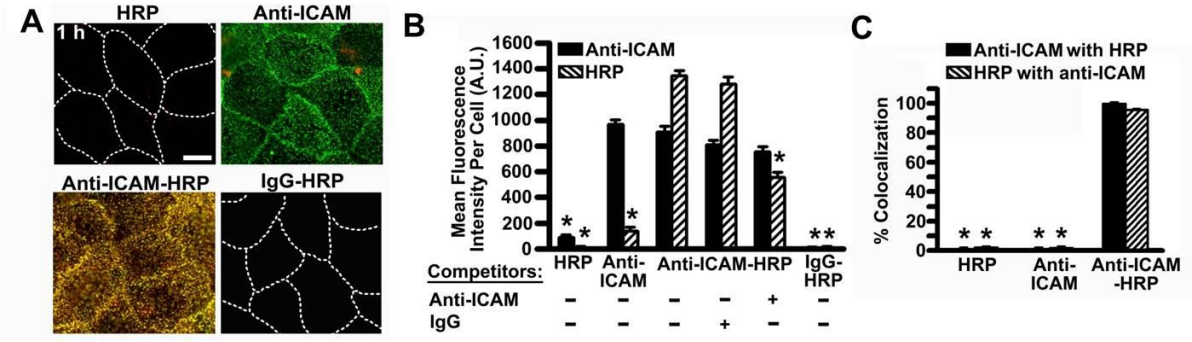

Figure 6.2. Specific binding of anti-ICAM-HRP conjugates to model gastrointestinal epithelial cells. (A) Fixed Caco-2 cells were incubated for 1 h at room temperature with non-conjugated HRP or anti-ICAM vs. anti-ICAM-HRP conjugates or control IgG-HRP conjugates. Incubations were performed either in control cell medium or medium containing anti-ICAM, to serve as a binding competitor, or non-specific IgG control. Anti-ICAM was immunostained with

FITC-labeled goat anti-mouse IgG (green), while HRP was immunostained with rabbit anti-HRP and TxR goat anti-rabbit IgG (red). Colocalization of anti-ICAM with HRP appears in yellow (green + red). Scale bar = 10 μm. Dashed lines mark the cell borders, as observed from phase-contrast microscopy. (B) The green FITC fluorescence was used to quantify binding of the anti-ICAM counterpart and the red TxR fluorescence was used to quantify binding of the HRP counterpart. (C) Colocalization was calculated as the percentage of anti-ICAM colocalized with HRP, or *vice versa*, relative to the total amount of anti-ICAM, or HRP, respectively. Data are Mean ± S.E.M. * Compares any condition against anti-ICAM-HRP in the absence of competitors ($p < 0.05$, Student's *t* test).

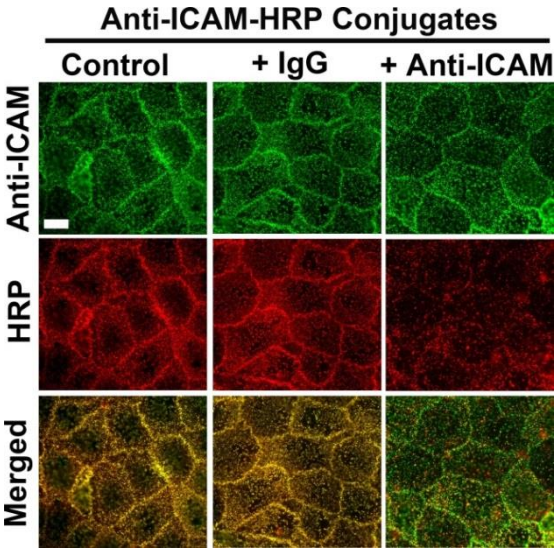

Figure 6.3. Binding of anti-ICAM-HRP conjugates to cells in the presence of competitors. Fixed Caco-2 cells were incubated for 1 h at room temperature with anti-ICAM-HRP conjugates either in control cell medium or cell medium containing anti-ICAM or non-specific IgG. Anti-ICAM was immunostained with FITC-labeled goat anti-mouse IgG (green) and HRP was immunostained with rabbit anti-HRP and TxR goat anti-rabbit IgG (red). Colocalization of anti-ICAM with HRP appears in yellow (green + red). Scale bar = 10 μm. Note that anti-ICAM competitor is detected by the corresponding secondary antibody. Hence, competition is visualized with respect to the HRP counterpart of conjugates.

In addition to fluorescence microscopy, we evaluated HRP activity of anti-ICAM-HRP conjugates bound to fixed cells (Fig. 6.4). Incubation with unconjugated anti-ICAM rendered no measurable HRP activity, as expected since no HRP component is attached to the naked antibody. In addition, incubation with unconjugated HRP did not result in significant activity, in agreement with the fact that the unconjugated enzyme did not bind to cells. This was also the case for IgG-HRP conjugates, in accord with their lack of binding observed above. Instead, anti-ICAM-HRP resulted in marked enzyme activity (equivalent to 127 pM), which was significantly reduced by co-incubation with anti-ICAM competitor

(42% of control), but not IgG (95% of control). Hence, HRP conjugated to anti-ICAM is specifically targeted to cells in an active form.

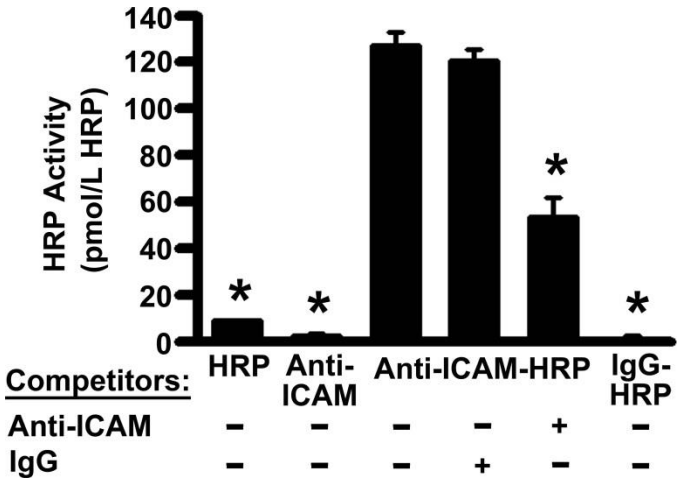

Figure 6.4. Enzyme activity of anti-ICAM-HRP conjugates bound to gastrointestinal epithelial cells. Fixed Caco-2 cells were incubated for 1 h at room temperature with non-conjugated HRP or anti-ICAM vs. anti-ICAM-HRP conjugates or control IgG-HRP conjugates. This was performed either in control cell medium or medium containing anti-ICAM, to compete for ICAM-1 binding sites, or non-specific IgG. Cells were washed to remove the non-bound counterparts and HRP substrate was then added to cells to measure HRP activity (pM HRP). Data are Mean ± S.E.M. * Compares any condition against anti-ICAM-HRP in the absence of competitors ($p < 0.05$, Student's *t* test).

6.2.3 Active Anti-ICAM-Enzyme Conjugates Are Internalized by Gastrointestinal Epithelial Cells

Having demonstrated binding specificity, we focused on the main question of this study: whether monomeric vs. multimeric binding to ICAM-1 by anti-ICAM-HRP conjugates induces uptake by cells, rendering intracellular enzyme activity. For this purpose, separation of the different conjugates species, as opposed to using the conjugate mixture, is paramount. Hence, we used AF4 to separate conjugates into two fractions: (1) the most prominent 233 kDa species (1:2 antibody-to-enzyme molar ratio), which binds to ICAM-1 in a monomeric manner as it contains only one antibody molecule; and (2) a prominent

>326 kDa (average = 686 kDa) species that is likely composed of larger conjugates or aggregates and, thus, binds to ICAM-1 in a multimeric manner as it contains more than one antibody molecule. The isolated monomeric vs. multimeric fractions as well as the unseparated anti-ICAM-HRP conjugate mixture were incubated with Caco-2 cells and then immunostained to distinguish surface-bound vs. internalized counterparts. As observed by the presence of single-labeled green anti-ICAM or HRP (arrows; Fig. 6.5A), the 686 kDa conjugate fraction providing multimeric binding showed uptake by cells when tracking either the antibody or enzyme counterparts (87% and 69% compared to the unseparated mixture), as expected. Most importantly, tracking the antibody and enzyme counterparts revealed that the 233 kDa conjugate was internalized by cells to an equivalent degree (100% and 91%) as the unseparated mixture. This demonstrates that monomeric binding to ICAM-1 by anti-ICAM-HRP conjugates induces internalization similar to that produced by multimeric species. Since this was the case and the main species in the conjugate mixture consisted of the 1:2 antibody-to-enzyme conjugate, we conducted the subsequent assays using said mixture.

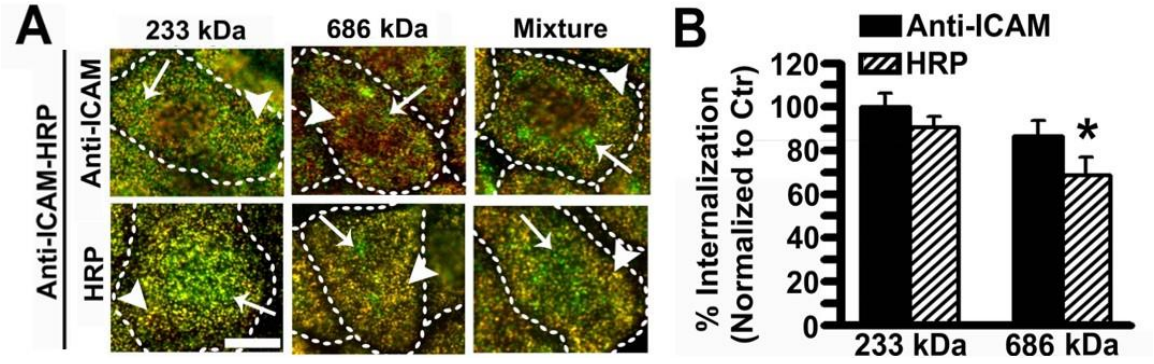

Figure 6.5. Uptake of anti-ICAM-HRP conjugates after monomeric vs. multimeric binding to gastrointestinal epithelial cells. The anti-ICAM-HRP conjugate mixture was separated into two main molecular weight fractions by AF4: a form corresponding to 1:2 antibody-to-enzyme molar ratio (233 kDa) and a form representing larger multimolecular or aggregated conjugates (>326 kDa; average = 686 kDa). (A) Caco-2 cells were incubated with the conjugate mixture vs. each one of

the separated conjugate fractions for a 30 min pulse period, washed, and then incubated with fresh medium for up to 1 h to track uptake. In parallel assays, either surface-bound anti-ICAM or HRP were immunostained to fluoresce in yellow (arrowheads), whereas internalized anti-ICAM or HRP were immunostained to fluoresce in green alone (arrows). Scale bar = 10 μm. Dashed lines mark the cell borders, as observed from phase-contrast microscopy. (B) The percentage of internalization of each conjugate fraction was obtained from micrograph analysis, which was normalized to that of the unseparated conjugated mixture used as a control (Ctr). Data are Mean ± S.E.M. * Compares each conjugate fraction against the control mixture ($p < 0.05$, Student's *t* test).

Moreover, the uptake of anti-ICAM-HRP conjugates was time-dependent: from 1 h to 3 h, the fluorescence corresponding to internalized anti-ICAM counterparts increased from 557 to 1254 A.U., and similarly, internalized HRP fluorescence increased from 739 to 995 A.U. (Fig. 6.6A-B, and Fig. 6.7). Tracking the HRP component, this level of uptake corresponded to ~34% of all cell-associated enzymes found at 3 h (Fig. 6.7C), similar to the rate of uptake observed for unconjugated anti-ICAM shown in Fig. 5.13. Therefore, uptake is likely mediated by the targeting antibody. Supporting this, amiloride diminished uptake of both the antibody and enzyme cargo components of the conjugate by 59% and 72% with respect to the control condition (Fig. 6.7D), demonstrating CAM-mediated endocytosis, as seen for the unconjugated antibody (Fig. 5.15).

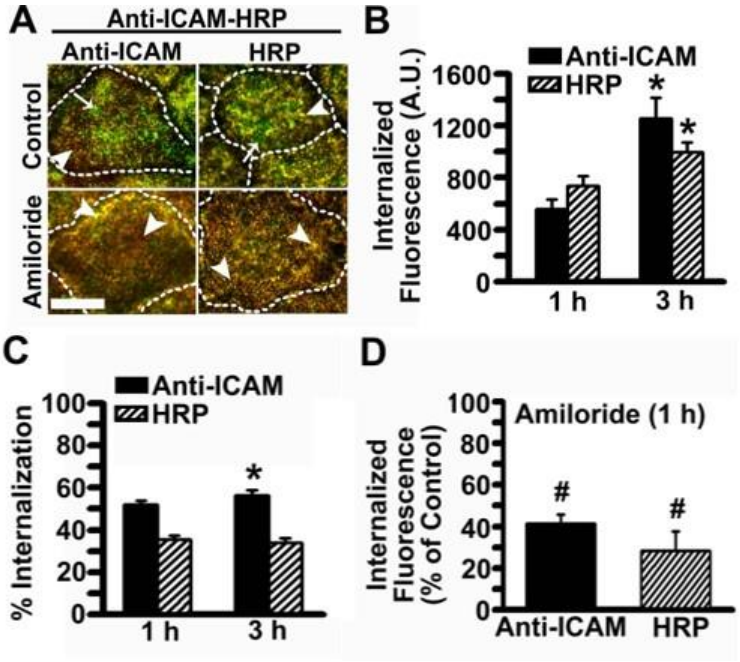

Figure 6.6. Uptake of the anti-ICAM HRP conjugate mixture by gastrointestinal epithelial cells. (A) The anti-ICAM-HRP conjugate mixture was incubated at 37 °C in the absence or presence of amiloride (an inhibitor of CAM-mediated endocytosis) with Caco-2 cells for 30 min to allow binding (pulse). Non-bound conjugates were removed by washing and cells were incubated with fresh medium for a total of 1 h or 3 h (only 1 h is shown). In parallel assays, either surface-bound anti-ICAM or HRP were immunostained to fluoresce in yellow (arrowheads), whereas internalized anti-ICAM or HRP were immunostained to fluoresce in green (arrows). Scale bar = 10 μm. Dashed lines mark the cell borders, as observed from phase-contrast microscopy. (B) The total internalized fluorescence per cell and the (C) percentage of internalization, either corresponding to anti-ICAM or HRP conjugate counterparts, were quantified using image analysis. (D) Uptake in cells treated with amiloride was quantified and compared to the control condition shown for 1 h in (C). Data are Mean ± S.E.M. * compares 3 h to 1 h for each conjugate component; # compares control vs. amiloride at 1 h; ($p < 0.05$, Student's *t* test).

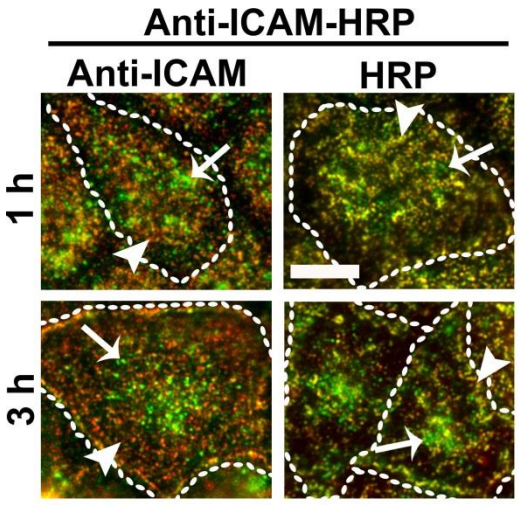

Figure 6.7. Time-dependent uptake of anti-ICAM HRP conjugates in gastrointestinal epithelial cells. Caco-2 cells were incubated with the anti-ICAM-HRP conjugate mixture for a 30 min pulse period, washed, and incubated with fresh medium for up to 1 or 3 h to track uptake. In parallel assays, either surface-bound anti-ICAM or HRP were immunostained to fluoresce in yellow (arrowheads), whereas internalized anti-ICAM or HRP were immunostained to fluoresce in green (arrows). Scale bar = 10 μm. Dashed lines mark the cell borders, as observed from phase-contrast microscopy.

Finally, we tested whether uptake of anti-ICAM-HRP conjugates could sustain HRP activity within cells (Fig. 6.8). To evaluate this, we examined the HRP activity of cells incubated with anti-ICAM-HRP conjugates vs. unconjugated anti-ICAM or HRP controls, which was performed with or without cell permeabilization. The rationale is that if cells are not permeabilized, the detectable HRP activity must come from the surface-bound fraction, while in permeabilized cells the enzyme substrate added would be accessible to both surface-bound and internalized HRP. Hence, the difference between these conditions shall render the internalized enzyme activity. As expected, in cells incubated with anti-ICAM-HRP conjugates, the activity detected after permeabilization (total activity) was 3.7-fold greater than that detected without permeabilization (surface activity); hence, 68% of the total HRP activity provided by anti-ICAM-HRP locates within the cell (Fig. 6.8A). In contrast, minimal HRP activity was detected in cells incubated with unconjugated HRP or anti-ICAM, whether or not cells were permeabilized (10- and 30-fold lower for permeabilized cells and 13- and 17-fold lower for non-permeabilized cells, respectively; Fig. 6.8A). This demonstrates insignificant contribution of endogenous cell peroxidases to the HRP activity measured, validating our method. Also, this result demonstrates that both surface and internalized enzyme activity are specifically delivered by anti-ICAM conjugates. Indeed, inhibition of the internalized HRP activity by amiloride (28% of the control condition; Fig. 6.8B) verifies the role of the CAM pathway in this process. As such, looking at the internalized activity alone (the difference between the activity in permeabilized vs. non-permeabilized cells), this was 9- and 45-fold greater for cells incubated with anti-ICAM-HRP conjugates vs. unconjugated HRP or anti-ICAM,

respectively (Fig. 6.8C), indicating the potential of conjugates to deliver active cargoes, such as enzymes, within target cells.

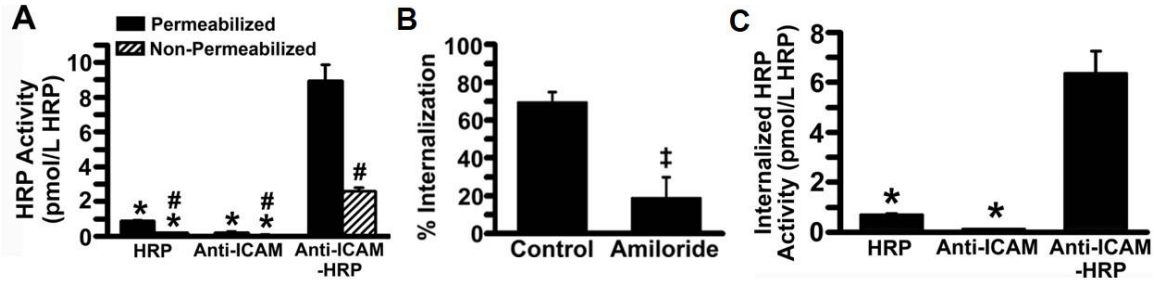

Figure 6.8. Enzyme activity delivered by anti-ICAM conjugates to gastrointestinal epithelial cells. (A) Caco-2 cells were incubated for 30 min at 37 °C with non-conjugated HRP or anti-ICAM vs. anti-ICAM-HRP conjugates in the absence or presence of amiloride (and inhibitor of CAM-mediated uptake). Non-bound conjugates were removed by washing and HRP substrate was added to measure HRP activity (pM HRP) in permeabilized cells (total internalized and cell surface-bound conjugate) vs. non-permeabilized cells (surface-bound fraction only) in parallel. The difference between these two measurements represents internalized activity (C). (B) The percentage of HRP activity internalized with respect to the total cell-associated activity was calculated from (A) in cells treated or not with amiloride. Data are Mean ± S.E.M. * Compares unconjugated counterparts to anti-ICAM-HRP conjugate; # compares permeabilized to non-permeabilized cells; ‡ compares amiloride vs. control; ($p < 0.05$, Student's *t* test).

6.2.4 Transport of Anti-ICAM-HRP Conjugates Into and Across Gastrointestinal Epithelial Monolayers

Having demonstrated the binding specificity of anti-ICAM-HRP, we then addressed the primary aim of this work, to assess whether monomeric binding by conjugates induces transport across cells. Previous characterization of anti-ICAM-HRP conjugates by SDS-PAGE and AF4 revealed a non-homogenous mixture consisting of (1) a predominant species with 2 HRP molecules conjugated per antibody (average molecular weight = 233 kDa), which contains a single copy of anti-ICAM and hence, binds to ICAM-1 in a monomeric manner, and (2) an aggregated species (average molecular weight = 686 kDa), which contains multiple copies of anti-ICAM and binds to ICAM-1 in a multimeric manner

(unpublished results under review). Thus, imperative to the objective of this study, we evaluated the transepithelial transport of the non-separated conjugate mixture vs. conjugates separated by AF4 into its respective monomeric (233 kDa) and multimeric (686 kDa) fractions (See Materials and Methods). By measuring the HRP activity of the basolateral (transported) fraction below cell monolayers over time, we demonstrated that monomeric ICAM-1-targeting by conjugates indeed led to delivery of HRP across these cells (Fig. 6.9). To our surprise, the monomeric, 233 kDa species delivered 10-fold and 2.6-fold greater HRP than the multimeric, 686 kDa fraction and the non-separated conjugate mixture, respectively (Fig. 6.9A). This trend was also observed in terms the rate of transport, P_{app}, which was 11-fold and 2.4-fold greater for 233 kDa conjugates relative to 686 kDa and non-separated conjugates (Fig. 6.9C). However, the percentage of transport with respect to the total cell-bound fraction, indicating the efficiency of the pathway, was ~50% for all molecular weight fractions (Fig. 6.9B). This suggests that the increase in absolute and rate of transport following monomeric binding resulted from enhanced initial uptake into cells. Taken together, monomeric binding to ICAM-1 led to transepithelial transport of conjugates, which did not increase in the presence of multimeric aggregates in the conjugate mixture. Considering that the non-separated conjugate mixture, produced a similar, although underestimated, level of transport, it was utilized for the remainder of transport studies.

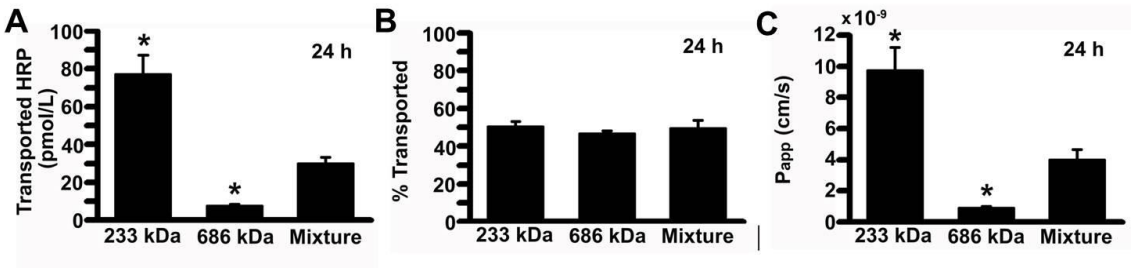

Figure 6.9. Transport of anti-ICAM-HRP conjugates after monomeric vs. multimeric binding to gastrointestinal epithelial monolayers. The anti-ICAM-HRP conjugate mixture was separated into two main molecular weight fractions by AF4: a form corresponding to 1:2 antibody-to-enzyme molar ratio (233 kDa) and a form representing larger multimolecular or aggregated conjugates (average = 686 kDa). Caco-2 cells cultured on transwell inserts were incubated with the conjugate mixture vs. each one of the separated conjugate fractions for 24 h at 37 ºC to allow transport into/across cells. HRP activity in the basolateral and cell fractions was measured using a spectrophotometric enzyme activity assay, and used to calculate (A) transported HRP activity (pmol/L), (B) the ratio of HRP activity found in the basolateral fraction to that in the combined basolateral and cell fractions (% transport), and (C) the rate of transport in terms of P_{app}. Data are Mean ± S.E.M. * compares values to the unseparated conjugate mixture ($p < 0.05$, Student's *t* test).

Similar to non-conjugated anti-ICAM, conjugates transported HRP across cells in a time-dependent manner: 2 pM HRP was transported across the cell monolayer by 1 h, accounting for 7% of the combined transported and cell fractions, which increased to 14 and 30 pM HRP, or 25 and 49% of the total cell-associated activity, by 5 h and 24 h (Fig. 6.10A-B). HRP activity in the basolateral chamber did not appear to result from endogenous peroxidase activity, as treatment with non-conjugated anti-ICAM produced negligible transport (3% of the level of anti-ICAM-HRP conjugates at 24 h) (Fig. 6.10C). In addition, conjugates enhanced transepithelial delivery by 2-fold relative to non-conjugated HRP (Fig. 6.10C). Nevertheless, a considerable amount of HRP was transported across cells, despite negligible association to cells (Fig. 6.9), perhaps owing to paracellular leakage or a non-specific transport mechanism. In contrast, minimal transport of IgG-HRP, which also does not associate to cells (Fig. 6.9), suggests that compounds of

this size do not undergo non-specific leakage and that targeted counterparts of similar size undergo specific, non-paracellular transport.

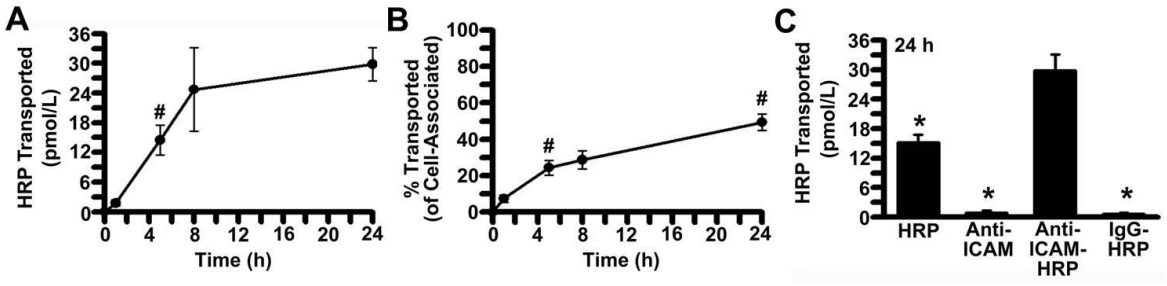

Figure 6.10. Transepithelial transport kinetics and specificity of anti-ICAM-HRP conjugates. Caco-2 cells cultured on transwell inserts were treated with anti-ICAM-HRP conjugates in the apical chamber for the indicated time intervals to allow intra- and transepithelial transport. To assess whether transport was specific to ICAM-1 binding, Caco-2 monolayers were also treated with non-conjugated HRP or anti-ICAM, or non-specific IgG-HRP conjugates. HRP activity in the basolateral and cell fractions was measured using a spectrophotometric enzyme activity assay, and used to calculate (A, C) transported HRP activity (pmol/L) or (B) the percent of transport, or the ratio of HRP activity found in the basolateral fraction to that in the combined basolateral and cell fractions. Data are Mean ± S.E.M. # compares each time point to the preceding one; * compares values to anti-ICAM-HRP conjugates ($p < 0.05$, Student's *t* test).

6.2.5 Anti-ICAM-HRP Conjugates Are Transported By a CAM-Mediated Pathway

Next, we evaluated whether conjugates traffic across cells by a vesicular, CAM-mediated pathway analogous to that utilized by anti-ICAM. First, we verified that transport of anti-ICAM-HRP was mediated by ICAM-1, given that the addition of an anti-ICAM competitor decreased accumulation of enzyme in the basolateral fraction by 76% relative to control, untreated conjugates, whereas the presence of IgG did not significantly alter transport (Fig. 6.11A). In identifying the contribution of CAM-endocytosis to transport, we demonstrated that EIPA inhibited both the amount and rate (P_{app}) of HRP activity transported by 60 and 92% of cells in the absence of an inhibitor (5h) (Fig. 6.11B). Moreover, similar to non-conjugated anti-ICAM, transport of conjugates did not seem to disrupt intercellular junctions between adjacent cells, as TEER values remained between 87 and 99% of values

for control, untreated cells over 24 h of transport. These results suggest that transport occurred by a vesicular pathway mediated by CAM-endocytosis, rather than a paracellular pathway.

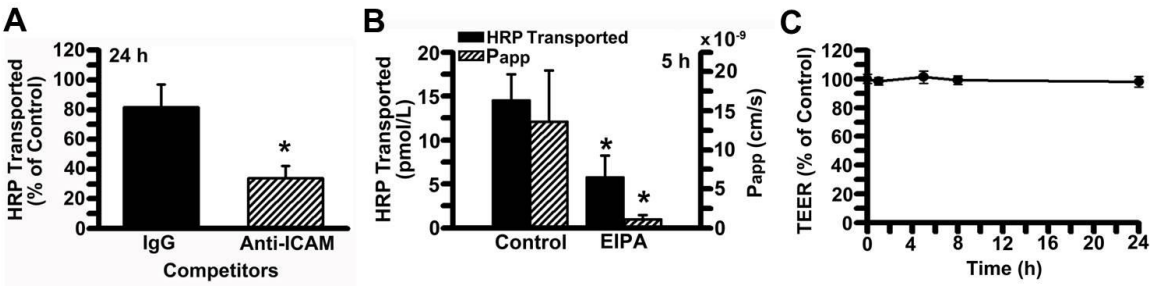

Figure 6.11. The mechanism of transport of anti-ICAM-HRP conjugates. (A) Caco-2 monolayers were incubated at 37 ºC for 24 h with anti-ICAM-HRP conjugates in the presence of anti-ICAM, to compete for ICAM-1 binding sites, or non-specific IgG. The HRP activity in the basolateral (transported) fraction was derived as described in Fig. 5, and normalized to control conditions in the absence of anti-ICAM or IgG. (B) Transport of anti-ICAM-HRP conjugates was assessed in the presence or absence of EIPA, an inhibitor of CAM-mediated endocytosis. Transport was expressed as the quantity HRP activity in the basolateral chamber (pM) as well as the rate of transport (P_{app}). (C) TEER was measured during transport of anti-ICAM-HRP conjugates across Caco-2 cells, to assess paracellular transport, and expressed as a percentage of values measured for untreated, control cells. Data are Mean ± S.E.M. * compares values to control cells treated with anti-ICAM-HRP ($p < 0.05$, Student's *t* test).

6.3 Discussion

Access of therapeutics into and across the GI epithelial lining, is imperative for the treatment disorders affecting the barrier itself and/or reaching the systemic circulation [6, 7, 52, 123]. Targeting drugs to cell-surface receptors involved in endocytosis has shown much success in this regard [6, 7, 52, 123]. In contrast to classical endocytic pathways, such as phagocytosis, clathrin- and caveolin-dependent endocytosis, and fluid-phase macropinocytosis, non-classical routes are less explored for this purpose. One such pathway that shows promise for drug delivery into and across cell barriers involves targeting to ICAM-1 [10, 13, 14]. Delivery of a model enzyme therapeutic across GI epithelial monolayers cells was previously demonstrated using multimeric targeting

strategies, i.e. anti-ICAM NCs carrying α-Gal, an enzyme used to treat Fabry disease [13]. In Chapter 5 of this dissertation, we demonstrated intracellular and transcellular transport of anti-ICAM in GI epithelial cells, revealing the potential of monomeric ICAM-1-targeting ligands as alternative drug vehicles that may provide distinct advantages with respect to multimeric targeting strategies [116]. In light of this work, this chapter examined whether such transport facilitates delivery of a therapeutic cargo, as was shown for multimeric counterparts.

For this purpose, we conjugated anti-ICAM to a drug cargo, represented here by the model enzyme, HRP. Our findings demonstrate that anti-ICAM-enzyme conjugates bind to ICAM-1 in a monomeric manner, and undergo specific transport into and across these cells. In parallel with anti-ICAM, anti-ICAM-enzyme conjugates are transported across cells by CAM-mediated transcytosis rather than a paracellular mechanism. This pathway was amenable to delivering HRP into and across GI epithelial cells, while preserving enzyme activity.

Specific binding to ICAM-1 on the GI epithelium has implications for minimizing clearance of freely circulating drug delivery systems, ultimately optimizing biodistribution to the site of absorption. Importantly, anti-ICAM retained its targeting ability after conjugation to an enzyme cargo, and preserved a considerable degree of enzyme activity upon binding to cells. In addition, uptake of monomeric anti-ICAM by ICAM-1 expressing cells may provide intracellular transport of therapeutic cargoes, as previously demonstrated in the case of multimeric binding to ICAM-1 [9, 12, 13, 25, 27, 30, 31, 35, 37, 86, 93, 112, 132-134, 164, 165, 169, 171]. Here, we examined cellular uptake of anti-ICAM conjugated to a model enzyme cargo, HRP. The conjugate mixture contained two major species: (a)

40% of the mixture contained a 233 kDa species, which corresponds to one antibody bearing two enzymes and, therefore binds to ICAM-1 in a monomeric manner; and (b) a 686 kDa fraction, which comprises 40% of the reaction and likely encompasses large conjugates or aggregates, and thus binds to ICAM-1 in a multimeric manner. The presence of both antibody and enzyme components of conjugates was verified by Western blot. As expected, binding was specifically driven by the anti-ICAM counterpart of conjugates. In accord with anti-ICAM uptake, endocytosis was found for anti-ICAM-HRP conjugates. Therefore, this strategy may be used for intracellular drug delivery via ICAM-1 in addition to published strategies that target ICAM-1 in a multimeric manner. Indeed, a similar degree of uptake (40-60% uptake) was observed between the unseparated conjugated mixture and conjugates species that bind to ICAM-1 in a monomeric (233 kDa) or multimeric (686 kDa) manner. This rate of uptake is similar to that of unconjugated anti-ICAM, further validating uptake upon monomeric binding. The process was abolished by an inhibitor of the CAM pathway, indicating its mediation by the antibody rather than the enzyme counterpart. Anti-ICAM-triggered uptake was further verified using IgG-HRP conjugates and unconjugated components.

Importantly, the enzyme counterpart of conjugates was active upon binding to the cell surface as well as after uptake, since significant activity was measured in both scenarios, and this was specific to ICAM-1-targeted counterparts. Efficient uptake of enzyme cargoes via ICAM-1 has been previously shown upon multimeric binding to cells [25, 30, 31, 181], including the case of anti-ICAM-coated nanoparticles loaded with α-Gal, which were observed to transcytose across Caco-2 cells [13]. Although the drug payload of anti-ICAM NCs that bind to ICAM-1 in a multimeric manner exceeded that of anti-

ICAM conjugates that bind in a monomeric fashion (~200 vs. 2 enzymes per targeting vehicle), the latter strategy provided greater targeting in terms of the number of enzyme molecules associated per cell (~4.5×10^5 vs. 2×10^5, respectively) and enzyme molecules internalized (~2×10^7 vs. 4×10^5 enzyme molecules per cell) [13]. This may be due to less steric hindrance between small antibody-enzyme conjugates binding to adjacent ICAM-1 molecules on the cell surface compared to ~250 nm antibody-coated nanocarriers. Hence, the smaller size afforded by monomeric vs. multimeric ligands may prove more beneficial in delivering therapeutics. Alternatively, this may be due to higher degradation of the enzyme cargo upon trafficking of anti-ICAM NCs to lysosomes, as previously shown [92], compared to low lysosomal transport and degradation of monomeric anti-ICAM. Whether these advantages hold true for other drug cargoes, such as smaller or more lipophilic agents, and upon administration *in vivo,* are aspects to be explored in future studies. Nevertheless, accumulation of monomeric ICAM-1-targeting vehicles within cells may benefit disorders affecting cell linings themselves, particularly GI epithelial and vascular complications where ICAM-1 is up-regulated by an inflammatory state, as in the case for inflammatory bowel disease, pathogenic infections, and atherosclerosis [19-22].

Importantly, transcytosis of anti-ICAM provided an avenue for delivery of an active drug cargo across GI epithelial cells, analogous to anti-ICAM NCs. Separation of anti-ICAM-enzyme conjugates into its respective molecular weight fractions revealed that such delivery was mediated by both monomeric and multimeric species. To our surprise, monomeric binding by conjugates induced significantly greater transport of enzymes across cells than multimeric counterparts. This was surprising considering that anti-ICAM NCs exceeded monomeric anti-ICAM in terms of the amount of enzymes transported

(4×10^5 vs. 4×10^4 molecules transported per cell at 24 h) and P_{app} (2×10^{-8} cm/s vs. 4×10^{-9} cm/s at 24 h) [13]. Therefore, multimeric formulations targeting ICAM-1 may benefit from the presence of a drug carrier rather than direct drug conjugation (multimeric conjugates), in terms of drug payload, uniform shape and orientation of targeting ligands, etc. Nevertheless, monomeric conjugates as well as multimeric conjugates and carriers behaved similarly with respect to the percentage of transport (40-50% at 24 h), indicating that the absolute amount of drug transport largely depends on initial cellular accumulation, which as noted above, was greater for ICAM-1 targeted NCs.

In addition, whereas the parameters characterizing transport of anti-ICAM NCs remained similar in the presence vs. absence of a drug cargo [13], conjugation of enzymes to anti-ICAM significantly reduced transport with respect to the unconjugated antibody. This may arise from discrepancies in the method of formulation; direct conjugation may compromise targeting and/or enzyme activity to a greater degree than non-covalent coating of the targeting ligand and enzymes onto the surface of nanocarriers. Moreover, in the latter formulation, many copies (i.e., >100) of targeting ligands and enzymes per NC results in a higher probability that the functionality of each NC is retained despite a fraction of the coat becoming denatured/deactivated. Another possibility for differences in transport between anti-ICAM-HRP and anti-ICAM is that conjugation significantly increases the size of anti-ICAM by ~50%, whereas coating of enzymes onto anti-ICAM NCs does not alter its size [13].

As demonstrated for anti-ICAM, anti-ICAM conjugated to an enzyme cargo is transported across cells by a vesicular CAM pathway, rather than a paracellular mechanism. This finding supports the observation that regardless of varying formulations,

such as monomeric vs. multimeric systems, presence vs. absence of a drug cargo, etc., targeting ICAM-1 leads to CAM-mediated transcytosis in cellular barriers [13]. This pairs well with previous reports indicating that CAM-mediated uptake and intracellular trafficking accommodates drug delivery systems with varying size, shape, targeting valency, and chemistry [25, 116, 132, 165]. In addition, extensive literature demonstrates that CAM-mediated endocytosis is amenable for the intracellular delivery of therapeutic and imaging agents, particularly enzyme cargoes [28, 30, 31, 36, 122, 132, 133, 165], providing efficient uptake while preserving their functional activity. Together with our observations using anti-ICAM NCs, the present work further supports that CAM-mediated transcytosis is also amenable for the delivery of active enzymes into and across cellular barriers.

6.4 Conclusion

The results in this chapter demonstrate that monomeric ligands targeted to ICAM-1 may serve as a vehicle for the delivery of active therapeutics into and across GI epithelial cells, significant for oral therapies aimed at treating the GI epithelium itself or accessing the systemic circulation. This provides a valuable alternative to multimeric carrier formulations in that it may offer distinct advantages for oral drug delivery, therefore expanding the range of clinical applications afforded by targeting ICAM-1.

Chapter 7: Overall Conclusions and Future Directions

7.1 Overall Conclusions

Among the various routes of drug administration, oral delivery through the GI tract is considered the most favorable for patients, healthcare workers, and manufacturers, owing to greater patient compliance, low cost, and fewer safety concerns relative to parenteral injections or infusions [1]. In light of these benefits, oral dosage forms represent the majority (90%) of all medicines and a substantial, USD $49 billion market [1]. However, efficient drug absorption by this route remains a major challenge due to various physiological barriers posed by the GI tract, including: (1) premature degradation and/or deactivation of drugs, e.g. by the low pH and proteolytic activity in the stomach; (2) poor mucus penetration and binding to the GI epithelium, resulting in low biodistribution to the site of drug absorption; and (3) suboptimal transport into GI epithelial cells, for treatment of GI pathologies, or across these cells for subsequent delivery into the systemic circulation [2, 3]. Numerous therapeutics entering the market are particularly susceptible to these barriers, including protein or peptide-containing biotherapeutics, necessitating more invasive routes of administration [2, 3]. Hence, the goal of this dissertation was to establish a strategy to improve oral delivery of therapeutics, particularly those with negligible oral bioavailability.

The work herein sought to achieve this goal by targeting therapeutics to ICAM-1, a cell-surface receptor located on the GI epithelial lining and various other tissues accessed by the systemic circulation [7, 13]. Extensive characterization by our lab has revealed significant potential of this strategy for both systemic delivery and oral delivery [13, 15,

27, 30, 31, 36-38]. In the context of oral delivery, we previously demonstrated that ICAM-1 targeted NCs were capable of efficient binding, uptake, and a novel means of transport across GI epithelial cells grown in culture [13]. Uptake and transepithelial transport relied on CAM-mediated endocytosis and transcytosis [13], which was favorable in that CAM-endocytosis has been previously characterized and optimized to deliver drugs and drug carriers with wide-ranging size, shape, chemistry, and targeting valency, while preserving the functionality of these cargoes [9, 12, 24-34]. In addition to the ability to fine-tune and regulate this pathway, CAM-transport did not induce prolonged opening of intercellular junctions that keep the epithelial permeability barrier intact, providing a relatively safe means of transport [13]. In addition, relative to NCs exploiting other transcytosis pathways, including NCs targeted to the B12 and Fc receptors, CAM-mediated transcytosis is more efficient in terms of the percentage of cell-bound NCs that are transported [13, 182, 183]. Importantly, this pathway enabled delivery of a model therapeutic cargo, enzymes for the treatment of Fabry disease, into and across these cells [13]. Apart from promising results in cell culture, oral gavage of ICAM-1 targeted antibodies either as single entities (anti-ICAM) or coated onto the surface of polymer NCs (anti-ICAM NCs) in mice revealed targeting of these systems to GI tissue [15]. However, the efficacy of these strategies was limited by enzymatic degradation of targeting antibodies in the stomach, reducing biodistribution to the small intestine, the main site of drug absorption [15].

These studies prompted the need to encapsulate ICAM-1 targeted systems for protection in the stomach and site-specific release in the small intestine, while preserving the function of targeting moieties. Ultimately, this would enable us to better evaluate the oral delivery potential of ICAM-1 targeting strategies *in vivo*, which additionally provides

a comparison to previous reports by our lab examining systemic delivery upon intravenous injections in mice [25, 27, 29-31, 37]. Encapsulation would not only benefit ICAM-1 targeted systems, but other drug delivery systems with labile targeting components that are susceptible to GI degradation, particularly those that are protein-based. In Chapter 4, we successfully addressed these requirements using alginate and chitosan-alginate hydrogel microspheres. Given that the binding and transport efficacy of anti-ICAM NCs was previously established in cultured GI epithelial cells, we characterized encapsulation of model antibody-coated NCs. Although there is extensive literature on utilization of alginate and chitosan-alginate hydrogels for effective oral delivery of therapeutics, including a wide range of delicate biological entities [16, 17, 47-49, 106-111], this application was not yet described for antibody-coated NCs, nor for other targeted drug delivery systems.

First, we demonstrated that we were able to adjust the size of alginate beads to conform to different *in vivo* applications: we formulated ~180 μm-diameter microspheres for mice studies (which were selected for the remainder of this work), as well as 2.8 mm-diameter beads for future studies in larger animals, such as rats. Both of these formulations exhibited uniform size, shape, and efficient loading of targeted NCs within the bead population, which did not differ in the presence of a chitosan shell. Moreover, the loading efficiency within microspheres exceeded that of previous works encapsulating large biological entities. We then confirmed that microspheres remained stable in storage conditions, and displayed pH-triggered release in GI conditions: they remained intact in gastric conditions and released their contents in intestinal conditions. We were able to further attenuate burst release by the addition of a chitosan shell, increasing chitosan shell concentration, and crosslinking the chitosan shell, yet we were not able to exert substantial

control over release kinetics using these strategies. Moreover, examination of encapsulated NCs after treatment in GI conditions revealed substantial targeting to ICAM-1 expressing endothelial and GI epithelial cells, even in the presence of digestive enzymes. Importantly, these results held true upon oral gavage of encapsulated NCs in mice. Relative to non-encapsulated NCs, microspheres provided significantly greater protection of NCs from degradation in all GI organs, site-specific release in the small intestine. Furthermore, we revealed that greater intestinal accumulation of NCs was attributed to ICAM-1 targeting. Therefore, this work provided an important foundation for studying the efficacy of ICAM-1, and potentially other, targeted platforms, for oral delivery *in vivo*. For example, this encapsulation method is not only limited to antibody-coated NCs but can be applied to systems with different targeting moieties, NCs, or drug-ligand conjugates in the absence of NCs, such as the anti-ICAM-enzyme conjugates described here.

Whereas our work on GI cell transport and encapsulation of ICAM-1 targeting strategies involved multimeric strategies employing anti-ICAM-coated carriers, Chapter 5 was dedicated to evaluating an alternative targeting platform utilizing monomeric ICAM-1 targeting, which would provide a novel opportunity for direct conjugation to therapeutics rather than loading onto NCs. In addition to providing a less complex formulation, monomeric targeting may endow distinct drug delivery outcomes, such as biodistribution, cellular binding and transport, metabolism, elimination, etc. These differences were first evaluated in vascular endothelial cells, to compare to extensive literature on CAM-mediated endocytosis of anti-ICAM NCs in these cells [12, 91-93]. Here we revealed, for the first time, uptake of monomeric ligands (i.e., anti-ICAM) by CAM-mediated endocytosis, although to a lower extent than multimeric counterparts. Rather than

lysosomal degradation encountered by multimeric platforms, we demonstrated that endocytosed monomeric anti-ICAM instead recycled to the plasma membrane, mimicking trafficking of its receptor in the absence of ligands. From a biological standpoint, these results alluded to novel roles for differential cellular regulation of ICAM-1 and its ligands. Furthermore, such regulation presented unique differences with respect to that of other cell-surface receptors. For example, in contrast to multimeric ICAM-1 ligands, multimeric ligands targeted to the Fc, transferrin, and B12 receptors were observed to avoid lysosomal degradation, while their monomeric counterparts trafficked to lysosomes [141, 182, 183]. These differences may arise from the fact that natural ligands to most receptors are monomeric, whereas ICAM-1 typically binds in a multimeric manner, e.g. to leukocytes and viruses [10]. In addition, while CAM-mediated endocytosis holds for both monomeric and multimeric ligands, the mechanism of endocytosis has been shown to switch upon monomeric vs. multimeric targeting to other receptors, as in the case of the B12 receptor [182]. From a drug delivery perspective, these observations exposed a novel avenue for intracellular drug delivery using monomeric ligands targeted to ICAM-1. This strategy may prove especially valuable for intracellular interventions, in light of minimal lysosomal degradation as compared with multimeric counterparts. Therefore, we subsequently explored these aspects in the context of improving oral delivery into GI epithelial cells.

In continuation of our findings in vascular endothelial cells, we then demonstrated that anti-ICAM undergoes similar uptake in GI epithelial cells by CAM-mediated endocytosis. Moreover, reduced uptake and minimal lysosomal trafficking and degradation relative to multimeric anti-ICAM NCs suggested that differential regulation of monomeric vs. multimeric ICAM-1 ligands may hold true for all cell types expressing ICAM-1.

Moreover, we revealed that such uptake led to transcytosis across a GI epithelial cell barrier model, as it did for multimeric formulations. Similar to anti-ICAM NCs [13], anti-ICAM were transported across cells by a CAM-mediated, rather than a paracellular, pathway, hence preserving cell barrier integrity. Hence, by characterizing an alternative carrier platform, we have expanded the range of oral drug delivery outcomes afforded by ICAM-1 targeting. This will also enables us to select an appropriate therapeutic intervention that caters to these distinct outcomes.

Furthermore, similar to anti-ICAM NCs, anti-ICAM provided substantial binding and intracellular delivery of a model enzyme cargo in GI epithelial cells, while preserving its enzyme activity. This finding is valuable for oral delivery of drugs, particularly biotherapeutics, with low innate affinity to and transport into/across the GI epithelial barrier. In addition, these results allow us to expand our knowledge and translation of enzyme delivery by ICAM-1 targeting, which has been a major focus of our lab. Uptake of biotherapeutics, or other drugs, into cells would be valuable for treating pathologies that affect the GI epithelial lining, such as infections, inflammatory bowel disease (Crohn's disease and ulcerative colitis), cancers, etc. where ICAM-1 is preferentially expressed [19-22].

Importantly, CAM-mediated transcytosis mediated delivery of active enzymes across the GI epithelial cell barrier, advocating the potential for oral delivery across these cells for access into the systemic circulation. Enzyme delivery by anti-ICAM was lower than that of anti-ICAM NCs, yet these comparisons do not take into account that delivery by the latter strategy was reported in terms of the total amount of enzymes transported regardless of functional activity [13]. Similar to CAM-mediated endocytosis, these results

demonstrate that CAM-mediated transcytosis is also flexible in that it caters to drug carriers and cargoes of different size, shape, and valency. Hence, monomeric vehicles targeted to ICAM-1 serves as a viable alternative to multimeric carriers for oral delivery across the GI epithelium.

Taken together, this dissertation has provided the groundwork for implementation of ICAM-1 targeting strategies for oral delivery: (1) in continuation of previous results demonstrating the efficacy of ICAM-1 targeted NCs for oral delivery, we encapsulated these NCs for protection in gastric conditions, site-specific release in intestinal conditions, and retention of targeting ability *in vitro*, cell culture, and animal models; (2) we explored monomeric ligands to ICAM-1 as an alternative carrier that provides distinct uptake and intracellular trafficking relative to former multimeric strategies, enabling a novel opportunity to deliver drugs into GI epithelial cells; and (3) we exploited this monomeric targeting strategy for delivery of active drugs into and across a model GI epithelial barrier. Therefore, this work establishes two complementary ICAM-1 targeting systems that endow different advantages for oral delivery, and the framework for evaluating the efficacy of these systems *in vivo*.

7.2 Future Directions

As noted above, the work performed in this dissertation has advocated the potential of ICAM-1 targeting strategies for improving oral absorption of therapeutics, as well as providing a foundation for studying these strategies *in vivo*. However, further

characterization and optimization has yet to be performed for future translation of these strategies.

First, the components used to formulate monomeric and multimeric ICAM-1 targeting systems thus far, including whole antibodies, polystyrene NCs, and enzyme drug cargoes, served as prototypes for facilitating their characterization and reducing the time, labor, and cost required to produce clinical-grade formulations. However, more clinically relevant alternatives may be used for future studies examining oral delivery by targeting ICAM-1. For example, while the work described herein employed whole antibodies from another species as the targeting ligand, this would lead to adverse immune reactions in patients, as well as potential detachment from drugs or drug carriers due to high shear stress in a physiological environment. Truncating the antibody to only include the variable region, the domain responsible for molecular recognition and binding, may result in less shear stress and minimize potential toxicity and immune recognition of antibody Fc regions. To address this, our lab has recently established a 17-mer linear peptide (γ3) as a viable substitute for targeting ICAM-1 from the systemic circulation [112]. Indeed, recent work demonstrated that γ3-coated NCs closely mimic the drug delivery parameters afforded by anti-ICAM NCs, in terms of targeting, CAM-endocytosis, lysosomal trafficking, and biodistribution upon intravenous administration in mice [112]. In addition, γ3 is likely to target ICAM-1 in different species (e.g., mouse, chimpanzee, and humans), which is suitable for the translation of ICAM-1-targeting platforms in future preclinical and clinical studies [112]. Hence, future studies may similarly utilize these peptides for oral delivery applications.

In addition, we could employ PLGA particles as an alternative to model polystyrene particles. PLGA is a biodegradable material that is already in several FDA-approved devices [58]. As noted in Chapter 3, ICAM-1 targeted PLGA particles demonstrated similar binding, internalization, intracellular trafficking characteristics as polystyrene counterparts. Future work may include confirming oral delivery achieved by anti-ICAM NCs presented in this thesis with PLGA particles, which has already been formulated and optimized in-house. Another benefit of using PLGA particles is the ability to chemically conjugate targeting moieties and polyethylene glycol (PEG) chains to the polymer end groups, which would endow greater stability of targeting entities on the particle surface in the GI lumen and post-GI trafficking [2]. We could also enhance the efficacy of monomeric ICAM-1 ligand-drug conjugates by PEG conjugation, which has been shown to increase mucus permeation and reduce enzymatic degradation, opsonization, and clearance by immune cells [8].

The work described previously and within this dissertation utilized enzymes as a model drug cargo, expanding upon the extensive studies performed by our lab demonstrated effective delivery of enzymes, particularly those used for the treatment of LSDs, in other cell types grown in culture and upon intravenous administration in mice [27, 30, 31, 36, 37, 94]. To further extend our knowledge on this application for oral delivery, future work may involve direct conjugation of a monomeric ICAM-1 ligand to more clinically relevant enzymes, such as α-Gal for the treatment of Fabry disease, and evaluation of drug activity as well as disease attenuation in cell culture and animal models. Furthermore, while α-Gal was used as a drug cargo for anti-ICAM NCs [13], the level of activity and disease attenuation was not yet tested following transport in GI epithelial cells.

Moreover, oral delivery applications involving direct conjugation or NC coupling to other types of therapeutics could be the subject of future studies employing ICAM-1 targeting strategies. Lipophilic drugs, for instance, would benefit from these strategies in terms of solubility in aqueous buffers but also cellular binding and regulation of transport.

In addition, the work conducted thus far on monomeric ICAM-1 ligand-drug conjugates demonstrated targeting and cellular transport in GI epithelial cell culture models. To further progress our knowledge on the potential of this strategy for oral delivery, future experiments will involve encapsulation of monomeric ICAM-1 ligands, as performed in this dissertation using multimeric platforms. Furthermore, in vivo characterization of drug delivery parameters (e.g., biodistribution, accumulation in tissues, etc.) could be permitted by future encapsulation of ICAM-1 targeted platforms with a drug cargo. Encapsulation of different formulations, such as monomeric vehicles and ICAM-1 targeted platforms coupled to a drug cargo, and enhanced control over release patterns, may warrant further optimization of chitosan-alginate microspheres. For example, we can optimize loading and release of these formulations by modulating alginate crosslinking density, e.g. using alginate with a higher guluronic acid content or adjusting the amount or type of divalent cations in the crosslinking media, or altering the pH, concentration, and crosslinking density of the chitosan coating, as explored herein and in previous literature [48, 49, 105]. We could also substitute alginate with alginate derivatives or other anionic hydrogels that are described for controlled release at neutral pH, including natural polymers (e.g., gellan gum, carrageenan, pectin, etc.) or synthetic polymers (e.g., polyacrylic and polymethacrylic acids) [4, 5, 16, 96]. In addition, it is likely that chitosan and genipin-crosslinked chitosan coatings do not significantly attenuate burst release in intestinal

conditions due to total or partial solvation of the chitosan shell at low pH [4]. This could be resolved in future studies by providing an additional layer of crosslinked alginate or by substituting chitosan with other cationic polymers that swell but do not dissolve in acidic medium, such as derivatized chitosan or poly-L-lysine [4, 16, 96, 107].

Importantly, the encapsulation method provided by this dissertation represents a valuable tool for future studies evaluating translation of ICAM-1 targeting strategies for oral delivery *in vivo*. Retention of ICAM-1 targeting of anti-ICAM NCs following release from microspheres will presumably allow for subsequent uptake into GI epithelial cells, although this has yet to be confirmed. Moreover, our previous work using anti-ICAM NCs and the present studies using anti-ICAM demonstrates that targeting ICAM-1 elicits delivery of therapeutics into GI epithelial cells. Distinct intracellular delivery outcomes have also been achieved as a result of: (1) differential endocytic routing taken by either targeting strategy; and (2) adjusting intracellular trafficking using chemical agents and carriers of different size, shape, and targeting valency [24, 25, 91, 122]. In light of these benefits, future work may involve ICAM-1 mediated delivery into the GI tissue for alleviation of GI disorders. For appropriate selection of a GI intervention, future experiments may involve quantification of the levels and distribution ICAM-1 expression throughout the various regions of the GI tract, and differential expression in healthy vs. diseased conditions. As previously noted, ICAM-1 is overexpressed in pathological conditions, as observed in the case of colon cancer, inflammatory bowel disease, and GI infections [19-22]. Hence, site-specific delivery to diseased tissues in the gut is conceivable. Indeed, our lab has recently established a model of intestinal inflammation in mice by dextran sulfate sodium (DSS)-induced colitis for this purpose. We could also

employ acid sphingomyelinase- or α-Gal-knockout mice, mimicking Niemman Pick and Fabry disease (two types of LSDs), which have been established in-house. Future experiments may evaluate whether biodistribution of ICAM-1 targeted systems favors inflamed tissues, as they did upon intravenous injection into disease-model mice.

Future studies may also probe the biological basis of CAM-mediated transcytosis, which has yet to be elucidated. In the case of transport across the vascular endothelial cells, the CAM pathway induced by anti-ICAM NCs presents similarities with ICAM-1 assisted transcellular transmigration of leukocytes across the vascular endothelial barrier, relevant to its biological role in mediating inflammation [113]. With regard to the intestinal epithelial barrier, a recent publication also revealed an analogous role for ICAM-1 in docking leukocytes to the apical surface of the intestinal epithelium, leading to transmigration across these cells [184]. Hence, future experiments may assess the overlap of cellular events regulating the transport of ICAM-1 targeted drug delivery systems with those observed during ICAM-1 mediated intestinal leukocyte transport, such as activation of the myosin light-chain kinase pathway.

Moreover, future work must assess the potential of ICAM-1 targeting for drug delivery into the systemic circulation via the oral route. For this purpose, the degradation status and targeting viability of ICAM-1 ligands can be assessed following transport across cultured GI epithelial monolayers, e.g. by Western blot, ELISA, and examining binding to a sub-epithelial cell lining cultured on the underside of transwells. Biodistribution of ICAM-1 targeted systems to the circulation and organs beyond the GI tract may also be evaluated upon oral gavage of microspheres in mice. These studies would allow us to determine whether further optimization of our models is needed to enhance their stability

following absorption by the GI tract, as well as select appropriate therapeutic interventions that reflect biodistribution patterns.

Taken together, this dissertation has established significant milestones for the advancement of ICAM-1 targeted systems for oral drug delivery: (1) we characterized an encapsulation strategy for evaluating oral delivery of ICAM-1 targeted systems *in vivo*; and (2) identified monomeric ICAM-1 targeting vehicles as a viable alternative to multimeric systems that enables intracellular delivery and (3) transcellular delivery of active therapeutics. These strategies show much promise for improving delivery of therapeutics into and across the GI tract, for interventions aimed at treating GI disorders and entering the systemic circulation via the oral route.

References

[1] F. Gabor, C. Fillafer, L. Neutsch, G. Ratzinger, M. Wirth, Improving oral delivery, Handb Exp Pharmacol, (2010) 345-398.
[2] V.K. Pawar, J.G. Meher, Y. Singh, M. Chaurasia, B. Surendar Reddy, M.K. Chourasia, Targeting of gastrointestinal tract for amended delivery of protein/peptide therapeutics: strategies and industrial perspectives, J Control Release, 196 (2014) 168-183.
[3] J. Renukuntla, A.D. Vadlapudi, A. Patel, S.H. Boddu, A.K. Mitra, Approaches for enhancing oral bioavailability of peptides and proteins, Int J Pharm, 447 (2013) 75-93.
[4] L.A. Sharpe, A.M. Daily, S.D. Horava, N.A. Peppas, Therapeutic applications of hydrogels in oral drug delivery, Expert Opin Drug Deliv, 11 (2014) 901-915.
[5] N.A. Peppas, K.M. Wood, J.O. Blanchette, Hydrogels for oral delivery of therapeutic proteins, Expert Opin Biol Ther, 4 (2004) 881-887.
[6] J.H. Hamman, P.H. Demana, E.I. Olivier, Targeting receptors, transporters and site of absorption to improve oral drug delivery, Drug Target Insights, 2 (2007) 71-81.
[7] S. Muro, Challenges in design and characterization of ligand-targeted drug delivery systems, J Control Release, 164 (2012) 125-137.
[8] V. Torchilin, Multifunctional and stimuli-sensitive pharmaceutical nanocarriers, Eur J Pharm Biopharm, 71 (2009) 431-444.
[9] J.-C. Murciano, S. Muro, L. Koniaris, M. Christofidou-Solomidou, D.W. Harshaw, S.M. Albelda, D.N. Granger, D.B. Cines, V.R. Muzykantov, ICAM-directed vascular immunotargeting of antithrombotic agents to the endothelial luminal surface, Blood, 101 (2003) 3977-3984.
[10] S. Muro, Intercellular Adhesion Molecule-1 and Vascular Cell Adhesion Molecule-1, in: W.C. Aird (Ed.) Endothelial biomedicine, Cambridge University Press, New York, 2007, pp. 1058-1070.
[11] R. Rothlein, M.L. Dustin, S.D. Marlin, T.A. Springer, A human intercellular adhesion molecule (ICAM-1) distinct from LFA-1, J Immunol, 137 (1986) 1270-1274.
[12] S. Muro, R. Wiewrodt, A. Thomas, L. Koniaris, S.M. Albelda, V.R. Muzykantov, M. Koval, A novel endocytic pathway induced by clustering endothelial ICAM-1 or PECAM-1, J Cell Sci, 116 (2003) 1599-1609.
[13] R. Ghaffarian, T. Bhowmick, S. Muro, Transport of nanocarriers across gastrointestinal epithelial cells by a new transcellular route induced by targeting ICAM-1, J Control Release, 163 (2012) 25-33.
[14] J. Hsu, J. Rappaport, S. Muro, Specific binding, uptake, and transport of ICAM-1-targeted nanocarriers across endothelial and subendothelial cell components of the blood-brain barrier, Pharm Res, 31 (2014) 1855-1866.
[15] V. Mane, S. Muro, Biodistribution and endocytosis of ICAM-1-targeting antibodies versus nanocarriers in the gastrointestinal tract in mice, Int J Nanomedicine, 7 (2012) 4223-4237.
[16] M. George, T.E. Abraham, Polyionic hydrocolloids for the intestinal delivery of protein drugs: alginate and chitosan--a review, J Control Release, 114 (2006) 1-14.
[17] K.Y. Lee, D.J. Mooney, Alginate: properties and biomedical applications, Prog Polym Sci, 37 (2012) 106-126.

[18] R. Rothlein, C. Wegner, Role of intercellular adhesion molecule-1 in the inflammatory response, Kidney Int, 41 (1992) 617-619.
[19] G.T. Huang, L. Eckmann, T.C. Savidge, M.F. Kagnoff, Infection of human intestinal epithelial cells with invasive bacteria upregulates apical intercellular adhesion molecule-1 (ICAM)-1) expression and neutrophil adhesion, J Clin Invest, 98 (1996) 572-583.
[20] R.C. Burns, J. Rivera-Nieves, C.A. Moskaluk, S. Matsumoto, F. Cominelli, K. Ley, Antibody blockade of ICAM-1 and VCAM-1 ameliorates inflammation in the SAMP-1/Yit adoptive transfer model of Crohn's disease in mice, Gastroenterology, 121 (2001) 1428-1436.
[21] T. Watanabe, T. Arakawa, K. Tominaga, Y. Fujiwara, K. Higuchi, T. Kuroki, Neutrophil accumulation in development gastric ulcer induced by submucosal injection of endothelin-1 in rats, Dig Dis Sci, 45 (2000) 880-888.
[22] Y. Maruo, A. Gochi, A. Kaihara, H. Shimamura, T. Yamada, N. Tanaka, K. Orita, ICAM-1 expression and the soluble ICAM-1 level for evaluating the metastatic potential of gastric cancer, Int J Cancer, 100 (2002) 486-490.
[23] W.M. Saltzman, M.L. Radomsky, K.J. Whaley, R.A. Cone, Antibody diffusion in human cervical mucus, Biophys J, 66 (1994) 508-515.
[24] A.J. Calderon, T. Bhowmick, J. Leferovich, B. Burman, B. Pichette, V. Muzykantov, D.M. Eckmann, S. Muro, Optimizing endothelial targeting by modulating the antibody density and particle concentration of anti-ICAM coated carriers, J Control Release, 150 (2011) 37-44.
[25] S. Muro, C. Garnacho, J.A. Champion, J. Leferovich, C. Gajewski, E.H. Schuchman, S. Mitragotri, V.R. Muzykantov, Control of endothelial targeting and intracellular delivery of therapeutic enzymes by modulating the size and shape of ICAM-1-targeted carriers, Mol Ther, 16 (2008) 1450-1458.
[26] R. Rossin, S. Muro, M.J. Welch, V.R. Muzykantov, D.P. Schuster, In vivo imaging of 64Cu-labeled polymer nanoparticles targeted to the lung endothelium, J Nucl Med, 49 (2008) 103-111.
[27] C. Garnacho, R. Dhami, E. Simone, T. Dziubla, J. Leferovich, E.H. Schuchman, V. Muzykantov, S. Muro, Delivery of acid sphingomyelinase in normal and niemann-pick disease mice using intercellular adhesion molecule-1-targeted polymer nanocarriers, J Pharmacol Exp Ther, 325 (2008) 400-408.
[28] O.S. Finikova, A.Y. Lebedev, A. Aprelev, T. Troxler, F. Gao, C. Garnacho, S. Muro, R.M. Hochstrasser, S.A. Vinogradov, Oxygen microscopy by two-photon-excited phosphorescence, Chemphyschem, 9 (2008) 1673-1679.
[29] J. Hsu, T. Bhowmick, S.R. Burks, J.P. Kao, S. Muro, Enhancing biodistribution of therapeutic enzymes in vivo by modulating surface coating and concentration of ICAM-1-targeted nanocarriers, J Biomed Nanotechnol, 10 (2014) 345-354.
[30] J. Hsu, L. Northrup, T. Bhowmick, S. Muro, Enhanced delivery of alpha-glucosidase for Pompe disease by ICAM-1-targeted nanocarriers: comparative performance of a strategy for three distinct lysosomal storage disorders, Nanomedicine, 8 (2012) 731-739.
[31] J. Hsu, D. Serrano, T. Bhowmick, K. Kumar, Y. Shen, Y.C. Kuo, C. Garnacho, S. Muro, Enhanced endothelial delivery and biochemical effects of alpha-galactosidase by ICAM-1-targeted nanocarriers for Fabry disease, J Control Release, 149 (2011) 323-331.

[32] C. Chittasupho, S.X. Xie, A. Baoum, T. Yakovleva, T.J. Siahaan, C.J. Berkland, ICAM-1 targeting of doxorubicin-loaded PLGA nanoparticles to lung epithelial cells, Eur J Pharm Sci, 37 (2009) 141-150.
[33] F.S. Villanueva, R.J. Jankowski, S. Klibanov, M.L. Pina, S.M. Alber, S.C. Watkins, G.H. Brandenburger, W.R. Wagner, Microbubbles targeted to intercellular adhesion molecule-1 bind to activated coronary artery endothelial cells, Circulation, 98 (1998) 1-5.
[34] E.N. Atochina, I.V. Balyasnikova, S.M. Danilov, D.N. Granger, A.B. Fisher, V.R. Muzykantov, Immunotargeting of catalase to ACE or ICAM-1 protects perfused rat lungs against oxidative stress, Am J Physiol, 275 (1998) L806-817.
[35] P.G. Bloemen, P.A. Henricks, L. van Bloois, M.C. van den Tweel, A.C. Bloem, F.P. Nijkamp, D.J. Crommelin, G. Storm, Adhesion molecules: a new target for immunoliposome-mediated drug delivery, FEBS Lett, 357 (1995) 140-144.
[36] S. Muro, E.H. Schuchman, V.R. Muzykantov, Lysosomal enzyme delivery by ICAM-1-targeted nanocarriers bypassing glycosylation- and clathrin-dependent endocytosis, Mol Ther, 13 (2006) 135-141.
[37] J. Papademetriou, C. Garnacho, D. Serrano, T. Bhowmick, E.H. Schuchman, S. Muro, Comparative binding, endocytosis, and biodistribution of antibodies and antibody-coated carriers for targeted delivery of lysosomal enzymes to ICAM-1 versus transferrin receptor, J Inherit Metab Dis, 36 (2013) 467-477.
[38] I.T. Papademetriou, C. Garnacho, E.H. Schuchman, S. Muro, In vivo performance of polymer nanocarriers dually-targeted to epitopes of the same or different receptors, Biomaterials, 34 (2013) 3459–3466.
[39] S. Muro, New biotechnological and nanomedicine strategies for treatment of lysosomal storage disorders, Wiley Interdiscip Rev Nanomed Nanobiotechnol, 2 (2010) 189-204.
[40] Z. Cai, Y. Wang, L.J. Zhu, Z.Q. Liu, Nanocarriers: a general strategy for enhancement of oral bioavailability of poorly absorbed or pre-systemically metabolized drugs, Curr Drug Metab, 11 (2010) 197-207.
[41] A. des Rieux, V. Fievez, M. Garinot, Y.J. Schneider, V. Preat, Nanoparticles as potential oral delivery systems of proteins and vaccines: a mechanistic approach, J Control Release, 116 (2006) 1-27.
[42] M.F. Francis, M. Cristea, F.M. Winnik, Exploiting the vitamin B12 pathway to enhance oral drug delivery via polymeric micelles, Biomacromolecules, 6 (2005) 2462-2467.
[43] H.H. Salman, C. Gamazo, M. Agueros, J.M. Irache, Bioadhesive capacity and immunoadjuvant properties of thiamine-coated nanoparticles, Vaccine, 25 (2007) 8123-8132.
[44] N. Mishra, S. Tiwari, B. Vaidya, G.P. Agrawal, S.P. Vyas, Lectin anchored PLGA nanoparticles for oral mucosal immunization against hepatitis B, J Drug Target, 19 (2011) 67-78.
[45] T. Stefanelli, A. Malesci, S.A. De La Rue, S. Danese, Anti-adhesion molecule therapies in inflammatory bowel disease: touch and go, Autoimmun Rev, 7 (2008) 364-369.
[46] P.L. Tuma, A.L. Hubbard, Transcytosis: crossing cellular barriers, Physiol Rev, 83 (2003) 871-932.

[47] A. Gupta, J.L. Terrell, R. Fernandes, M.B. Dowling, G.F. Payne, S.R. Raghavan, W.E. Bentley, Encapsulated fusion protein confers "sense and respond" activity to chitosan-alginate capsules to manipulate bacterial quorum sensing, Biotechnol Bioeng, 110 (2013) 552-562.
[48] X.Y. Li, L.J. Jin, Y.N. Lu, Y.H. Zhen, S.Y. Li, L.H. Wang, Y.P. Xu, Chitosan-alginate microcapsules for oral delivery of egg yolk immunoglobulin (IgY): effects of chitosan concentration, Appl Biochem Biotechnol, 159 (2009) 778-787.
[49] A.K. Anal, D. Bhopatkar, S. Tokura, H. Tamura, W.F. Stevens, Chitosan-alginate multilayer beads for gastric passage and controlled intestinal release of protein, Drug Dev Ind Pharm, 29 (2003) 713-724.
[50] L.D. Wood, E. Montgomery, Structure and innervation of hollow viscera, in: J.F. Reinus, D. Simon (Eds.) Gastrointestinal Anatomy and Physiology: The Essentials, John Wiley & Sons, Ltd, Chichester, West Sussex, PO19 8SQ, UK, 2014.
[51] B. Alberts, A. Johnson, J. Lewis, M. Raff, K. Roberts, P. Walter, Molecular Biology of the Cell, 4th edition, 4th ed., Garland Science, New York, 2002.
[52] R. Duncan, S.C. Richardson, Endocytosis and intracellular trafficking as gateways for nanomedicine delivery: opportunities and challenges, Mol Pharm, 9 (2012) 2380-2402.
[53] Y. Yun, Y.W. Cho, K. Park, Nanoparticles for oral delivery: targeted nanoparticles with peptidic ligands for oral protein delivery, Adv Drug Deliv Rev, 65 (2013) 822-832.
[54] H.H. Salman, C. Gamazo, P.C. de Smidt, G. Russell-Jones, J.M. Irache, Evaluation of bioadhesive capacity and immunoadjuvant properties of vitamin B(12)-Gantrez nanoparticles, Pharm Res, 25 (2008) 2859-2868.
[55] K.B. Chalasani, G.J. Russell-Jones, A.K. Jain, P.V. Diwan, S.K. Jain, Effective oral delivery of insulin in animal models using vitamin B12-coated dextran nanoparticles, J Control Release, 122 (2007) 141-150.
[56] S. Jain, V.V. Rathi, A.K. Jain, M. Das, C. Godugu, Folate-decorated PLGA nanoparticles as a rationally designed vehicle for the oral delivery of insulin, Nanomedicine (Lond), 7 (2012) 1311-1337.
[57] V. Fievez, L. Plapied, A. des Rieux, V. Pourcelle, H. Freichels, V. Wascotte, M.L. Vanderhaeghen, C. Jerôme, A. Vanderplasschen, J. Marchand-Brynaert, Y.J. Schneider, V. Préat, Targeting nanoparticles to M cells with non-peptidic ligands for oral vaccination, Eur J Pharm Biopharm, 73 (2009) 16-24.
[58] P.N. Gupta, K. Khatri, A.K. Goyal, N. Mishra, S.P. Vyas, M-cell targeted biodegradable PLGA nanoparticles for oral immunization against hepatitis B, J Drug Target, 15 (2007) 701-713.
[59] T. Hou, Y. Li, W. Zhang, J. Wang, Recent developments of in silico predictions of intestinal absorption and oral bioavailability, Comb Chem High Throughput Screen, 12 (2009) 497-506.
[60] J. Shaji, V. Patole, Protein and Peptide drug delivery: oral approaches, Indian J Pharm Sci, 70 (2008) 269-277.
[61] Y. Nakada, N. Awata, C. Nakamichi, I. Sugimoto, The effect of additives on the oral mucosal absorption of human calcitonin in rats, J Pharmacobiodyn, 11 (1988) 395-401.
[62] D.Z. Liu, E.L. LeCluyse, D.R. Thakker, Dodecylphosphocholine-mediated enhancement of paracellular permeability and cytotoxicity in Caco-2 cell monolayers, J Pharm Sci, 88 (1999) 1161-1168.

[63] E.S. Swenson, W.B. Milisen, W. Curatolo, Intestinal permeability enhancement: efficacy, acute local toxicity, and reversibility, Pharm Res, 11 (1994) 1132-1142.
[64] B. Steffansen, C.U. Nielsen, B. Brodin, A.H. Eriksson, R. Andersen, S. Frokjaer, Intestinal solute carriers: an overview of trends and strategies for improving oral drug absorption, Eur J Pharm Sci, 21 (2004) 3-16.
[65] L.M. Bareford, P.W. Swaan, Endocytic mechanisms for targeted drug delivery, Adv Drug Deliv Rev, 59 (2007) 748-758.
[66] S. Muro, M. Koval, V. Muzykantov, Endothelial endocytic pathways: gates for vascular drug delivery, Curr Vasc Pharmacol, 2 (2004) 281-299.
[67] D.T. Wiley, P. Webster, A. Gale, M.E. Davis, Transcytosis and brain uptake of transferrin-containing nanoparticles by tuning avidity to transferrin receptor, Proc Natl Acad Sci U S A, (In press. DOI: 10.1073/pnas.1307152110) (2013).
[68] W. Xia, P.S. Low, Folate-targeted therapies for cancer, J Med Chem, 53 6811-6824.
[69] L. Johannes, R.G. Parton, P. Bassereau, S. Mayor, Building endocytic pits without clathrin, Nat Rev Mol Cell Biol, 16 (2015) 311-321.
[70] G.M. Pauletti, F.W. Okumu, R.T. Borchardt, Effect of size and charge on the passive diffusion of peptides across Caco-2 cell monolayers via the paracellular pathway, Pharm Res, 14 (1997) 164-168.
[71] N. Salamat-Miller, T.P. Johnston, Current strategies used to enhance the paracellular transport of therapeutic polypeptides across the intestinal epithelium, Int J Pharm, 294 (2005) 201-216.
[72] M. Chittchang, N. Salamat-Miller, H.H. Alur, D.G. Vander Velde, A.K. Mitra, T.P. Johnston, Poly(L-lysine) as a model drug macromolecule with which to investigate secondary structure and microporous membrane transport, part 2: diffusion studies, J Pharm Pharmacol, 54 (2002) 1497-1505.
[73] J.R. Turner, Intestinal mucosal barrier function in health and disease, Nature Reviews Immunology, 9 (2009) 799-809.
[74] M.A. Deli, Potential use of tight junction modulators to reversibly open membranous barriers and improve drug delivery, Biochimica et Biophysica Acta, 1788 (2009) 892-910.
[75] C.C. Lee, J.A. MacKay, J.M. Frechet, F.C. Szoka, Designing dendrimers for biological applications, Nat Biotechnol, 23 (2005) 1517-1526.
[76] S. Sadekar, H. Ghandehari, Transepithelial transport and toxicity of PAMAM dendrimers: implications for oral drug delivery, Adv Drug Deliv Rev, 64 (2012) 571-588.
[77] K.M. Kitchens, M.E. El-Sayed, H. Ghandehari, Transepithelial and endothelial transport of poly (amidoamine) dendrimers, Adv Drug Deliv Rev, 57 (2005) 2163-2176.
[78] D.S. Goldberg, H. Ghandehari, P.W. Swaan, Cellular entry of G3.5 poly (amido amine) dendrimers by clathrin- and dynamin-dependent endocytosis promotes tight junctional opening in intestinal epithelia, Pharm Res, 27 (2010) 1547-1557.
[79] T. Minko, R.I. Pakunlu, Y. Wang, J.J. Khandare, M. Saad, New generation of liposomal drugs for cancer, Anticancer Agents Med Chem, 6 (2006) 537-552.
[80] S.M. Moghimi, J. Szebeni, Stealth liposomes and long circulating nanoparticles: critical issues in pharmacokinetics, opsonization and protein-binding properties, Prog Lipid Res, 42 (2003) 463-478.
[81] B.M. Discher, Y.Y. Won, D.S. Ege, J.C. Lee, F.S. Bates, D.E. Discher, D.A. Hammer, Polymersomes: tough vesicles made from diblock copolymers, Science, 284 (1999) 1143-1146.

[82] F. Ahmed, D.E. Discher, Self-porating polymersomes of PEG-PLA and PEG-PCL: hydrolysis-triggered controlled release vesicles, J Control Release, 96 (2004) 37-53.
[83] J. Panyam, V. Labhasetwar, Biodegradable nanoparticles for drug and gene delivery to cells and tissue, Adv Drug Deliv Rev, 55 (2003) 329-347.
[84] E.A. Simone, T.D. Dziubla, V.R. Muzykantov, Polymeric carriers: role of geometry in drug delivery, Expert Opin Drug Deliv, 5 (2008) 1283-1300.
[85] T.D. Dziubla, V.R. Muzykantov, Synthetic carriers for vascular delivery of protein therapeutics, Biotechnol Genet Eng Rev, 22 (2006) 267-298.
[86] S. Muro, T. Dziubla, W. Qiu, J. Leferovich, X. Cui, E. Berk, V.R. Muzykantov, Endothelial targeting of high-affinity multivalent polymer nanocarriers directed to intercellular adhesion molecule 1, J Pharmacol Exp Ther, 317 (2006) 1161-1169.
[87] T. Bhowmick, E. Berk, X. Cui, V.R. Muzykantov, S. Muro, Effect of flow on endothelial endocytosis of nanocarriers targeted to ICAM-1, J Control Release, 157 (2012) 485-492.
[88] Y. Takei, Y. Nishimura, S. Kawano, H. Nagai, A. Ohmae, H. Fusamoto, T. Kamada, Expression of ICAM-1 is involved in the mechanism of liver injury during liver transplantation: therapeutic usefulness of the F(ab')2 fragment of an anti-ICAM-1 monoclonal antibody, Transplant Proc, 28 (1996) 1103-1105.
[89] A.F. Kavanaugh, H. Schulze-Koops, L.S. Davis, P.E. Lipsky, Repeat treatment of rheumatoid arthritis patients with a murine anti-intercellular adhesion molecule 1 monoclonal antibody, Arthritis Rheum, 40 (1997) 849-853.
[90] D.E. Hallahan, S. Virudachalam, Intercellular adhesion molecule 1 knockout abrogates radiation induced pulmonary inflammation, Proc Natl Acad Sci U S A, 94 (1997) 6432-6437.
[91] S. Muro, M. Mateescu, C. Gajewski, M. Robinson, V.R. Muzykantov, M. Koval, Control of intracellular trafficking of ICAM-1-targeted nanocarriers by endothelial Na+/H+ exchanger proteins, Am J Physiol Lung Cell Mol Physiol, 290 (2006) L809-817.
[92] S. Muro, C. Gajewski, M. Koval, V.R. Muzykantov, ICAM-1 recycling in endothelial cells: a novel pathway for sustained intracellular delivery and prolonged effects of drugs, Blood, 105 (2005) 650-658.
[93] D. Serrano, T. Bhowmick, R. Chadha, C. Garnacho, S. Muro, Intercellular adhesion molecule 1 engagement modulates sphingomyelinase and ceramide, supporting uptake of drug carriers by the vascular endothelium, Arterioscler Thromb Vasc Biol, 32 (2012) 1178-1185.
[94] J. Hsu, J. Hoenicka, S. Muro, Targeting, endocytosis, and lysosomal delivery of active enzymes to model human neurons by ICAM-1-targeted nanocarriers, Pharm Res, 32 (2015) 1264-1278.
[95] R. Manthe, S. Muro, Lysosomes and nanotherapeutics: diseases, treatments, and side effects, in: V. Torchilin (Ed.) Handbook of Nanobiomedical Research, World Scientific, 2014, pp. 261-305.
[96] T. Coviello, P. Matricardi, C. Marianecci, F. Alhaique, Polysaccharide hydrogels for modified release formulations, J Control Release, 119 (2007) 5-24.
[97] L. Serra, J. Domenech, N.A. Peppas, Engineering design and molecular dynamics of mucoadhesive drug delivery systems as targeting agents, Eur J Pharm Biopharm, 71 (2009) 519-528.

[98] N.A. Peppas, P. Bures, W. Leobandung, H. Ichikawa, Hydrogels in pharmaceutical formulations, Eur J Pharm Biopharm, 50 (2000) 27-46.
[99] B. Balakrishnan, R. Banerjee, Biopolymer-based hydrogels for cartilage tissue engineering, Chem Rev, 111 (2011) 4453-4474.
[100] D.J. Mastropietro, H. Omidian, K. Park, Drug delivery applications for superporous hydrogels, Expert Opin Drug Deliv, 9 (2012) 71-89.
[101] T. Yoshida, T.C. Lai, G.S. Kwon, K. Sako, pH- and ion-sensitive polymers for drug delivery, Expert Opin Drug Deliv, 10 (2013) 1497-1513.
[102] K.A. Watkins, R. Chen, pH-responsive, lysine-based hydrogels for the oral delivery of a wide size range of molecules, Int J Pharm, 478 (2015) 496-503.
[103] B. Kim, S.H. Lim, W. Ryoo, Preparation and characterization of pH-sensitive anionic hydrogel microparticles for oral protein-delivery applications, J Biomater Sci Polym Ed, 20 (2009) 427-436.
[104] T.W. Wong, Chitosan and its use in design of insulin delivery system, Recent Pat Drug Deliv Formul, 3 (2009) 8-25.
[105] S. Takka, A. Gürel, Evaluation of chitosan/alginate beads using experimental design: formulation and in vitro characterization, AAPS PharmSciTech, 11 (2010) 460-466.
[106] M. Chávarri, I. Marañón, R. Ares, F.C. Ibáñez, F. Marzo, M.e.C. Villarán, Microencapsulation of a probiotic and prebiotic in alginate-chitosan capsules improves survival in simulated gastro-intestinal conditions, Int J Food Microbiol, 142 (2010) 185-189.
[107] S. Sugiura, T. Oda, Y. Aoyagi, R. Matsuo, T. Enomoto, K. Matsumoto, T. Nakamura, M. Satake, A. Ochiai, N. Ohkohchi, M. Nakajima, Microfabricated airflow nozzle for microencapsulation of living cells into 150 micrometer microcapsules, Biomed Microdevices, 9 (2007) 91-99.
[108] L.S. Kontturi, M. Yliperttula, P. Toivanen, A. Määttä, A.M. Määttä, A. Urtti, A laboratory-scale device for the straightforward production of uniform, small sized cell microcapsules with long-term cell viability, J Control Release, 152 (2011) 376-381.
[109] G. D'Orazio, P. Di Gennaro, M. Boccarusso, I. Presti, G. Bizzaro, S. Giardina, A. Michelotti, M. Labra, B. La Ferla, Microencapsulation of new probiotic formulations for gastrointestinal delivery: in vitro study to assess viability and biological properties, Appl Microbiol Biotechnol, (2015).
[110] S. Koch, C. Schwinger, J. Kressler, C. Heinzen, N.G. Rainov, Alginate encapsulation of genetically engineered mammalian cells: comparison of production devices, methods and microcapsule characteristics, J Microencapsul, 20 (2003) 303-316.
[111] R.P. Lanza, R. Jackson, A. Sullivan, J. Ringeling, C. McGrath, W. Kuhtreiber, W.L. Chick, Xenotransplantation of cells using biodegradable microcapsules, Transplantation, 67 (1999) 1105-1111.
[112] C. Garnacho, D. Serrano, S. Muro, A fibrinogen-derived peptide provides intercellular adhesion molecule-1-specific targeting and intraendothelial transport of polymer nanocarriers in human cell cultures and mice, J Pharmacol Exp Ther, 340 (2012) 638-647.
[113] D. Serrano, S. Muro, Endothelial Cell Adhesion Molecules and Drug Delivery Applications, in: H. Aranda-Espinoza (Ed.) Mechanobiology of the Endothelium, Science Publishers, Maryland, 2014.

[114] S. Muro, Muzykantov, V.R., Murciano, J., Characterization of endothelial internalization and targeting of antibody-enzyme conjugates in cell cultures and in laboratory animals, in: C.M. Niemeyer (Ed.) Methods in molecular biology. Bioconjugation protocols., Humana Press, Totowa, New Jersey, 2004, pp. 21-36.
[115] M.E. Wiseman, C.W. Frank, Antibody adsorption and orientation on hydrophobic surfaces, Langmuir, 28 (2012) 1765-1774.
[116] R. Ghaffarian, S. Muro, Distinct subcellular trafficking resulting from monomeric vs multimeric targeting to endothelial ICAM-1: implications for drug delivery, Mol Pharm, 11 (2014) 4350-4362.
[117] A.J. Calderon, V. Muzykantov, S. Muro, D.M. Eckmann, Flow dynamics, binding and detachment of spherical carriers targeted to ICAM-1 on endothelial cells, Biorheology, 46 (2009) 323-341.
[118] R. Wiewrodt, A.P. Thomas, L. Cipelletti, M. Christofidou-Solomidou, D.A. Weitz, S.I. Feinstein, D. Schaffer, S.M. Albelda, M. Koval, V.R. Muzykantov, Size-dependent intracellular immunotargeting of therapeutic cargoes into endothelial cells, Blood, 99 (2002) 912-922.
[119] H.O. Chen, C. Martoni, S. Prakash, Genipin cross-linked polymeric chitosan-alginate microcapsules for oral delivery: in-vitro analysis, International Journal of Polymer Science, 16 (2009).
[120] A. Lu, Microfluidic generation of anisotropic capsules, in: Department of Chemical and Biomolecular Engineering, University of Maryland, College Park., College Park, MD, 2015, pp. 71.
[121] H. Onishi, K. Koyama, O. Sakata, Y. Machida, Preparation of chitosan/alginate/calcium complex microparticles loaded with lactoferrin and their efficacy on carrageenan-induced edema in rats, Drug Dev Ind Pharm, 36 (2010) 879-884.
[122] S. Muro, X. Cui, C. Gajewski, J.-C. Murciano, V.R. Muzykantov, M. Koval, Slow intracellular trafficking of catalase nanoparticles targeted to ICAM-1 protects endothelial cells from oxidative stress, Am J Physiol, Cell Physiol, 285 (2003) C1339-1347.
[123] L. Rajendran, H.J. Knolker, K. Simons, Subcellular targeting strategies for drug design and delivery, Nat Rev Drug Discov, 9 (2010) 29-42.
[124] Y. Zhang, W. Wei, P. Lv, L. Wang, G. Ma, Preparation and evaluation of alginate-chitosan microspheres for oral delivery of insulin, Eur J Pharm Biopharm, 77 (2011) 11-19.
[125] J.Y. Hou, L.N. Gao, F.Y. Meng, Y.L. Cui, Mucoadhesive microparticles for gastroretentive delivery: preparation, biodistribution and targeting evaluation, Mar Drugs, 12 (2014) 5764-5787.
[126] A. Trapani, A. Lopedota, M. Franco, N. Cioffi, E. Ieva, M. Garcia-Fuentes, M.J. Alonso, A comparative study of chitosan and chitosan/cyclodextrin nanoparticles as potential carriers for the oral delivery of small peptides, Eur J Pharm Biopharm, 75 (2010) 26-32.
[127] B. Manickam, R. Sreedharan, M. Elumalai, 'Genipin' - the natural water soluble cross-linking agent and its importance in the modified drug delivery systems: an overview, Curr Drug Deliv, 11 (2014) 139-145.
[128] E. Simone, B.J. Zern, A.-M. Chacko, J.L. Mikitsh, E. Blankemeyer, S. Muro, R.V. Stan, V. Muzykantov, Endothelial Targeting of Polymeric Nanoparticles Stably Labeled with Radioisotopes: from Synthesis to PET Imaging, Biomaterials, In Press (2012).

[129] E. Berk, Muzykantov, VR., Muro, S., Binding and uptake of anti-ICAM-1 coated nanoparticles by flow adapted endothelial cells, 9 th Annual Respiration Research Retreat, 9 (2003).
[130] I.J. Hidalgo, T.J. Raub, R.T. Borchardt, Characterization of the human colon carcinoma cell line (Caco-2) as a model system for intestinal epithelial permeability, Gastroenterology, 96 (1989) 736-749.
[131] I. Papademetriou, Z. Tsinas, J. Hsu, S. Muro, Combination-targeting to multiple endothelial cell adhesion molecules modulates binding, endocytosis, and in vivo biodistribution of drug nanocarriers and their therapeutic cargoes, J Control Release, 188 (2014) 87-98.
[132] S. Muro, A DNA-Device that Mediates Selective Endosomal Escape and Intracellular Delivery of Drugs and Biologicals, Adv Funct Mater, 24 (2014) 2899-2906.
[133] A.J. Hamilton, S.L. Huang, D. Warnick, M. Rabbat, B. Kane, A. Nagaraj, M. Klegerman, D.D. McPherson, Intravascular ultrasound molecular imaging of atheroma components in vivo, J Am Coll Cardiol, 43 (2004) 453-460.
[134] G.E. Weller, F.S. Villanueva, E.M. Tom, W.R. Wagner, Targeted ultrasound contrast agents: in vitro assessment of endothelial dysfunction and multi-targeting to ICAM-1 and sialyl Lewisx, Biotechnol Bioeng, 92 (2005) 780-788.
[135] G.E. Weller, M.K. Wong, R.A. Modzelewski, E. Lu, A.L. Klibanov, W.R. Wagner, F.S. Villanueva, Ultrasonic imaging of tumor angiogenesis using contrast microbubbles targeted via the tumor-binding peptide arginine-arginine-leucine, Cancer Res, 65 (2005) 533-539.
[136] M.F. Kiani, H. Yuan, X. Chen, L. Smith, M.W. Gaber, D.J. Goetz, Targeting microparticles to select tissue via radiation-induced upregulation of endothelial cell adhesion molecules, Pharm Res, 19 (2002) 1317-1322.
[137] P. Guo, J. Huang, L. Wang, D. Jia, J. Yang, D.A. Dillon, D. Zurakowski, H. Mao, M.A. Moses, D.T. Auguste, ICAM-1 as a molecular target for triple negative breast cancer, Proc Natl Acad Sci U S A, 111 (2014) 14710-14715.
[138] A.C. Anselmo, S. Kumar, V. Gupta, A.M. Pearce, A. Ragusa, V. Muzykantov, S. Mitragotri, Exploiting shape, cellular-hitchhiking and antibodies to target nanoparticles to lung endothelium: Synergy between physical, chemical and biological approaches, Biomaterials, 68 (2015) 1-8.
[139] R.J. Desnick, E.H. Schuchman, Enzyme replacement therapy for lysosomal diseases: lessons from 20 years of experience and remaining challenges, Annu Rev Genomics Hum Genet, 13 (2012) 307-335.
[140] V.I. Brown, M.I. Greene, Molecular and cellular mechanisms of receptor-mediated endocytosis, DNA Cell Biol, 10 (1991) 399-409.
[141] E.W. Marsh, P.L. Leopold, N.L. Jones, F.R. Maxfield, Oligomerized transferrin receptors are selectively retained by a lumenal sorting signal in a long-lived endocytic recycling compartment, J Cell Biol, 129 (1995) 1509-1522.
[142] W. Xia, P.S. Low, Folate-targeted therapies for cancer, J Med Chem, 53 (2010) 6811-6824.
[143] P. Oh, P. Borgstrom, H. Witkiewicz, Y. Li, B.J. Borgstrom, A. Chrastina, K. Iwata, K.R. Zinn, R. Baldwin, J.E. Testa, J.E. Schnitzer, Live dynamic imaging of caveolae pumping targeted antibody rapidly and specifically across endothelium in the lung, Nat Biotechnol, 25 (2007) 327-337.

[144] I. Mellman, H. Plutner, P. Ukkonen, Internalization and rapid recycling of macrophage Fc receptors tagged with monovalent antireceptor antibody: possible role of a prelysosomal compartment, J Cell Biol, 98 (1984) 1163-1169.
[145] I. Mellman, H. Plutner, Internalization and degradation of macrophage Fc receptors bound to polyvalent immune complexes, J Cell Biol, 98 (1984) 1170-1177.
[146] K.L. Singer, K.E. Mostov, Dimerization of the polymeric immunoglobulin receptor controls its transcytotic trafficking, Mol Biol Cell, 9 (1998) 901-915.
[147] B.D. Grant, J.G. Donaldson, Pathways and mechanisms of endocytic recycling, Nat Rev Mol Cell Biol, 10 (2009) 597-608.
[148] O. Barreiro, M. Yanez-Mo, J.M. Serrador, M.C. Montoya, M. Vicente-Manzanares, R. Tejedor, H. Furthmayr, F. Sanchez-Madrid, Dynamic interaction of VCAM-1 and ICAM-1 with moesin and ezrin in a novel endothelial docking structure for adherent leukocytes, Journal of Cell Biology, 157 (2002) 1233-1245.
[149] C.V. Carman, C.-D. Jun, A. Salas, T.A. Springer, Endothelial cells proactively form microvilli-like membrane projections upon intercellular adhesion molecule 1 engagement of leukocyte LFA-1., J Immunol, 171 (2003) 6135-6144.
[150] A.M. Hopkins, A.W. Baird, A. Nusrat, ICAM-1: targeted docking for exogenous as well as endogenous ligands, Adv Drug Deliv Rev, 56 (2004) 763-778.
[151] J.M. Greve, G. Davis, A.M. Meyer, C.P. Forte, S.C. Yost, C.W. Marlor, M.E. Kamarck, A. McClelland, The major human rhinovirus receptor is ICAM-1, Cell, 56 (1989) 839-847.
[152] E. Rieder, A.E. Gorbalenya, C. Xiao, Y. He, T.S. Baker, R.J. Kuhn, M.G. Rossmann, E. Wimmer, Will the polio niche remain vacant?, Dev Biol (Basel), 105 (2001) 111-122; discussion 149-150.
[153] B.S. Stein, H.H. Sussman, Demonstration of two distinct transferrin receptor recycling pathways and transferrin-independent receptor internalization in K562 cells, J Biol Chem, 261 (1986) 10319-10331.
[154] R.G. Anderson, M.S. Brown, U. Beisiegel, J.L. Goldstein, Surface distribution and recycling of the low density lipoprotein receptor as visualized with antireceptor antibodies, J Cell Biol, 93 (1982) 523-531.
[155] J.H. Jo, M.S. Kwon, H.O. Choi, H.M. Oh, H.J. Kim, C.D. Jun, Recycling and LFA-1-dependent trafficking of ICAM-1 to the immunological synapse, J Cell Biochem, 111 (2010) 1125-1137.
[156] M.S. Diamond, D.E. Staunton, S.D. Marlin, T.A. Springer, Binding of the integrin Mac-1 (CD11b/CD18) to the third immunoglobulin-like domain of ICAM-1 (CD54) and its regulation by glycosylation, Cell, 65 (1991) 961-971.
[157] P. Norris, R.N. Poston, D.S. Thomas, M. Thornhill, J. Hawk, D.O. Haskard, The expression of endothelial leukocyte adhesion molecule-1 (ELAM-1), intercellular adhesion molecule-1 (ICAM-1), and vascular cell adhesion molecule-1 (VCAM-1) in experimental cutaneous inflammation: a comparison of ultraviolet B erythema and delayed hypersensitivity, J Invest Dermatol, 96 (1991) 763-770.
[158] S.C. van Ijzendoorn, Recycling endosomes, J Cell Sci, 119 (2006) 1679-1681.
[159] A. Zeigerer, M.A. Lampson, O. Karylowski, D.D. Sabatini, M. Adesnik, M. Ren, T.E. McGraw, GLUT4 retention in adipocytes requires two intracellular insulin-regulated transport steps, Mol Biol Cell, 13 (2002) 2421-2435.

[160] J.G. Lock, J.L. Stow, Rab11 in recycling endosomes regulates the sorting and basolateral transport of E-cadherin, Mol Biol Cell, 16 (2005) 1744-1755.
[161] M. Fabbri, S. Di Meglio, M.C. Gagliani, E. Consonni, R. Molteni, J.R. Bender, C. Tacchetti, R. Pardi, Dynamic partitioning into lipid rafts controls the endo-exocytic cycle of the alphaL/beta2 integrin, LFA-1, during leukocyte chemotaxis, Mol Biol Cell, 16 (2005) 5793-5803.
[162] O. Ullrich, S. Reinsch, S. Urbé, M. Zerial, R.G. Parton, Rab11 regulates recycling through the pericentriolar recycling endosome, J Cell Biol, 135 (1996) 913-924.
[163] P. Shah, V. Jogani, T. Bagchi, A. Misra, Role of Caco-2 cell monolayers in prediction of intestinal drug absorption, Biotechnol Prog, 22 (2006) 186-198.
[164] N. Zhang, C. Chittasupho, C. Duangrat, T.J. Siahaan, C. Berkland, PLGA nanoparticle--peptide conjugate effectively targets intercellular cell-adhesion molecule-1, Bioconjug Chem, 19 (2008) 145-152.
[165] E. Mastrobattista, G. Storm, L. van Bloois, R. Reszka, P.G. Bloemen, D.J. Crommelin, P.A. Henricks, Cellular uptake of liposomes targeted to intercellular adhesion molecule-1 (ICAM-1) on bronchial epithelial cells, Biochim Biophys Acta, 1419 (1999) 353-363.
[166] A.M. Powelka, J. Sun, J. Li, M. Gao, L.M. Shaw, A. Sonnenberg, V.W. Hsu, Stimulation-dependent recycling of integrin beta1 regulated by ARF6 and Rab11, Traffic, 5 (2004) 20-36.
[167] Z. Mamdouh, X. Chen, L.M. Pierini, F.R. Maxfield, W.A. Muller, Targeted recycling of PECAM from endothelial surface-connected compartments during diapedesis, Nature, 421 (2003) 748-753.
[168] J. Millán, L. Hewlett, M. Glyn, D. Toomre, P. Clark, A.J. Ridley, Lymphocyte transcellular migration occurs through recruitment of endothelial ICAM-1 to caveola- and F-actin-rich domains, Nat Cell Biol, 8 (2006) 113-123.
[169] K.S. Choi, S.H. Kim, Q.Y. Cai, S.Y. Kim, H.O. Kim, H.J. Lee, E.A. Kim, S.E. Yoon, K.J. Yun, K.H. Yoon, Inflammation-specific T1 imaging using anti-intercellular adhesion molecule 1 antibody-conjugated gadolinium diethylenetriaminepentaacetic acid, Mol Imaging, 6 (2007) 75-84.
[170] R.C. Gunawan, D.T. Auguste, Immunoliposomes That Target Endothelium In Vitro Are Dependent on Lipid Raft Formation, Molecular Pharmaceutics, 7 (2010) 1569-1575.
[171] S. Park, S. Kang, A.J. Veach, Y. Vedvyas, R. Zarnegar, J.Y. Kim, M.M. Jin, Self-assembled nanoplatform for targeted delivery of chemotherapy agents via affinity-regulated molecular interactions, Biomaterials, 31 (2010) 7766-7775.
[172] S. Muro, Strategies for delivery of therapeutics into the central nervous system for treatment of lysosomal storage disorders, Drug Delivery and Translational Research, 2 (2012) 169-186.
[173] C.E. Haug, R.B. Colvin, F.L. Delmonico, H. Auchincloss, Jr., N. Tolkoff-Rubin, F.I. Preffer, R. Rothlein, S. Norris, L. Scharschmidt, A.B. Cosimi, A phase I trial of immunosuppression with anti-ICAM-1 (CD54) mAb in renal allograft recipients, Transplantation, 55 (1993) 766-772; discussion 772-763.
[174] W. Dippold, B. Wittig, W. Schwaeble, W. Mayet, K.H. Meyer zum Buschenfelde, Expression of intercellular adhesion molecule 1 (ICAM-1, CD54) in colonic epithelial cells, Gut, 34 (1993) 1593-1597.

[175] B.R. Yacyshyn, M.B. Bowen-Yacyshyn, L. Jewell, J.A. Tami, C.F. Bennett, D.L. Kisner, W.R. Shanahan, Jr., A placebo-controlled trial of ICAM-1 antisense oligonucleotide in the treatment of Crohn's disease, Gastroenterology, 114 (1998) 1133-1142.
[176] K. Kusterer, J. Bojunga, M. Enghofer, E. Heidenthal, K.H. Usadel, H. Kolb, S. Martin, Soluble ICAM-1 reduces leukocyte adhesion to vascular endothelium in ischemia-reperfusion injury in mice, Am J Physiol, 275 (1998) G377-380.
[177] T. Zimmerman, F.J. Blanco, Inhibitors targeting the LFA-1/ICAM-1 cell-adhesion interaction: design and mechanism of action, Curr Pharm Des, 14 (2008) 2128-2139.
[178] V.R. Muzykantov, Targeting of superoxide dismutase and catalase to vascular endothelium, Journal of Controlled Release, 71 (2001) 1-21.
[179] T. Maritzen, H. Schachtner, D.F. Legler, On the move: endocytic trafficking in cell migration, Cell Mol Life Sci, 72 (2015) 2119-2134.
[180] D.W. Shortt, D. Roessner, P.J. Wyatt, Absolute measurement of diameter distributions of particles using multiangle light scattering photometer coupled with flow field-flow fractionation., American Lab, (1996) 21-28.
[181] Q.A. Thai, G. Pradilla, F.G. Legnani, R.M. Kretzer, W. Hsu, R.J. Tamargo, Lysis of intracerebral hematoma with stereotactically implanted tissue plasminogen activator polymers in a rabbit model, J Neurosurg, 105 (2006) 424-429.
[182] R. Fowler, D. Vllasaliu, F.F. Trillo, C. Alexander, H. Horsley, B. Smith, I. Whitcomb, M. Eaton, S. Stolnik, Nanoparticle transport in epithelial cells: pathway switching through bioconjugation, Small, 9 (2013) 3282-3294.
[183] D.B. Tesar, N.E. Tiangco, and P.J. Bjorkman, Ligand valency affects transcytosis, recycling and intracellular trafficking mediated by the neonatal Fc receptor, Traffic 7 (2006) 1127-1142.
[184] R. Sumagin, A.Z. Robin, A. Nusrat, C.A. Parkos, Transmigrated neutrophils in the intestinal lumen engage ICAM-1 to regulate the epithelial barrier and neutrophil recruitment, Mucosal Immunology 7 (2014) 905–915.

Peer-Reviewed Publications

R. Ghaffarian, T. Bhowmick, S. Muro. (2012). Transport of nanocarriers across gastrointestinal epithelial cells by a new transcellular route induced by targeting ICAM-1. *Journal of Controlled Release*. 163: 25-33.

R. Ghaffarian and S. Muro. (2013). Models and Methods to Evaluate Transport of Drug Delivery Systems Across Cellular Barriers**.** *Journal of Visualized Experiments*. 80):e50638.

R. Ghaffarian and S. Muro. (2014). Distinct subcellular trafficking resulting from monomeric vs multimeric targeting to endothelial ICAM-1: implications for drug delivery. *American Chemical Society - Molecular Pharmaceutics*. 11(12): 4350-62.

***R. Ghaffarian**, A. Abouzeid, W. Vreeland, and S. Muro. (In preparation). Endocytosis of monomeric ICAM-1 targeting moieties provides intracellular transport of active enzyme conjugates in epithelial cells.*

***R. Ghaffarian**, A. Abouzeid, W. Vreeland, and S. Muro. (In preparation). Monomeric ICAM-1 targeting moieties provides transcellular transport of active enzyme conjugates across gastrointestinal epithelial cells.*

***R. Ghaffarian**, H. Oh, T. Smith, S.R. Raghavan, and S. Muro. (In preparation). Encapsulation of ICAM-1 targeted nanocarriers into chitosan-alginate microspheres provides gastric protection and controlled release for oral drug delivery*.

International and National Conference Abstracts and Proceedings

R. Ghaffarian and S. Muro. (Dec 2012). Effect of valency on the sub-cellular transport induced by ICAM-1-targeting. *Nanomedicine and Drug Delivery Symposium 2012*. Atlantic City, NJ. Poster presentation.

V. Mane, **R. Ghaffarian**, and S. Muro. (Jul. 2012). ICAM-1-targeted nanocarriers are endocytosed in the gastrointestinal tract of mice. *The 39th Annual Meeting and Exposition of the Controlled Release Society*. Québec, Canada. Oral presentation.

R. Ghaffarian, T. Bhowmick, S. Muro. (Apr. 2012). A novel mechanism of transcytosis of drug carriers across gastrointestinal epithelial cells mediated by ICAM-1. *Experimental Biology 2012*. San Diego, CA. Poster presentation.

R. Ghaffarian, T. Bhowmick, S. Muro. (Feb. 2012). Transport of α-galactosidase coupled to ICAM-1-targeted nanocarriers across gastrointestinal epithelial cells. *World*

Organization for Research on Rare Lysosomal Disorders (WORLD) Symposium. San Diego, CA. Oral presentation.

R. Ghaffarian, T. Bhowmick, S. Muro. (Nov. 2011). Transport of ICAM-1-targeted nanocarriers across gastrointestinal epithelial cells occurs via the transcellular, not paracellular, route. *The 3rd Annual Meeting of the American Society for Nanomedicine*. Shady Grove, MD. Poster and oral presentation

R. Ghaffarian, A. Bagal, S.R. Raghavan, S. Muro. (Oct. 2011). pH-sensitive hydrogels for encapsulation and controlled release of antibody-coated nanocarriers for oral drug delivery. *Biomedical Engineering Society 2011 Annual Fall Meeting*. Hartford, CT. Poster presentation.

R. Ghaffarian, O. Ayyub, P. Kofinas, S. Muro. (Aug. 2011). Targeting to ICAM-1 induces transport of polymer carriers across gastrointestinal epithelial cells. *The 38th Annual Meeting and Exposition of the Controlled Release Society*. National Harbor, MD. Poster presentation.

V. Mane, **R. Ghaffarian**, T. Bhowmick, S. Muro. (Aug. 2011). Biodistribution of ICAM-1-targeting nanocarriers in the gastrointestinal tract in mice. *The 38th Annual Meeting and Exposition of the Controlled Release Society*. National Harbor, MD. Oral presentation.

R. Ghaffarian, T. Bhowmick, S. Muro. (May 2011). ICAM-1-targeted transport of drug carriers across gastrointestinal epithelial cells. *The 6th Annual Cancer Nanobiology Think Tank*. Frederick, MD. Poster presentation.

R. Ghaffarian, T. Bhowmick, S. Muro. (Oct. 2010). Transcellular transport of nanocarriers across gastrointestinal epithelial cells by targeting ICAM-1. *Biomedical Engineering Society 2010 Annual Fall Meeting*. Austin, TX. Oral presentation.

Local Symposium Abstracts and Proceedings

R. Ghaffarian, H. Oh, T. Smith, S.R. Raghavan, and S. Muro. (Apr. 2015). Encapsulation of ICAM-1 targeted nanocarriers for oral delivery of lysosomal enzymes. *Graduate Research Interaction Day.* College Park, MD. Oral presentation.

R. Ghaffarian and S. Muro. (Nov 2014). Direct conjugation of a model enzyme to anti-ICAM provides specific transport across cellular barriers. *Bioscience Research and Technology Review Day.* College Park, MD. Poster presentation.

R. Ghaffarian and S. Muro. (Oct 2014). Oral delivery of biological therapeutics. *Inventor's Panel, 2014 Fischell Festival*. College Park, MD. Oral presentation.

R. Ghaffarian and S. Muro. (Nov 2013). ICAM-1 mediates distinct intracellular trafficking of ligands with different valency: implications for biology and drug delivery. *Innovation Venture Fair, Bioscience Research and Technology Review Day.* College Park, MD. Poster presentation.

R. Ghaffarian and S. Muro. (Nov 2012). Oral delivery of biological therapeutics. *Innovation Venture Fair, Bioscience Research and Technology Review Day.* College Park, MD. Oral presentation.

R. Ghaffarian and S. Muro. (Oct 2012). Valency determines route of sub-cellular transport of drug carriers targeted to ICAM-1. *The 2012 Fischell Festival*. College Park, MD. Poster presentation.

R. Ghaffarian, A. Bagal, S.R. Raghavan, S. Muro. (Oct. 2011). Design of chitosan-gellan gum capsules for gastric protection and intestinal release of targeted nanocarriers. *The 2011 Fischell Festival.* College Park, MD. Poster presentation.

R. Ghaffarian, S. Muro. (Mar. 2011). Transport of drug delivery carriers across the gastrointestinal epithelium by targeting ICAM-1. *University of Maryland/National Cancer Institute Partnership for Cancer Technology Workshop*. College Park, MD. Poster presentation.

R. Ghaffarian, T. Bhowmick, S. Muro. (Nov. 2010). ICAM-1-targeted nanocarriers as a strategy for drug delivery across the intestinal epithelium. *Bioscience Research and Technology Review Day*. College Park, MD. Poster presentation.

R. Ghaffarian, T. Bhowmick, S. Muro. (Apr. 2010). ICAM-1-targeted nanocarriers as a strategy for drug delivery across the intestinal epithelium. In *11th Annual Howard Hughes Medical Institute Research Symposium*. College Park, MD. Poster presentation.

Awards and Fellowships

Best Presentation, Category - Physical Determinants of Health — April 2015
Graduate Research Interaction Day

First Place, Business Pitch Competition, — December 2012
Bioscience Research and Technology Review Day

Young Investigator Award and Best Poster — November 2011
American Society for Nanomedicine

Invention of the Year — May 2011
UMD Office of Technology Commercialization

NSF Graduate Research Fellowship — August 2011 – August 2014